الجمهورية الجزائرية الديمقراطية الشعبية

People's Democratic Republic of Algeria

وزارة التعليم العالي والبحث العلمي

Ministry of Higher Education and Scientific Research

Mustapha Stambouli University

Mascara

جامعة مصطفى اسطمبولي

معسكر

Faculty of Science and Technology

Department of Mechanical Engineering

كلية العلوم والتكنولوجيا

قسم الهندسة الميكانيكية

DOCTORAL THESIS

Entitled

Contribution of Numerical Methods in Design of Implantological Systems

***Presented by*: Ouldyerou Abdelhak**

11/10/2023

Members of the jury:

Noureddine Della	**Full Professor**	**University of Mascara**	**President**
Laid Aminallah	**Full Professor**	**University of Mascara**	**Supervisor**
Ali Merdji	**Full Professor**	**University of Mascara**	**Co-Supervisor**
Abdelkader Ziadi	**Full Professor**	**University of Ain Tmouchent**	**Examiner**
El Bahri Ould Chikh	**Full Professor**	**University of Mascara**	**Examiner**
Abdelghani May	**Full Professor**	**Polytechnic Military School - Algiers**	**Examiner**
Mohamed Chabbi Ziane	**Full Professor**	**Dental Ziane office manager - Oran**	**Invited**

Academic year: 2022-2023

Dedications and Acknowledgements

First and foremost, I want to express my gratitude to Allah, the Almighty, the Most Gracious, and the Most Merciful, for His blessings that enabled me to finish this thesis and my studies.

To my beloved family, who has consistently supported and encouraged me throughout my academic journey, I dedicate this thesis. Your unwavering love and belief in me have been the driving force behind my success. I am eternally grateful to my parents for their constant support.

I would like to express my deepest gratitude to my supervisor, Professor Laid Aminallah, and my co-supervisor, Professor Ali Merdji, for their invaluable guidance, supervision, and assistance throughout this thesis.

I am also grateful to Dr. Hassan Mehboob for his support and encouragement during my PhD journey. His expertise and guidance have been immensely valuable.

I am also grateful to all my friends for their unwavering support and encouragement.

Abstract

Dense titanium implants have become a popular choice for orthopedic surgery due to their biocompatibility and corrosion resistance. However, they can cause stress shielding, which leads to bone loss around the implant due to the mismatch between the implant's higher stiffness and the lower stiffness of the surrounding bone. Stress shielding is a common problem in dental implantology. To address this issue, researchers have developed various strategies, including modifying the implant's surface properties or design, using materials with lower stiffness, and developing novel implant design such as using porous bioamaterials that can stimulate bone growth and regeneration around the implant. The use of the finite element method and mechanostat theory has been proposed to better understand the stress and strain distribution in the implant-bone interface and to develop strategies to minimize stress shielding. In this study, a finite element model with porous titanium and low stiffness was used to simulate the stress and strain distribution in a the bone and implant under different loading conditions. The mechanostat theory was applied to predict bone behavior and remodeling. However, the use of different implant stiffness was found to affect the strain intensity in the host bone. Our findings suggest that porous implants can promote bone ingrowth and enhance the implant's stability by allowing the bone to grow into the implant's surface. In addition, the finite element method and mechanostat theory can be useful tools to optimize dental implant design and prevent stress shielding in silico-analysis.

Keywords: Porosity, titanium, finite element, dental implant, mechanostat, stress-shielding, bone atrophy, FGM, 3D modeling

الملخص:

أصبحت غرسات التيتانيوم ذات الكثافة العالية خيارًا شائعًا لجراحة العظام نظرًا لتوافقها الحيوي ومقاومتها للتآكل. ومع ذلك ، يمكن أن تسبب هذه الغرسات ظاهرة الحماية من الإجهاد stress shielding ، مما يؤدي إلى فقدان العظام حول الزرع بسبب عدم التطابق بين الصلابة العالية للغرسة والصلابة المنخفضة للعظم المحيط. الوقاية من الإجهاد مشكلة شائعة في زراعة الأسنان. لمعالجة هذه المشكلة ، طور الباحثون استراتيجيات مختلفة ، بما في ذلك تعديل خصائص سطح الزرع أو تصميمه ، واستخدام مواد ذات صلابة أقل ، وتطوير تصميم جديد للزرع مثل استخدام المواد الحيوية المسامية التي يمكن أن تحفز نمو العظام وتجديدها حول الغرسة. تم اقتراح استخدام طريقة العناصر المحدودة ونظرية الميكانيوستات لفهم توزيع الإجهاد والانفعال بشكل أفضل في واجهة عظام الزرع ولتطوير استراتيجيات لتقليل الحماية من الإجهاد. في هذه الدراسة ، تم استخدام نموذج العناصر المحدودة مع التيتانيوم المسامي والصلابة المنخفضة لمحاكاة توزيع الإجهاد والانفعال في العظم والغرسة تحت ظروف تحميل مختلفة. تم تطبيق نظرية الميكانوستات للتنبؤ بسلوك العظام وإعادة تشكيلها. وجد أن استخدام غرسات ذات صلابة مختلفة له تأثير على توزيع الاجهادات على مستوى العظم. تشير النتائج التي توصلنا إليها إلى أن الغرسات المسامية يمكن أن تعزز نمو العظام وتعزز استقرارها من خلال السماح للعظم بالنمو في سطح الغرسة. بالإضافة إلى ذلك ، يمكن أن تكون طريقة العناصر المحدودة ونظرية الميكانيوستات أدوات مفيدة لتحسين تصميم زراعة الأسنان ومنع الحماية من الإجهاد.

Résumé :

Les implants en titane denses sont devenus un choix populaire pour la chirurgie orthopédique en raison de leur biocompatibilité et de leur résistance à la corrosion. Cependant, ils peuvent provoquer une protection contre les contraintes, ce qui entraîne une perte osseuse autour de l'implant en raison de l'inadéquation entre la rigidité plus élevée de l'implant et la rigidité plus faible de l'os environnant. La protection contre les contraintes (Stress-shielding) est un problème courant dans l'implantologie dentaire. Pour résoudre ce problème, les chercheurs ont développé diverses stratégies, notamment en modifiant les propriétés de surface de

l'implant ou la conception, en utilisant des matériaux avec une rigidité plus faible et en développant une nouvelle conception d'implant tel que l'utilisation de biomatériaux poreux qui peuvent stimuler la croissance et la régénération osseuses autour de l'implant. L'utilisation de la méthode d'éléments finis et de la théorie du mécanostat a été proposée pour mieux comprendre la distribution de contrainte et de déformation dans l'interface implantaire et pour développer des stratégies pour minimiser le stress-shielding. Dans cette étude, un modèle d'éléments finis avec du titane poreux et une faible rigidité a été utilisé pour simuler la distribution des déformations et des contraintes dans l'os et l'implant dans différentes conditions de chargement. La théorie du mécanostat a été appliquée pour prédire le comportement et le remodelage osseux. Cependant, l'utilisation de différentes rigidité implantaire s'est avérée affecter l'intensité de la déformation dans l'os. Nos résultats suggèrent que les implants poreux peuvent favoriser la dérivation des os et améliorer la stabilité de l'implant en permettant à l'os de se développer dans la surface de l'implant. De plus, la méthode des éléments finis et la théorie du mécanostat peuvent être des outils utiles pour optimiser la conception de l'implant dentaire et prévenir le stress-shielding en silico-analyse.

Table of Contents

List of Figures

List of Tables

Abbreviations

με	Microstrain
3D	Three Dimensional
AM	Additive manufacturing
ATZ	Alumina toughened zirconia
BCC	Body-centered cubic
C3D10	10 node tetrahedral elements
CAD	Computer aided design
CAM	Computer-aided manufacturing
CC	Cubic-cross
CFR-PEEK	Carbon-fiber-reinforced polyetheretherketone
CT	Computed Tomography
DICOM	Digital Imaging and Communications in Medicine
E	Young's modulus
FCC	Face-centered cubic
FE	Finite element
FGM	Functionally graded materials

GPa	Gigapascal
HA	Hydroxyapatite
HU	Hounsfield units
L	Length
LSA	Laser surface alloying
Max	Maximum
MIM	Metal injection molding
Min	Minimum
mm	Millimeter
MPa	Megapascal
MRI	Magnetic resonance imaging
N	Newton
NURBS	Non-uniform rational basis spline
Octa	Octahedron
Octa-c	Octahedron-cross
P	Porosity
PEEK	polyetheretherketone

PLA	Polylactic acid
PLGA	poly(lactic-co-glycolic acid)
PLLA	Poly-L-lactic acid
PMMA	Poly(methyl methacrylate)
Po	Pore size
PVDF	Polyvinylidene fluoride
RVE	Representative Volume Element
S	Stimulus
SD	Strut diameter
SLM	Selective laser melting
SLS	Selective laser sintering
STL	Standard stereo-lithography
Ti	Titanium
Ti-6Al-4V	90% titanium, 6% aluminum, 4% vanadium
U	Strain energy density
UMAT	User Material
ZTA	Zirconia Toughened Alumina

α	Alpha
β	Beta
γ	Gamma
δ	Delta
ε	strain tensor
N	Poisson's Ratio
ρ	Rho (bone density)
σ	stress tensor
ψ	Psi
σ_e	Von Mises stress
ε_i	Strain intensity
σ_1, σ_2, σ_3	Principal's stresses
ε_{oct}	Octahedral shear (equivalent) strain

Chapter I Introduction and background

The skeletal system is a complex system contains mainly bones and cartilages, it protects the body's vital organs. There are around 206 bones (excluding teeth) in a human skeleton [1], they occupy between 12% and 15% of the whole-body weight [2]. The bone tissue is multifunctional and biological material. When we talk about skeletal system in the context of biomechanics, we must always mention the interactions between joints, muscles, and bones. Our knowledge of the composition and characteristics of bones allows us to know their potential resistance, mechanical support and protection. **Figure I.1** shows the skeletal elements.

1. Cranial bones (27)
2. Mandible
3. Hyrod
4. Cervical vertebrae (7)
5. Clavicle (2)
6. Scapula (2)
7. Sternum
8. Ribs (24)
9. Humerus (2)
10. Ulna (2)
11. Radius (2)
12. Os coxae (2)
13. Sacrum
14. Coccyx (3-5)
15. Carpals (16)
16. Metacarpals (10)
17. Phalanges (28)
18. Femur (2)
19. Patella (2)
20. Tibia (2)
21. Fibula (2)
22. Tersals (14)
23. Metatarsals (10)
24. Foot phalanges (28)

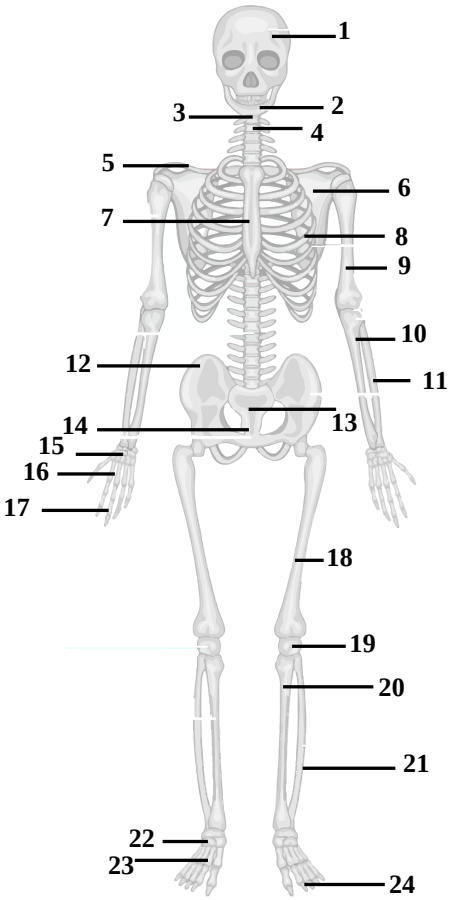

Figure I.1 *The skeletal elements* [3].

I.1 Bones functions

Bone's mechanical functions are by far the most well-known and researched. The function of the bone is to adapt to avoid fractures caused by repetitive loading (dynamic cyclic loading) at

physiological levels. Because of its strength and stiffness, the bone also serves as a form of protection for the body and play a central role in maintaining mineral homeostasis and hematopoiesis [2][4]. Research has shown that bones also perform an important endocrine function [5][6].

I.2 Composition of bones

Bone is composed of an organic matrix, minerals and water. Organic matrix includes bone cells (osteoblasts, osteoclasts, and osteocytes) and materials made by osteoblasts: proteoglycans, glycoproteins and collagen. Minerals contains hydroxyapatite, calcium, phosphate and it make up about 65% of bone's weight, organic matrix about 25%, and 10% is water [7](**Figure I.2**). Bone is the primary calcium depot in the body, it is present in an amount of about 1000 grams and 99% with phosphate in the skeleton [8].

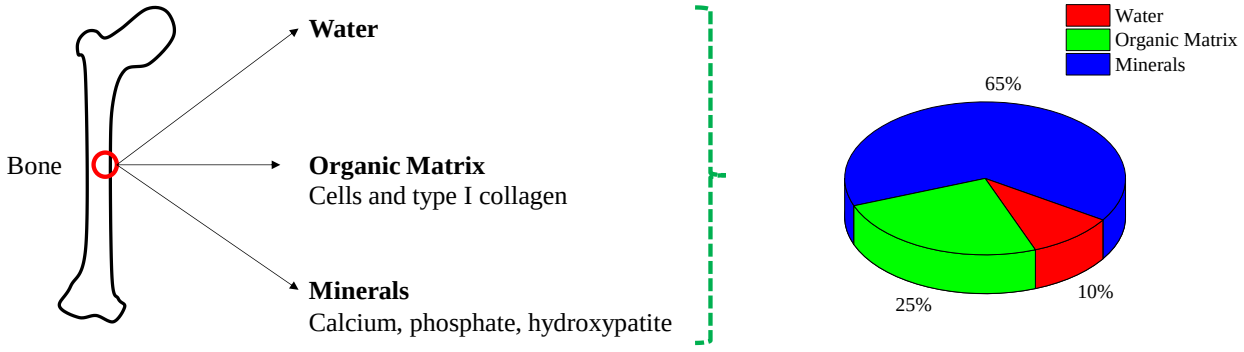

Figure I.2 *The composition of the bone.*

I.3 Bone cells

Bone is living tissue made up of different cell types (osteoblasts and osteoclasts) that either make new bone or destroy old bone, keeping bone homeostasis by a dynamic's equilibrium of cells [3].

I.3.1 Osteoblasts cells

The osteoblasts are secretory cells, responsible for the bone-production cells. They form a protein matrix called osteoid during osteoblastic activity [9]. Osteoblasts cells are small, nucleated and single cells (mono).

I.3.2 Osteoclasts cells

The osteoclasts are large cells as compared to osteoblasts; they are responsible for bone destruction (in bone removable processes). Osteoblasts cells are multinucleated [10].

I.3.3 Osteocytes cells

Osteocytes are created when osteoblasts embed themselves in the bone's mineral matrix and take on characteristics. Osteocytes cells can release proteins to osteoblasts and osteoclasts cells.

I.3.4 Osteogenic cells

Osteogenic cells are cells that have a significant impact on bone growth and healing. These cells, which can be found in the bone marrow, are the forerunners of the more specialized bone cells (osteocytes and osteoblasts).

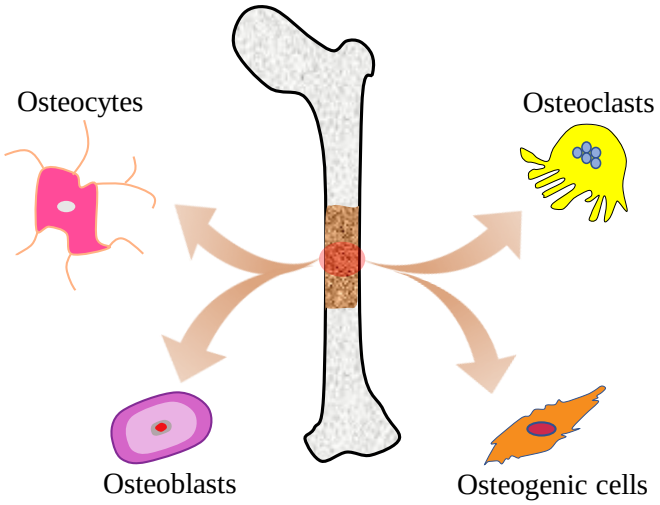

Figure I.3 *bone cells.*

I.4 Bone remodeling, formation and resorption

Bone remodeling (or bone metabolism) is the process of bone renewal and microdamage repair, it performed by groups of cells on a local level. Each cycle of bone remodeling lasts about 200 days [11]. The bone remodeling cycle begins with the activation of osteoclasts cells, which leads to a phase of bone resorption. After bone resorption period, osteoblasts cells go through a phase of bone formation. The bone remodelling is highly regulated, where bone turnover being higher at night and lower during the day. Endocrine hormones like cortisol, oxytocin, and melatonin, as well as local factors like peroxisome proliferator activated receptor Y and clock genes, control this cycle. As a result, the mechanical properties of bone tissue change because of agin, maturation, aging, pathologic processes.

The process by which bones are shaped or reshaped by the independent action of osteoblasts and osteoclasts cells is known as bone modeling.

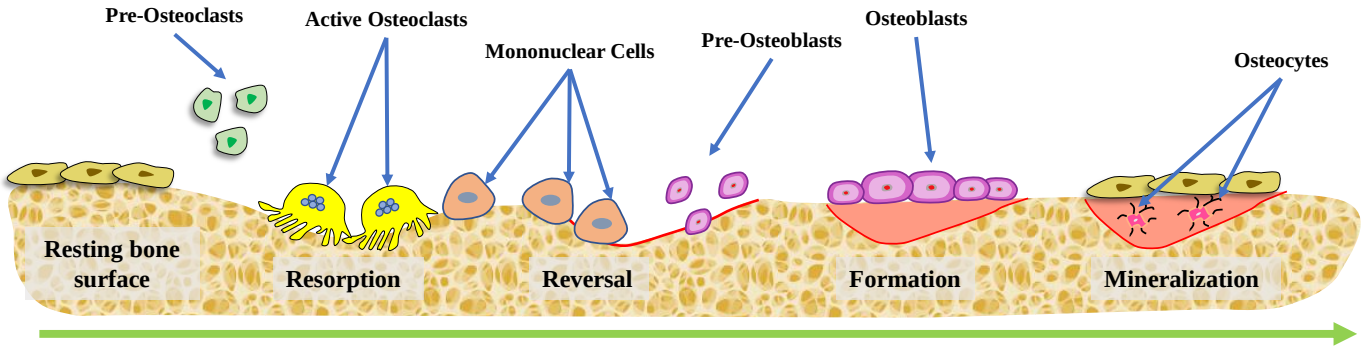

Figure I.4 *The process of bone remodeling.*

I.4.1 Loading and bone remodeling

Bone remodelling and modeling in humans are load-driven, the mechanical loading such as strain is necessary for bone growth maintenance. Without mechanical loading, bone formation decreases and resorption increases (atrophy state). **Figure I.5** show the concept of bone remodeling in an alveolar bone.

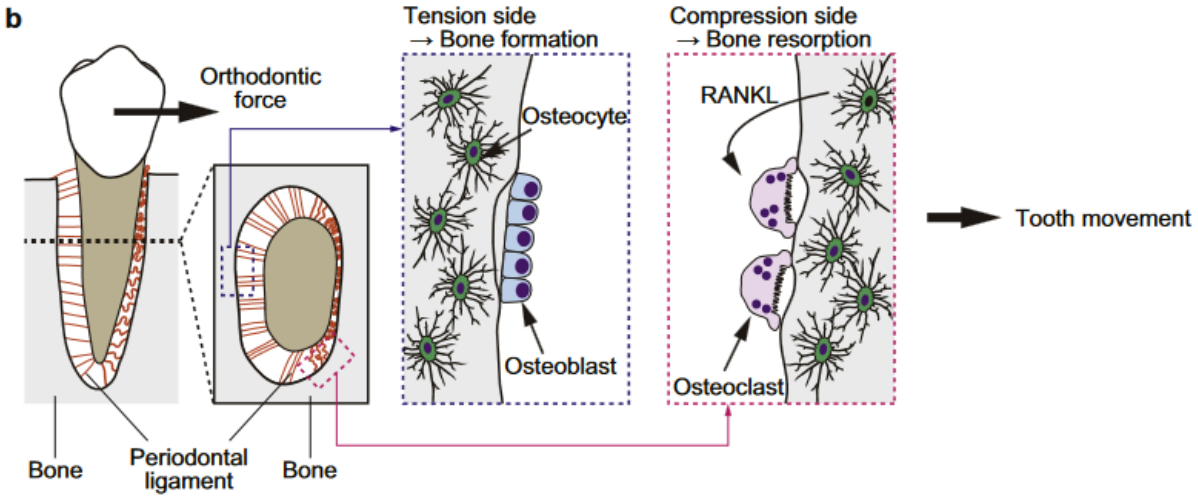

Figure I.5 *Alveolar bone remodeling in orthodontic tooth movement (OTM)* [12].

I.4.2 Wolff's law

Wolff's law [13] state that the bone tissue can adapts in size and shape to external physiological loading under which it is applied, and that bone will remodel itself over time. Wolff stated the relationship between principal stress (or strain) and internal bone tissue.

I.4.3 The mechanostat theory of Frost

Harold Frost proposed the mechanostat theory in the 1980s [14], he described how bone behaves and responds differently under mechanical stimuli based on microstrain levels. The five fundamental principles of the mechanostat theory [15] are illustrated in **Figure I.6.**

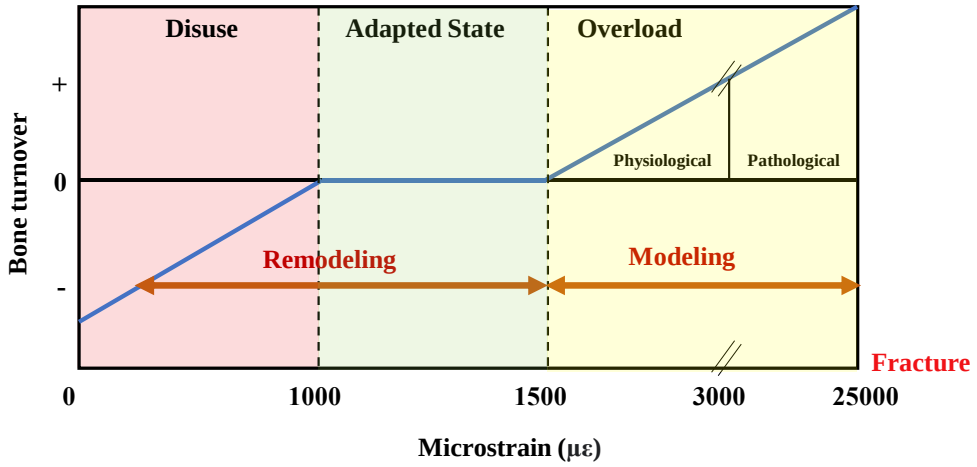

Figure I.6 *The five fundamental principles of the mechanostat theory of Frost.*

I.5 Osteoporosis

Osteoporosis is a bone metabolic disease and the most common bone disorder associated with low bone mass and characterized by bone architectural deterioration, resulting in bone fragility and increasing the risk of fracture [16]. The major cause of osteoporosis is unbalanced bone remodeling, when bone resorption exceeds bone formation. There are primary osteoporosis and secondary osteoporosis. Primary osteoporosis usually occurs in older people (50 years or above), this is often due to decreased estrogen hormones after menopause [17]. Secondary osteoporosis occurs as a result of some medications that cause low bone mineral and it more common in men than in women [18]. There are other bone disorders than osteoporosis, such as Paget's disease, osteosarcoma, osteogenesis imperfecta, and Ricket's disease, which are all distinct from normal bone architecture. **Figure I.7** shows the comparison of normal and osteoporotic bones.

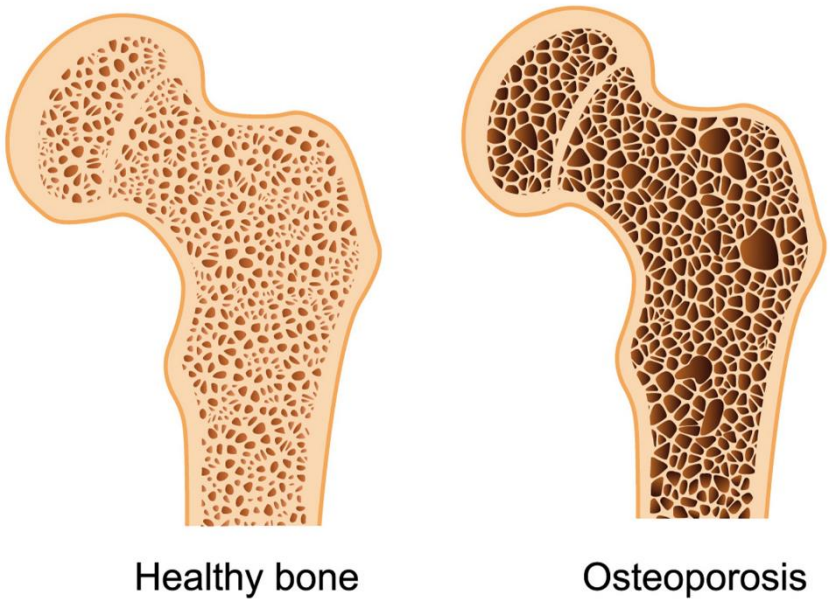

Figure I.7 *Comparison of normal and osteoporotic bones* [19].

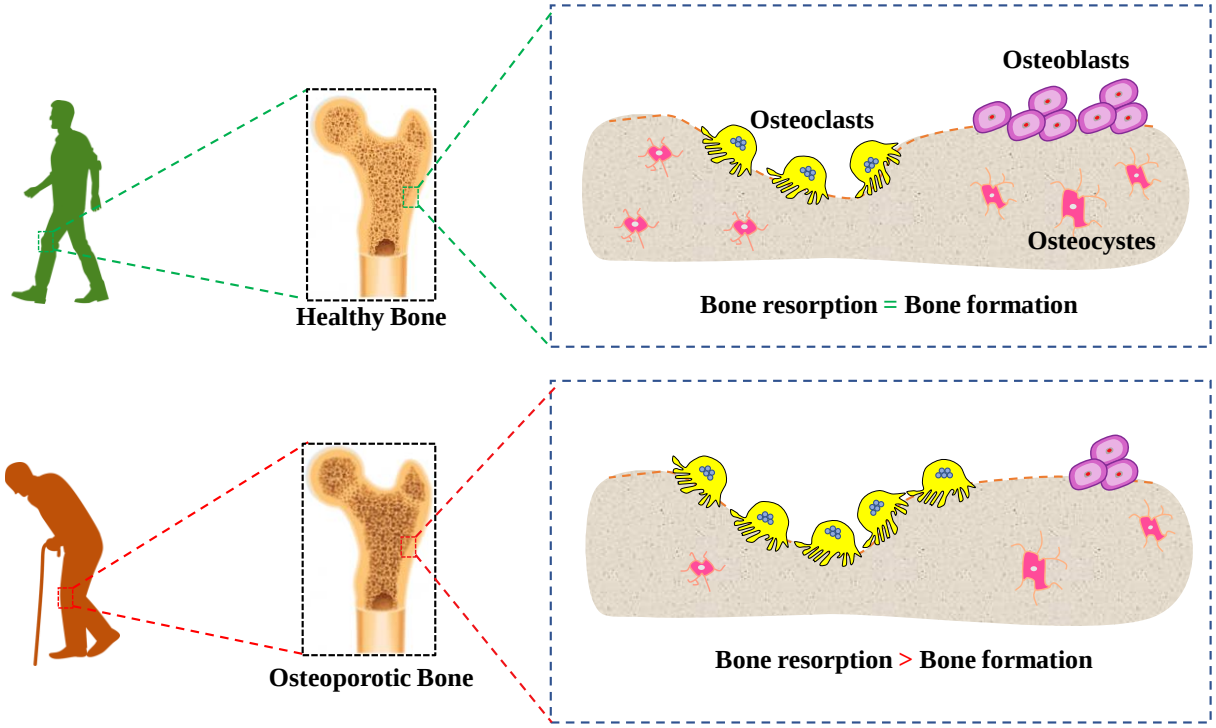

Figure I.8 *bone resorption versus bone formation in health and osteoporotic bones*

I.6 Bones as multiscale material

bone is organized in a hierarchical structure. To better understand this structure, its best to evaluate bone at three levels from nano to macro scales.

I.6.1 The nanoscale structure of bone

At nanoscale, bone is nano biocomposite, it's constituted of type I collagen elastic fibrils that biomineralized with hydroxyapatite crystals. Any disturbance at the level of these molecules may lead to poor bone quality [20] .

I.6.2 The microscale structure of bone

Most bone types display either woven or lamellar tissue at the microscale. The lamellar bone is a type of tissue that can be primary or secondary, and its typically easily identifiable [21]. Around the periosteal and endocortical surfaces, lamellae are structured circumferentially [22]. **Figure I.9** show the woven and lamellar bones.

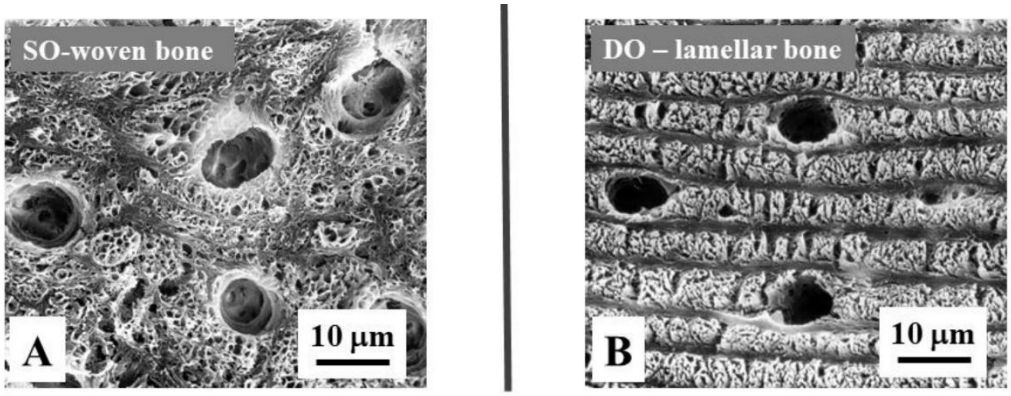

Figure I.9 *The woven and lamellar bones at microscale level* [23].

I.6.3 The macroscale structure of bone

Bones are classified at the macroscopic level into cortical bone (compact bone) and cancellous bone (trabecular bone because it's made up of trabecular struts), each with its own functions and characteristics.

I.6.3.1 Cortical (Compact) bone

Cortical bone is the most solid and dense tissue, it represents around 80 % of the total skeleton [24]. Cortical bone encapsulates trabecular bone, it's structurally well-organized, densely packed, stiffer, and texturally smooth [25]. It can withstand higher stresses.

I.6.3.2 Cancellous (trabecular) bone

Cancellous bone is also called spongy bone or trabecular bone, its covered by cortical bone. It's porous composite material which has the texture of a meshwork of bone (trabeculae) with many interconnected gaps that contain red bone marrow, this meshwork allows it to store a lot of energy of bone marrow imparted by loading impacts [25]. **Figure I.10** show the hierarchical structure of bone.

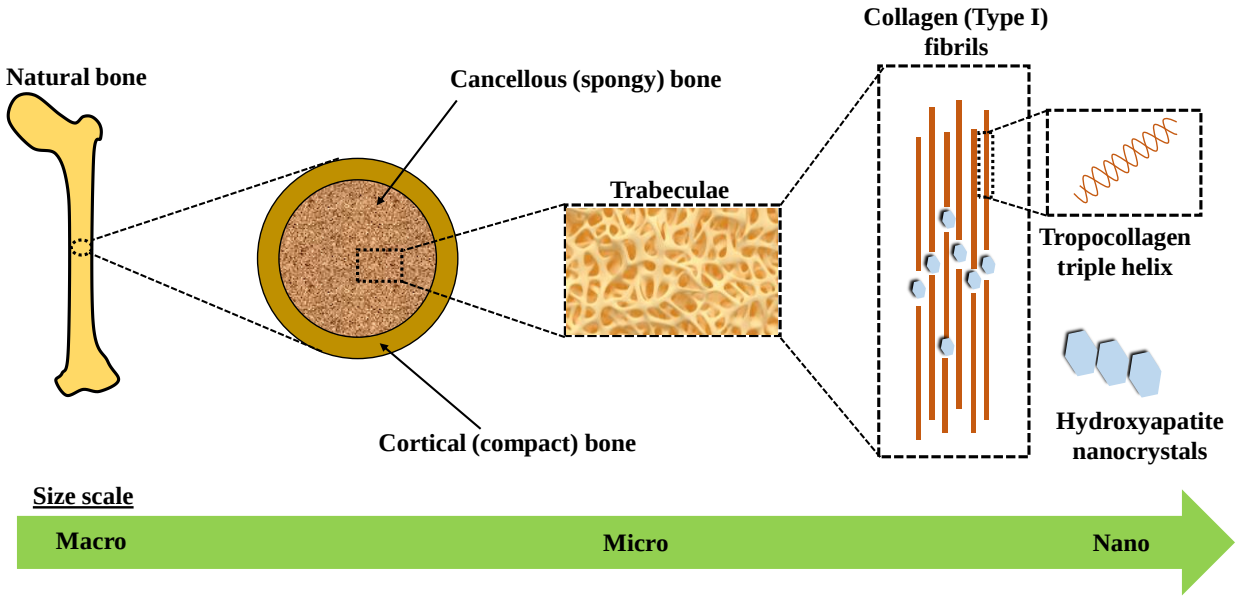

Figure I.10 *The hierarchical structure of bone* [26].

I.7 Mechanical properties of bone tissue

Mechanical testing and methods have been a direct way to assess the mechanical behavior of bone tissue, these methods based on the fundamental principles of material strength (mechanics of materials), continuum mechanics and fracture mechanics.

When bone tissue is subjected to external forces, the response of the tissue depends on a number of factors, such as the type of loading (tensile, compression, shear, bending or combinations), the nature of the loading (loading continuous monotonic, cyclic), and loading magnitude. Mechanical tests quantify stresses, displacements, and deformations, which are fundamental variables that explain bone characteristics' and have been examined at various length scales using a variety of methodologies.

I.7.1 Elasticity

Based on linear theory of elasticity, the elastic behavior characterizes the reversible deformation, i.e. the initial dimensions of the sample can be returned after removing the applied load. It can be mathematically described by the generalized Hooke's law.

The bone tissue is an exception, it doesn't obey Hook's law because its bio-composite material and the relation between stress and strain is nonlinear. Therefore, the material behavior of bone tissue (cortical and cancellous bones) is anisotropic. Anisotropy property means different properties in different directions. Several studies have evaluated the orthogonal or anisotropic mechanical properties of bone tissue [27][28].

I.7.2 Cortical bone

The longitudinal elastic modulus of cortical bone was found to be greater than the transverse elastic modulus, thus, cortical bone can be considered as a transversely isotropic material [27][29]. **Figure I.11** show the stress-strain curve for bovine cortical bone. The mechanical characteristics of cortical bone span a wide range of values influenced by a variety of factors including age, gender, animal species dissimilarity, and testing methods used. For example, the stress-strain curves of bones with and without osteoporosis under tensile testing have a different pattern, as shown in **Figure I.11** The mechanical property parameters of the two stress–strain curves of **Figure I.12** are listed in **Table I.1**. Moreover, there is a lot of data that varies from one study to another.

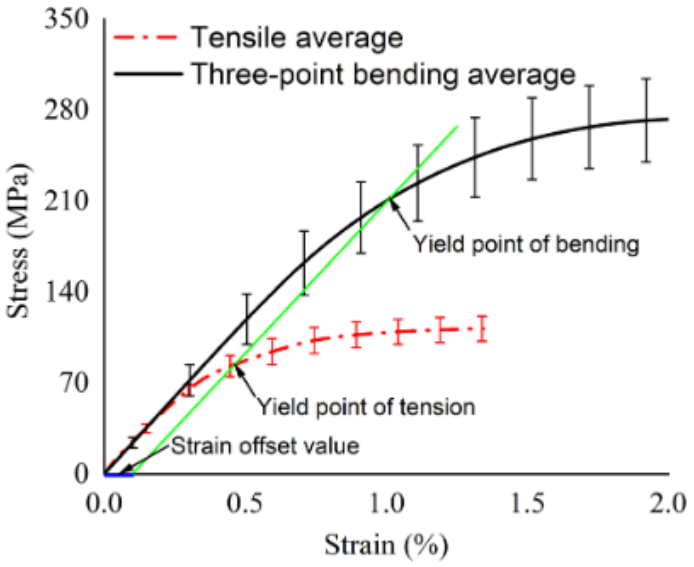

Figure I.11 *Stress–strain curves for cortical bone tested along the longitudinal direction* [30].

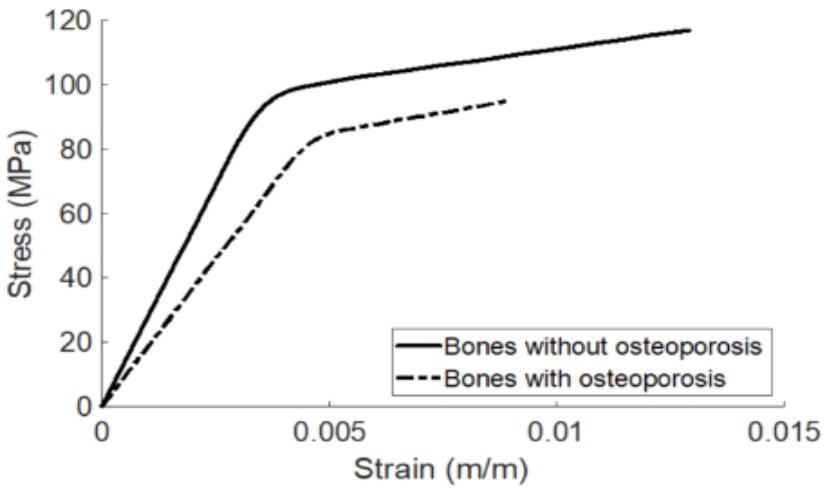

Figure I.12 *The stress–strain curves of bones with and without osteoporosis* [31].

Cortical bone's mechanical characteristics vary with strain rate ($\dot{\varepsilon}$). In general, stiffness and strength increase as the strain rate increases .This is a bone characteristic. It's a viscoelastic material. Furthermore, studies showed that the ultimate strength is more sensitive to strain rate than elastic modulus [32]. The Young's modulus is relatively constant, as shown in **Figure I.13**.

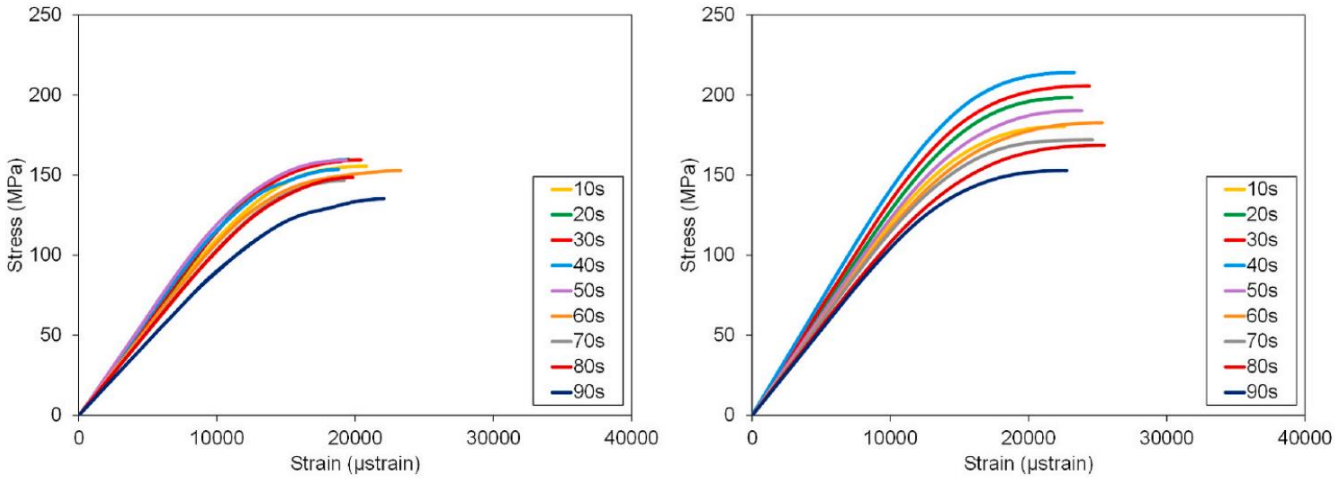

Figure I.13 *Stress-strain curves of rib bone for each decade at 0.005 strain/s (left) and 0.5 strain/s (right) [32].*

Table I.1 Mechanical properties of normal and osteoporotic bones [31].

Name of the Mechanical Property Parameter	Osteoporotic bone	Normal bone (without osteoporosis)
Range of the elastic region (in strain) (m/m)	0–0.0063	0–0.0043
Range of the plastic region (in strain) (m/m)	0.0063–0.0089	0.0043–0.0129
Proportional limit (in stress) (MPa)	77.0934	80.3718
Elastic limit (in stress) (MPa)	88.3528	98.6828
Failure strength (in stress) (MPa)	94.9280	116.9657
Brittleness coefficient (Dimensionless)	0.7079	0.3333
Modulus of resilience (MJ/m3)	0.3394	0.2450
Modulus of toughness (MJ/m3)	0.5778	1.1751
Modulus of elasticity (MPa)	18283.2314	27544.2425
Tangent modulus (MPa)	2490.2230	2118.0671
Strain hardening parameter (MPa)	2882.8784	2294.5076

I.7.3 Cancellous bone

In cancellous bone, the strength is greater in compression rather than in tension and lowest in shear, just like in cortical bone. The linear elastic region in cancellous bone is not clear because the nonlinearity is present at low stress levels [9]. Several studies have found that the Young's modulus ranges between 0.8 and 16.9 gigapascals [33], for many considerations, such as measuring methods, mechanical testing (bending, tensile, compression), ultrasonic methods, nanoindentation, finite element method. The study on samples from different anatomical sites also gives different results. For example, it has been reported that the Young’s modulus varies between the mandible, tibia, vertebra, and femur [34][35].

I.7.3.1 viscoelasticity

Bone has a viscoelastic behavior same as cortical bone, due to many factors, including the properties of collagen and movements of fluids within the pores, as well as the organization of hierarchical tissues. Both cortical and cancellous bones exhibit creep and stress relaxation, phase lag between stress and strain during oscillatory loading [36]. Both exhibit strain rate sensitivity when subjected to loading. Bone viscoelasticity has been evaluated beyond the elastic limit by many researchers [37][38]. Aging and diseases can alter the viscoelastic behavior of bone, which can cause fragility and damage [39].

I.7.3.2 Bone mass and density

Bone mineral density (BMD) is the amount of calcium in a given volume of bone material. This measurement makes it possible in particular to determine the mechanical behavior, it is measured by X-ray diffraction. Since the density influences the stiffness considerably, this means that the Young's modulus varies according to the density. It’s very important to test bone mineral density of those who have osteoporosis. **Figure I.14** show an example of the relationship between bone density and Young’s modulus. Many scientific research have worked this relationship.

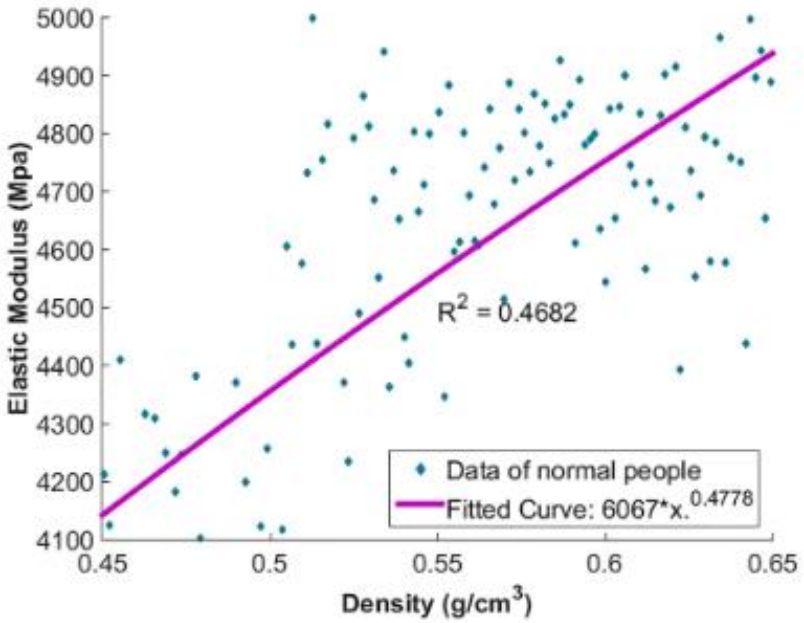

Figure I.14 *Relationship between the density and elastic modulus* [40]**.**

I.8 The masticatory system

The masticatory system is a complicated functional unit associated with teeth, bones (the mandible or lower jaw, the maxilla or upper jaw), temporomandibular joint (TMJ), and the muscles directly or indirectly involved in mastication (Including lips and tongue) [41]. The mastication system is the series of actions from swallowing to ingestion. Understanding the biomechanical functions of the jaw is very important in clinical dentistry. Hence, dentists must know how mastication normally occurs. Today, these functions have become clear and have a great importance in prosthodontics, orthodontics, dentofacial orthopaedics, periodontics, Oral and maxillofacial pathology, and surgery.

I.8.1 The upper jaw

The upper jaw also knows as maxilla, its facial fixed bone which contains the maxillary sinus and divides the nasal and oral canals. The maxilla holds the upper teeth and supports the nose.

I.8.2 The lower jaw

The lower jaw also knows as mandible, it's the largest bone in the human skull, It helps with chewing, maintains the position of the lower teeth, and defines the lower jawline. The mandible is inferior to the maxilla and is composed of a body, ramus, condyloid (mandibular condyle) and coronoid process. **Figure I.15** depicts a human's lower jaw.

I.8.3 The temporomandibular joint

The temporomandibular joint is formed by the condyloid process and the mandibular fossa the temporal bone.

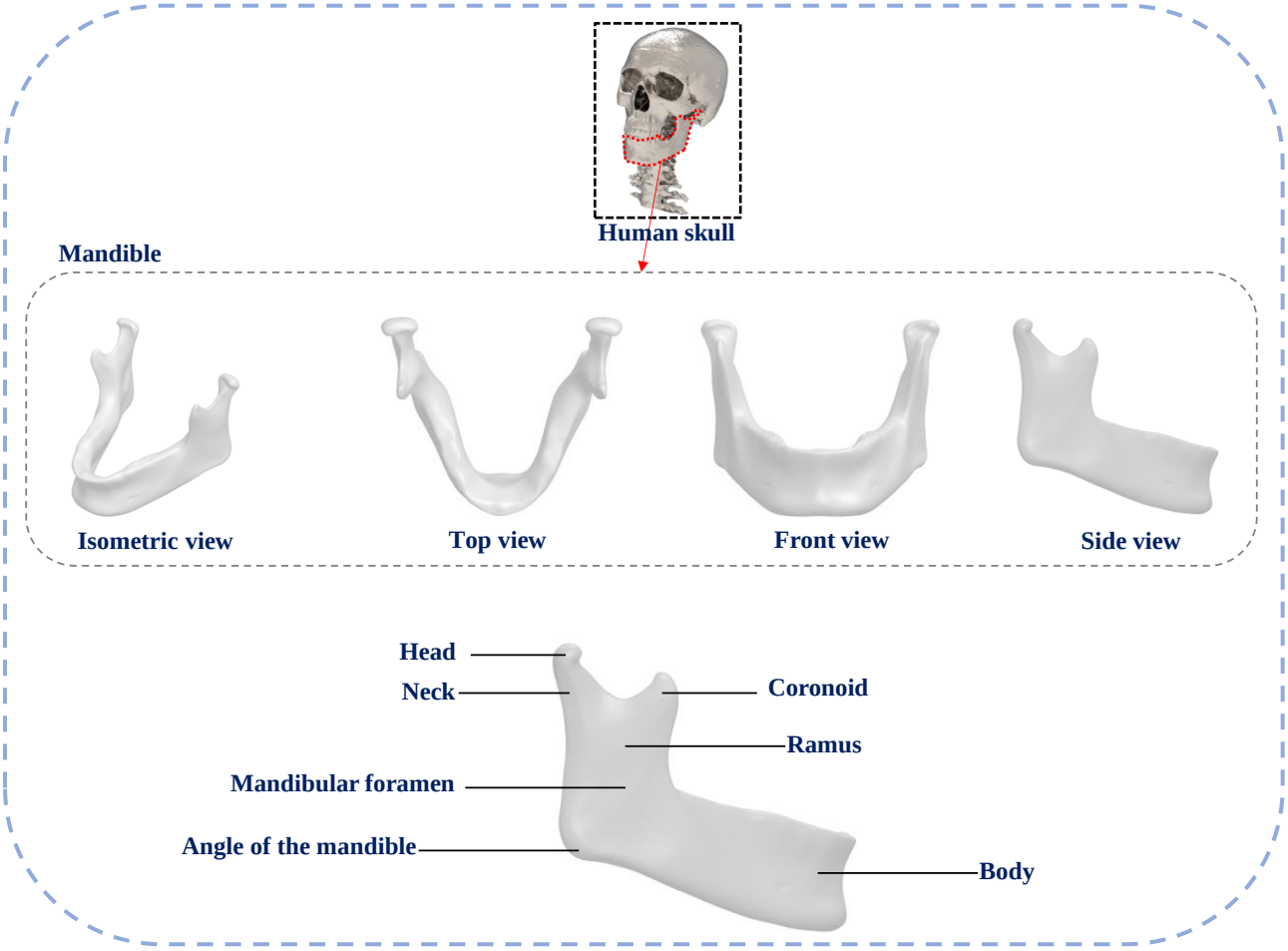

Figure I.15 *The lower jaw.*

I.8.4 Chewing physiology

Mastication is the very complex mechanical and rhythmic act during which, the food is cut, crushed then ground by a synergistic work of the teeth, lips, cheeks and tongue, under the action of saliva. Many systems are involved in chewing including teeth, tongue and muscles. Teeth for cutting, tearing and crushing. The tongue plays a part in the mastication system as well; it shifts food from right to left so that the molars can grind it. The most crucial muscles for mastication function are the temporal (anterior and posterior), masseter (superficial and deep), medial pterygoid, lateral pterygoid (superior and inferior), and digastric muscles. The masticatory muscles are depicted in **Figure I.16**.

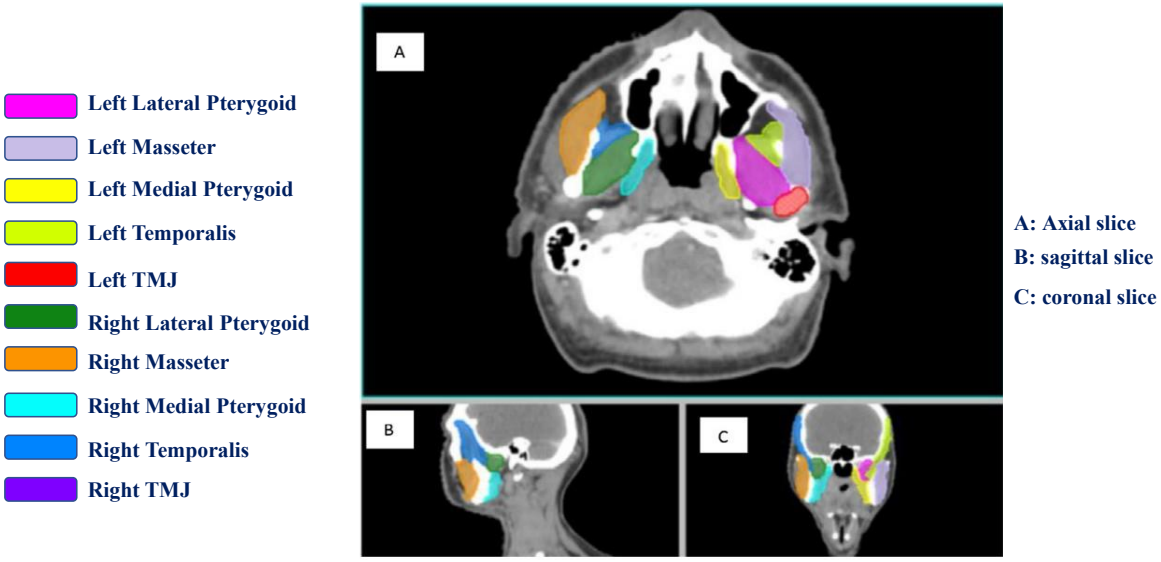

Figure I.16 *Muscles involved in mastication* [42].

Chewing force is usually measured using strain gauges or with a gnathodynamometer, which is a dental medical instrument. An Italian professor used it for the first time in 1681 [43]. A human's biting force is approximately 500 N on average [44][45]. Numerous studies have discovered that the maximal voluntary biting force (MVBF) is a reliable indication of masticatory function [46][47][48].

I.9 Age-related tooth loss

Teeth are important for chewing food, speaking, communicating socially, loosing these essential structures may have a negative effect on people's quality life. In general, tooth loss appears to be linked with older age. Many previous studies [49][50] have evaluated the risk factors of tooth loss, dental caries and periodontal disease are two main causes of tooth loss. **Figure I.17** show the bone resorption in mandible bone because of tooth loss.

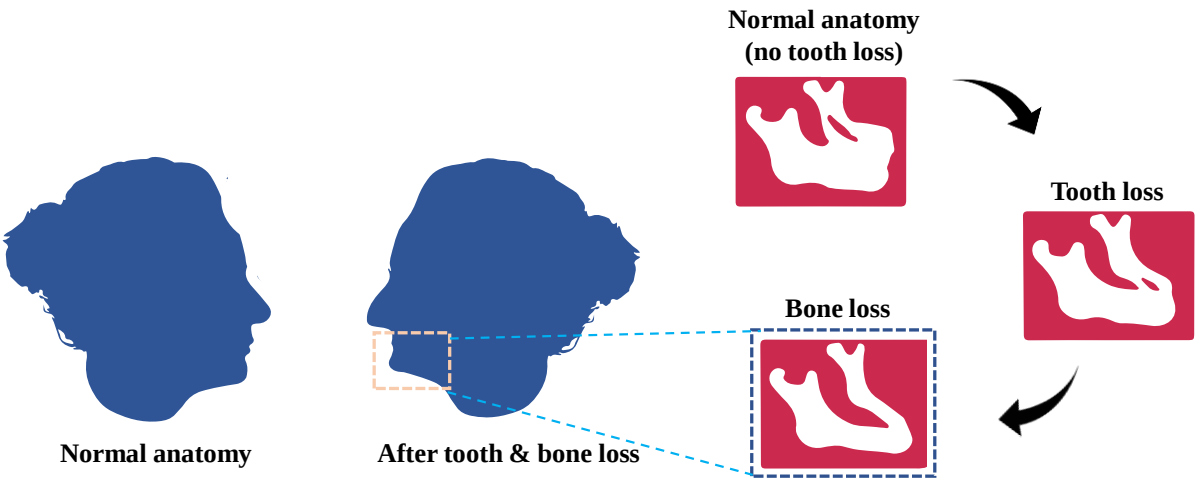

Figure I.17 *The anatomy of mandible bone due to the tooth loss*

I.10 Edentulous patient complications

Edentulism, often known as tooth lessness, is the absence of teeth (complete tooth loss). The World Health Organization identified edentulism as a significant global public health problem that has a significant impact on both oral and general health status [51]. Additionally, edentulous patient have a higher chance of developing several systemic diseases such as chronic kidney disease ..etc. Therefore, researchers in the field of oral health care are working to prevent tooth loss by promoting oral health, or even by replacing missing teeth with various prosthodontic procedures.

I.11 Removable Partial Dentures

Patients with missing tooth can be treated with different types of prostheses. Removable partial dentures are common option of restoration for partial dentition. It is commonly utilized in clinical practurce. Kennedy (1925) divided removable partial dentures into four categories [52] based on where the edentulous space was in patients with tooth loss. The Kennedy categorization of removable partial dentures is shown in **Figure I.18**.

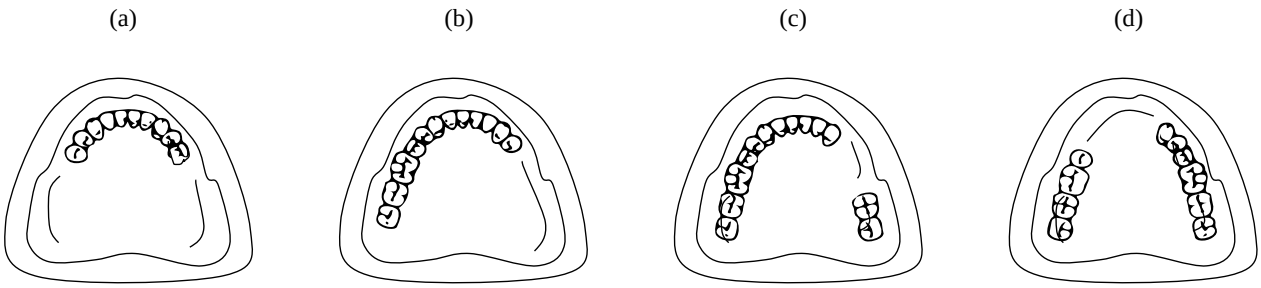

Figure I.18 *Kennedy classification of removable partial dentures.*

(a) Class I: Bilaterally located edentulous spaces, posterior to natural teeth.

(b): Class II: A unilateral edentulous space located posterior to natural teeth.

(c): Class III: A unilateral edentulous space with natural teeth remaining both anterior and posterior to it.

(d): Class IV: A single, but bilateral (crossing the midline) edentulous space located anterior to the remaining natural teeth.

I.12 Conventional Denture Prostheses

Conventional denture prostheses are removable prostheses that rehabilitate the whole dentition . Partial and complete edentulism can treated with conventional dental prostheses. Nowdays, these prostheses are well fabricated due to the introduction of CAD/CAM (Computer-aided

design/computer-aided manufacturing) technology in dentistry [53], from data acquisition to fabrication (**Figure I.19**).

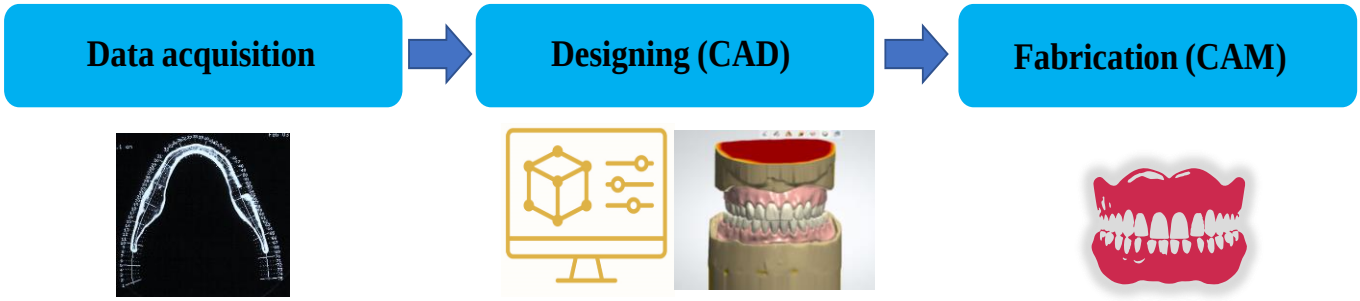

Figure I.19 *Main process for denture prostheses fabrication.*

I.13 Implant dentistry

Implant dentistry is a branch of general dentistry, concerned with replacing teeth with prosthetics (implants), as well as oral surgery. The practice of modern implant dentistry has developed throughout years, especially since osseointegration was discovered by Branemark [54]. Nowadays, advancements in digital dentistry, accurate and precise diagnostic tools, such as three-dimensional imaging, and proper treatment planning, which is essential to any clinical process, have all been made possible by new understanding to provide the best treatment outcomes. The demand for implant therapy has increased from the public for aesthetic reasons,

I.13.1 Implant-Supported Prostheses

A key element of contemporary prosthodontics is the dental implant, as it has replaced removable prostheses. It was proved that any patient wearing an adaptable denture may benefit from implant prosthodontics as a viable treatment option, provided the requisite systemic and local requirements for implant treatment can be satisfied. The availability of implants offers new approaches to solve problems caused by missing teeth.

I.13.2 Structure of the dental implant system

The components of a dental implant include the crest module, apex, body, abutment, crown, and screw. The crest module is the top part of the implant, and it sits above the gum line. The apex is the bottom part of the implant, and it's inserted into the jawbone. The body of the implant connects the crest module and the apex. The abutment is a small connector that attaches to the implant body, and it supports the crown. The crown is the visible part of the implant, and it resembles a natural tooth. The screw is used to secure the abutment to the implant body, and it has threads that match the pitch, width, and depth of the implant. All of these components work together to create a stable and durable replacement tooth that looks and functions like a natural tooth. The components of dental implants are shown in **Figure I.20**.

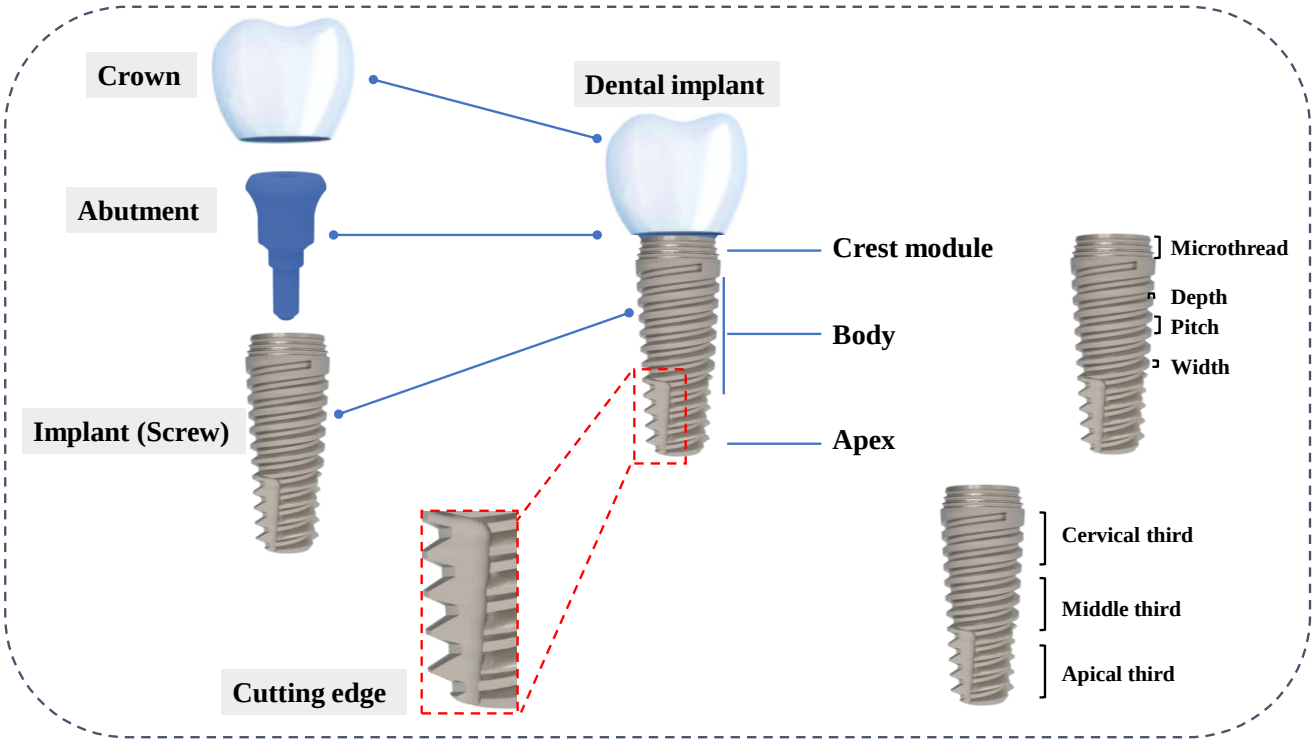

Figure I.20 *Structure of dental implant system.*

I.13.3 Osseoinegration

Osteocytes grow directly into titanium implants, resulting in complete integration of the foreign body into the bone. This phenomena called osseointegration (the term: “functional ankylosis” is also used), it was discovered by Branemark [54]. Due to this scientific fact, dental implants as well orthopaedic implants have been developed with great clinical performance. Studies have shown osseointegration occurs through a uniform and complex process that can take several months. Stages of the osseointegration process are determined biologically [55]. After implant placement, comes the first stage which is the formation of woven bone around the implant (inert object), it can rapidly form a trabecular scaffold and vascular network (compared to trabacular bone, newly woven bone is noticeably darker). Stage 2 involves reinforcement of the primary spongiosa, with deposition of parallel-fibered and lamellar bone, this stage consists of adaptation of bone mass to load. Stage 3, beginning around 12 weeks, consists of bone modeling and remodeling (adaptation of bone structure).

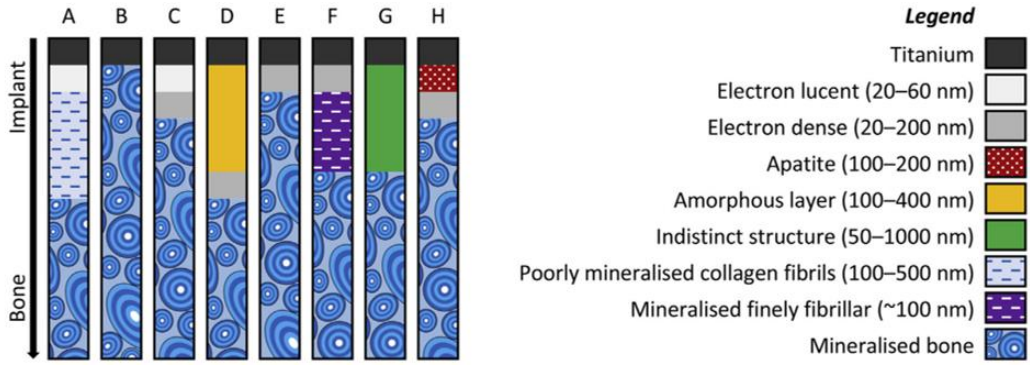

Figure I.21 *Different ultrastructural arrangements between bone and implant [55].*

There are plenty of biomaterials that are used in implantology. Titanium and titanium alloy (Ti6A14V) have been the most widely used of these materials. **Figure I.21** describes the ultrastructural contact between implant and bone from different experimental and clinical conditions (literature). The implant surface is surrounded with osteonal/lamellar bone, osteoclasts

(OC) and osteocytes (OT) are also welded directly with implant, as illustrated in **Figure I.22** Moreover, at the interface between the implant surface and bone, complex physical and chemical reactions occur at multiscale. Many cells are involved in the process of osseointegration (**Figure I.23**)

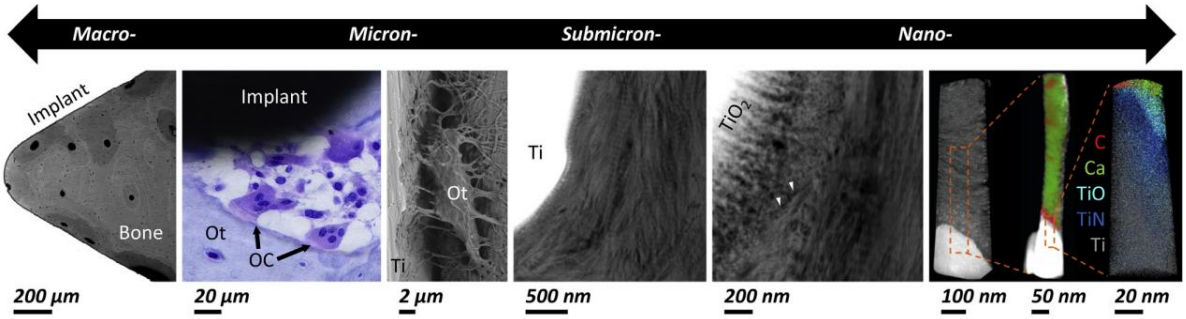

Figure I.22 *Bone-Ti implant interface [55].*

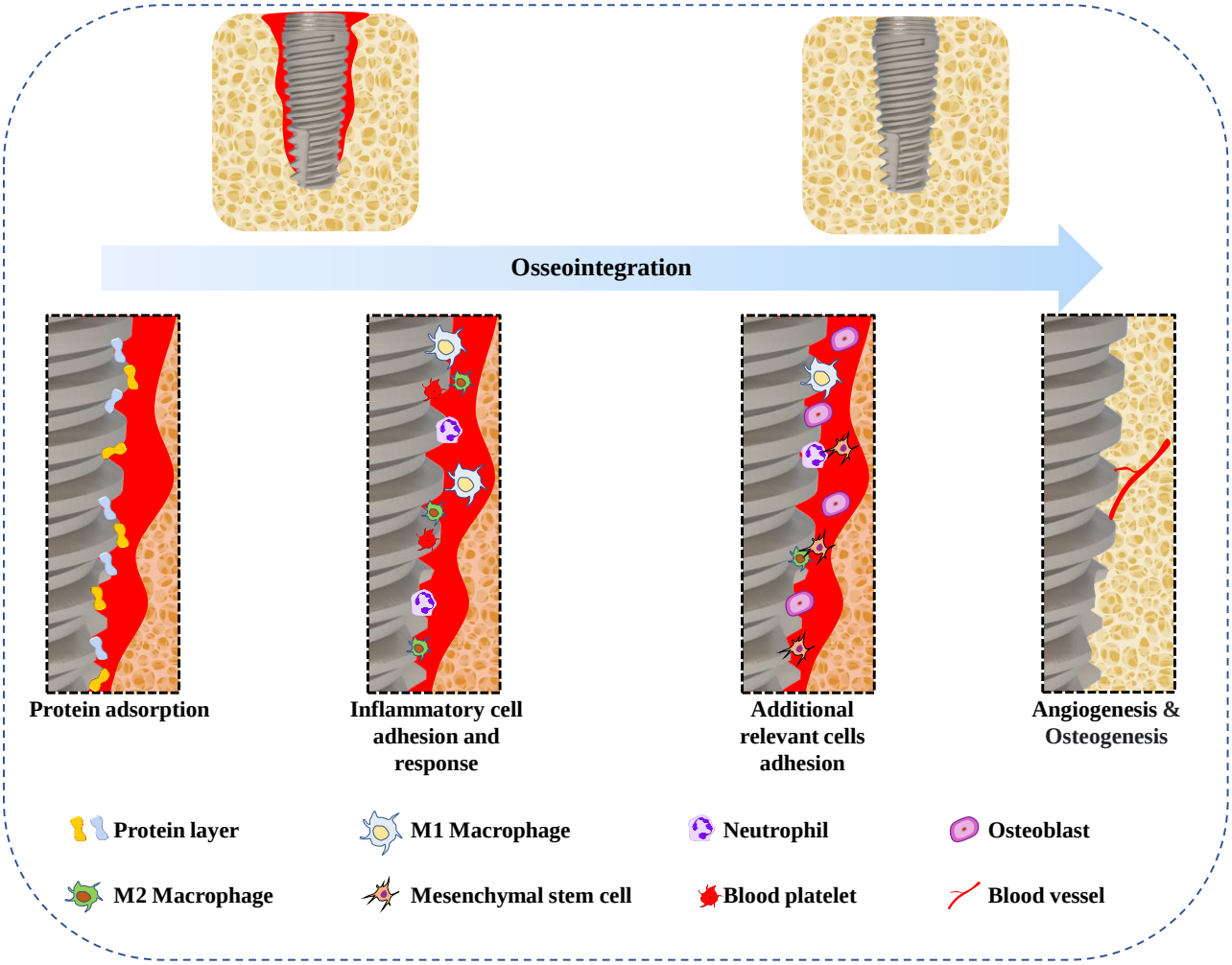

Figure I.23 *Process of osseointegration.*

I.14 Implant stability

I.14.1 Primary stability

Primary stability is defined as the mechanical anchorage immediately after implant insertion. It is obtained by surface of contact between the implant and bone. It is crucial for the development of osseointegration [56] and helps determine the implant's prognosis, which in turn influences the selection of the best loading protocol. The quality and quantity of the contact area between the implant and the bone provide primary stability. The contact area can be measured in percentage. Several factors related to the bone (bone quality and quantity) and implant type (implant length, diameter, surface type, and macro design) influence the bone implant contact (BIC). Low-density

trabecular bone (more porous) has a lower of BIC and can lead to uneven and concentrated force distribution from implant to bone which can result to excessive microstrain, implant mobility and failure. Overall, higher bone density has a higher BIC, and consequently, the greater the bone density, the greater the primary stability. Primary stability of implants is considered a prognostic factor for osseointegration and an indication of bone quality [57]. The implants macro-design might represent a key factor on primary stability. A study has showed that implants with a more aggressive thread distance could increase primary stability [58].

I.14.2 Secondary stability

Secondary stability refers to the formation of new bone around the implant. After implant placement, the bone surrounding the newly placed implant is reorganized, and during this process, primary stability is gradually replaced by secondary stability. Secondary stability is given by the level of osseointegration. This refers to the concept of an anatomical and functional junction formed directly between the living bone and implant without the presence of fibrous matter. **Figure I.24** shows the primary and secondary stability in function of time.

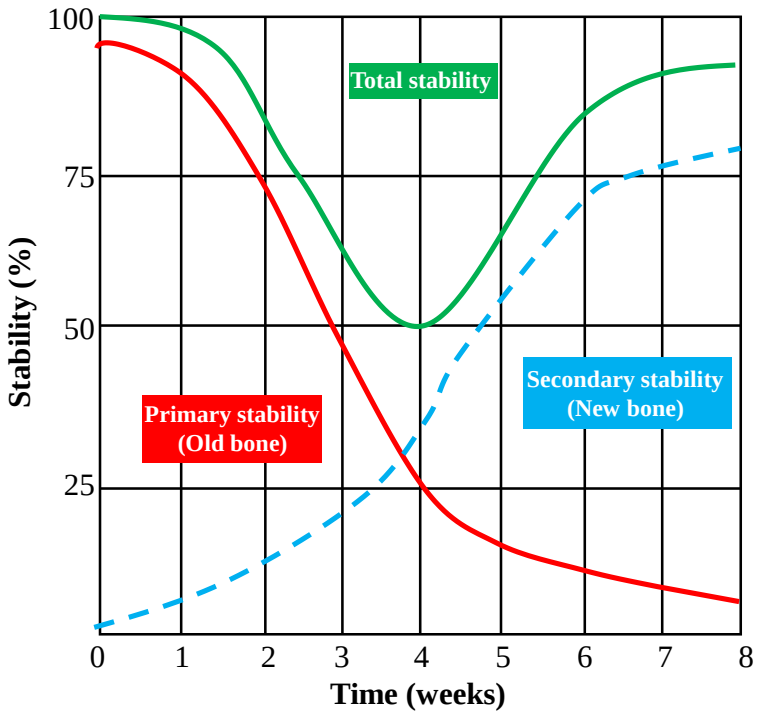

Figure I.24 *Primary and secondary stability in function of time.*

In the trabecular bone, secondary stability begins with the formation of a blood clot, filling the gap between the implant and remaining bone. The fibrinogen in the blood attaches to the implant, allowing for preferential adsorption of platelets to the implant surface, and their immediate degranulation, releasing factors attracting undifferentiated cells to the site.

Various techniques have been used to assess implant stability during osseointegration and at the time of insertion. Resonance frequency analysis (RFA), developed by Meredith et al. in 1996 [59], is a non-invasive technique for examining the stability and stiffness of the implant-bone interface. The implant stability quotient (ISQ), which runs from 1 (lowest implant stability) to 100 (best implant stability), is used to quantify implant stability. Successful implantation has reported ISQ levels ranging from 57 to 82 [60]. However, to achieve adequate implant stability, ISQ values during implant insertion should be lower than 60 [61]. **Figure I.25** illustrates the surgical procedure to measure the implant stability.

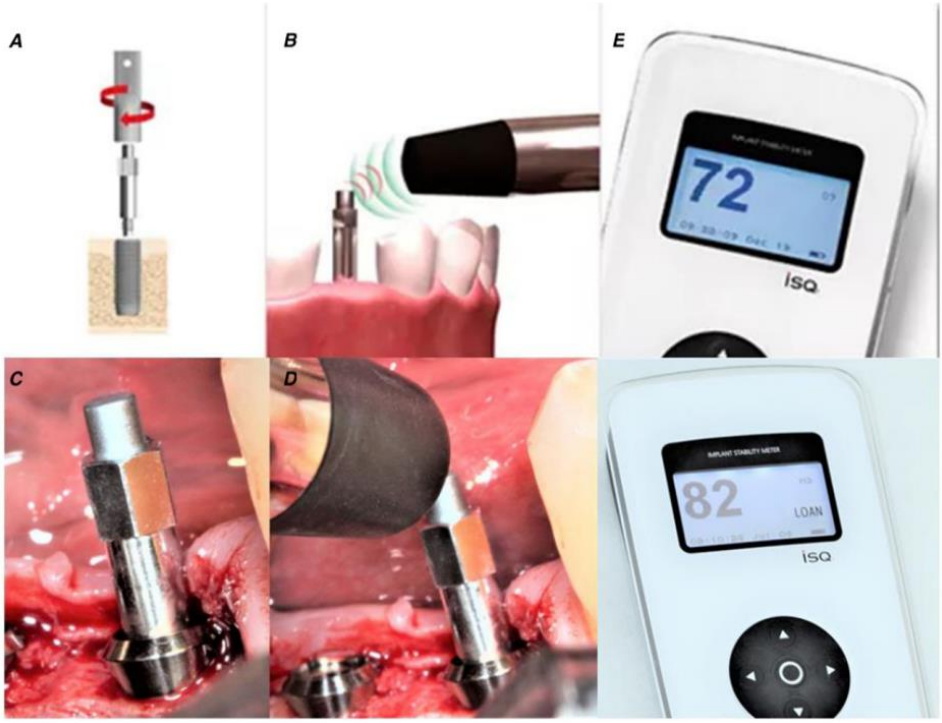

Figure I.25 *The resonance frequency analysis (RFA)* [56]*: (A) insertion of the measurement adapter, (b) resonance frequencies measured with the device, (c) implant with adapter in situ, (D) RFA-measurement from the vestibular side, and (E) implant stability meter with implant stability quotient (ISQ) values for the evaluation*

I.15 Mandibular bone Quality

Several types of mandibular bone and several classifications according to its densities and compositions have been recognized and make it possible to determine their quality and quantity. The crestal cortical bone thickness and the inner cancellous bone density determine the amount and quality of the host bone.

The structure of the mandibular bone is classified by four qualities according to Lekholm and Zarb (1985, [62]) as shown in the **Figure I.26**.

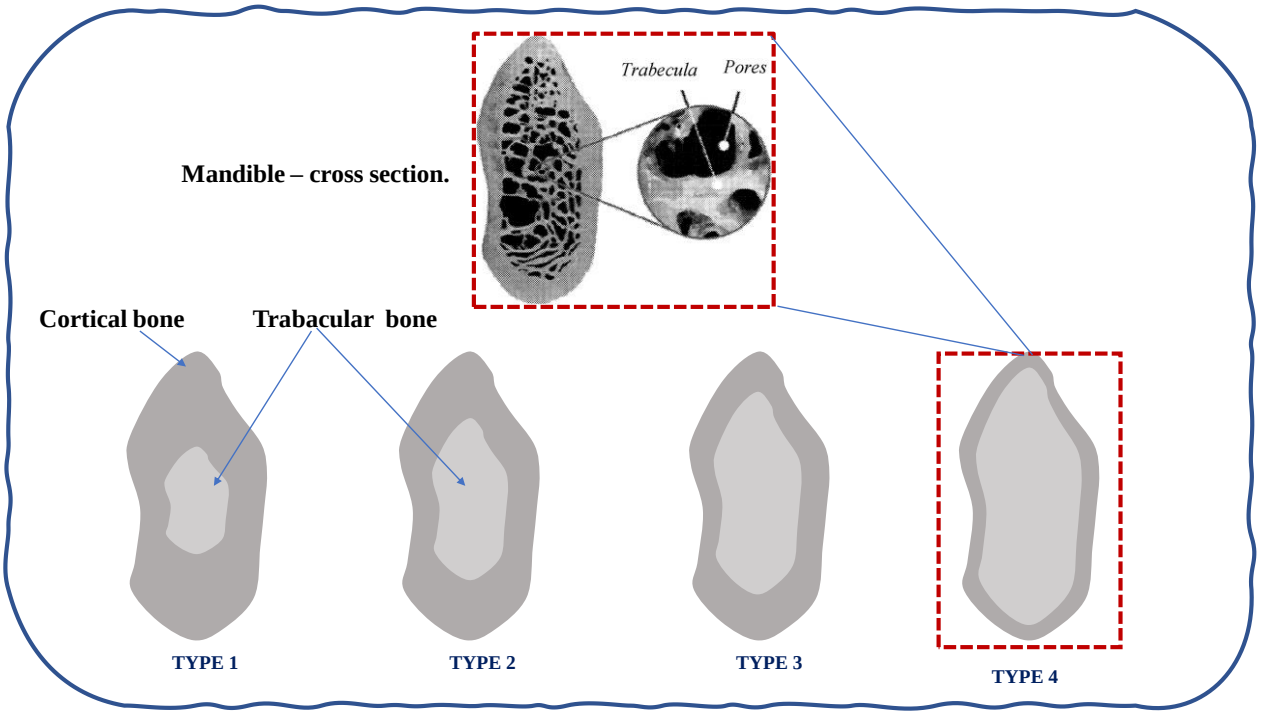

Figure I.26 *Classification of Lekholm and Zarb.*

The remaining alveolar bone was divided into four types:

Type 1: A homogeneous and compact tissue essentially composes the bone.

Type 2: A core of dense cancellous bone surrounded by a thick layer of compact bone.

Type 3: A core of dense cancellous bone surrounded by a thin layer of cortical bone.

Type 4: A core of low-density cancellous bone surrounded by a very thin layer of cortical bone.

Subsequently, Mish [63] proposed a classification of bone density based on clinical drilling. He measured bone density in Houndsfield units (HU) for different mandibular sites, **Table *I.2*** shows the five types of densities (D1-D5) identified by Mish in different jaw positions.

Table I.2 Bone density classification by Misch.

Bone density	Description	Location
Density 1	Dense cortical bone	Anterior mandible
Density 2	Porous cortical bone and dense trabecular bone	Anterior and posterior mandible Anterior maxilla

Density 3	Thin and porous cortical bone and thin trabecular bone	Anterior and posterior maxilla
Density 4	Thin trabecular bone	posterior maxilla
Density 5	Non-mineralized bone	-

To measure bone density, computed tomography (CT) has been utilized frequently. CT axial images have 260,000 pixels, each pixel in a CT image has a certain HU level which is associated with the density of the bone tissue. **Table *I.3*** shows the classification of bone density by Misch and Lekholm and Zarb based on computed tomography scan.

Table I.3 Classification of bone density by Misch, and Lekholm and Zarb based on Hounsfield units by CT scan.

Mish Bone Density	**Bone density range (HU)**	**Lekholm and Zarb Bone Quality**	**Bone density range (HU)**
D1	>1250 HU	**Q1**	>850 HU
D2	850–1250 HU	**Q2**	500–850 HU
D3	350–850 HU	**Q3**	0-500 HU
D4	150–350 HU	**Q4**	<0
D5	<150 HU	**-**	-

I.16 Marginal Bone loss

Marginal bone loss has been one of the criteria to define implant success (the most referred definitions of implant success are permissive of a 1 mm marginal bone loss (MBL) for the first year and an annual rate of 0.2 mm in next years). Early bone loss, considered to be mainly physiological, happens rapidly during the early healing phase from implant installation to one year after loading [58]. [59]. Early bone loss may cause periimplantitis, which is frequently thought of as the initial stage before progressive bone loss, it can be be influenced by many factors such as implant position, occlusal loading, implant-abutment connection type, plaque accumulation,

implant macrodesign, neck design, smoking, bone quality and quantity, abutment height [59]. According to a systematic review [64], osseointegrated dental implants with internal connections exhibited lower marginal bone loss than implants with external connections. Another review [65] indicated that cement-retained, fixed implant-supported restorations showed less marginal bone loss than screw-retained. On the other hands, a meta-analysis showed that micro thread design in the implant neck can reduce the amount of MBL (Marginal bone loss) [66].

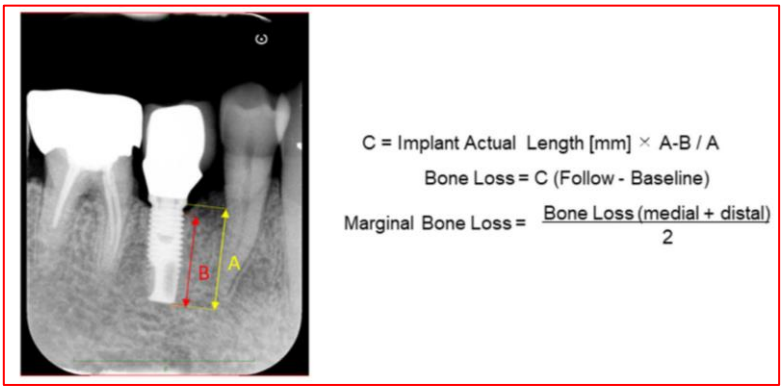

Figure I.27 *The measurement of marginal bone loss (MBL) based on radiography* [67].

Figure I.27 shows the measurement of marginal bone loss (MBL) on dental radiography. The reference points for the measurements are the implant platform (the horizontal interface between the implant and the abutment), the implant tip, and the first bone-implant contact (FBIC). The length from the implant platform to the FBIC defines the marginal bone level. The marginal bone level is measured in mm using the ratio of the real implant length and the length from the implant platform to the tip on the images.

I.17 Implant success

Several criteria have been proposed to evaluate the osseointegration and implant success. The most recognized criteria were established by Albrektsson et al. [68] Initially, accepted vertical bone loss was set at 1.5 mm during the first year and 0.1 mm for the following years. These criteria were

later revised, and the accepted vertical bone loss was changed to 0.2 mm annually after the first year of service [69].

Criteria for implant success [70]:

– An individual unattached implant is immobile when tested clinically.

– The radiograph does not demonstrate any evidence of preimplant radiolucency.

– Vertical bone loss is less than 0.2 mm annually after the first year of service of the implant.

– Individual implant performance is characterized by an absence of persistent or irreversible signs and symptoms such as pain, infections, neuropathies, paresthesia, or violation of the mandibular canal.

– Success rates of 85% at the end of a 5-year observation period and 80% at the end of a 10-year period are minimum criteria for success.

I.18 Dental biomaterials

Biomaterials are substances that interact with the human or animal body for therapeutic reasons, such as replacing a damaged part part of the body. Modern biomaterials are one of the main features that have increased the quality and duration of human life, especially after excessive research in vivo and vitro. Over the past years, several biomaterials (ceramics, metals, polymers) have been used to treat, restore and replace more different parts of the human body, including skin, muscle tissue, blood vessels, nerve fibers, bone tissue. The current state of the implant market can be viewed as an expectation of a massive invasion of new ideas and materials. Therefore, biomaterials must have certain biological, mechanical, chemical properties. According to the nature of the body's response to the implant, biomaterials are classified as bioinert (non-toxic but biologically inactive), bioactive (biologically active and osseointegrated with bone tissue), biocompatible (**Figure I.28**). Nowadays, biomaterials are an integral part of dentistry and can offer a unique bone

and soft tissue regeneration system for use in implantology, oral surgery, maxillofacial surgery and periodontology.

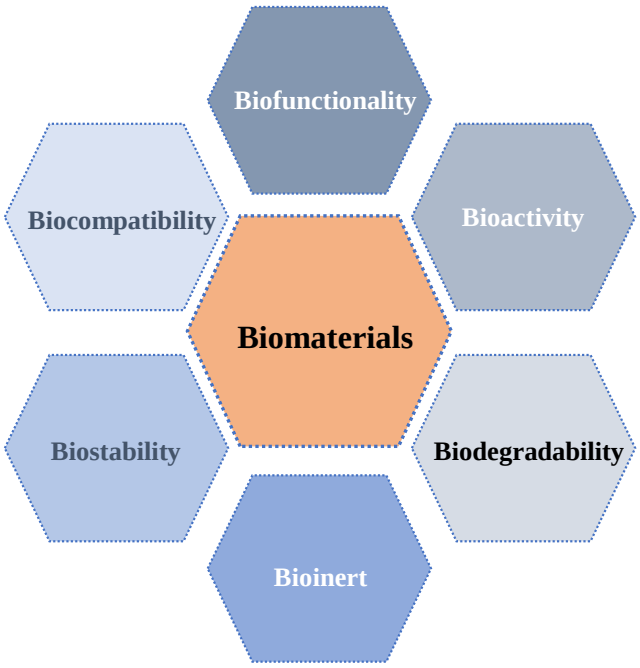

Figure I.28 *The main characteristics of effective biomaterials.*

I.18.1 Bioinert

The body will not interact in any manner with bioinert materials when they are ingested, and the materials themselves will not be affected. This is the first extreme stage with such full inertness in terms of chemical and biological processes.

I.18.2 Bioactivity

The second stage is bioactivity of the materials, it can form a biochemical link with the body as soon as they enter, for example taking part in tissue regeneration. Bioactive materials release ions or molecules that promote the attachment and growth of cells and tissues, leading to improved healing and integration of the implant with the surrounding tissue. Examples of bioactive materials used in dental implants include calcium phosphate ceramics, which can stimulate bone growth and improve osseointegration, and bioactive glass, which can promote the formation of a layer of

hydroxyapatite on the implant surface, leading to improved bonding with surrounding tissue. The development of bioactive dental biomaterials has the potential to significantly improve the success rates and long-term outcomes of dental implant procedures.

I.18.3 Biocompatibility

A biomaterial used in dental implants must be biocompatible, meaning that it should not cause any adverse reaction in the human body. This includes inflammation, infection, or rejection. Titanium and its alloys are the most commonly used materials for dental implants due to their excellent biocompatibility. They have been extensively studied and found to be safe for use in the human body. In addition to titanium, other materials such as zirconia and ceramics are also used in dental implants, and have also been found to be biocompatible. The biocompatibility of a biomaterial used in dental implants is critical for the long-term success of the implant, as it ensures that the implant can function properly without causing any harm to the patient.

I.18.4 Biostability and biodegradability

Biostability and biodegradability are two important properties that must be considered when selecting biomaterials for dental implants. Biostability refers to the ability of a material to maintain its structural integrity and physical properties over time without undergoing significant degradation or breakdown. This property is crucial in ensuring that the dental implant remains stable and functional for an extended period of time, without deteriorating or causing any harm to the surrounding tissues. Materials such as titanium and ceramics are known for their excellent biostability, making them suitable for use in dental implants. On the other hand, biodegradability refers to the ability of a material to be broken down and absorbed by the body over time. Biodegradable materials are advantageous in that they eliminate the need for implant removal surgery, which is necessary when using non-degradable materials. However, biodegradable

materials must also be carefully selected to ensure that they degrade at an appropriate rate, and that their degradation products do not cause any adverse reactions in the body. Biodegradable materials such as polymers are being developed for use in dental implants, but more research is needed to assess their biocompatibility, biodegradability, and long-term effectiveness. In conclusion, a balance between biostability and biodegradability must be struck when selecting biomaterials for dental implants, to ensure optimal patient outcomes.

I.19 Biomaterials Class

Biomaterials are materials that are specifically designed to interact with biological systems, such as living tissues or organs. They are used in a wide range of medical applications, including dental implants, orthopedic implants, drug delivery systems, and tissue engineering. Biomaterials can be classified into several categories based on their chemical composition, structure, and properties. One way to classify biomaterials is based on their origin. Naturally-derived biomaterials are those that are obtained from natural sources such as animal tissues, plants, or microorganisms. Examples of naturally-derived biomaterials include collagen, hyaluronic acid, chitosan, and silk. Synthetic biomaterials, on the other hand, are those that are synthesized in the laboratory using chemical or physical methods. Examples of synthetic biomaterials include polyethylene glycol (PEG), polylactic acid (PLA), and polyglycolic acid (PGA). Another way to classify biomaterials is based on their chemical composition. Metals, ceramics, polymers, and composites are the four main types of biomaterials based on their chemical composition. Each of these materials has unique properties that make them suitable for different medical applications. Metals are strong, durable, and biocompatible, making them ideal for use in load-bearing applications such as orthopedic implants. Ceramics are hard and brittle, but they are also biocompatible and can withstand high temperatures, making them suitable for dental implants and bone grafts. Polymers are lightweight, flexible, and can be easily shaped, making them useful for drug delivery systems and tissue engineering.

Composites are a combination of two or more types of materials, and can be tailored to have specific mechanical, chemical, or biological properties.

I.19.1 Metals

Metals are one of the most commonly used biomaterials for dental implants due to their excellent mechanical properties and biocompatibility. Specifically, titanium and its alloys are the preferred materials for dental implants due to their ability to form a stable oxide layer on the surface, which allows for integration with the surrounding bone. This integration, known as osseointegration, is critical for the success of dental implants as it provides stability and support for the replacement tooth or bridge. In addition to titanium, other metals such as cobalt-chromium and stainless steel have been used in dental implants, but they are less commonly used due to concerns over corrosion and biocompatibility. Overall, metals are a reliable and effective biomaterial for dental implants, providing patients with a long-lasting and durable solution for tooth replacement. One potential concern with metal dental implants is the possibility of allergic reactions. While rare, some patients may have an allergic reaction to certain metals, such as nickel, which is commonly found in stainless steel. However, allergy testing prior to implantation can help identify any potential issues and alternative materials can be used if necessary. Overall, metals are a reliable and effective choice for dental implants, providing a long-lasting and durable solution for tooth replacement. The success rates of metal dental implants are high, with studies showing a 10-year success rate of over 90%. Ongoing research is focused on improving the surface properties of metal implants to promote faster and more reliable osseointegration, as well as developing new metal alloys that can further enhance the performance.

I.19.2 Ceramics

Ceramics are another type of biomaterial commonly used in dental implants due to their biocompatibility, high strength, and aesthetic properties. Dental ceramics are typically composed of metal oxides, such as alumina, zirconia, or a combination of both. They can be manufactured using a variety of techniques, such as sintering, casting, or computer-aided design and manufacturing (CAD/CAM). Ceramics are highly resistant to wear and can withstand high compressive forces, making them an excellent option for dental crowns, bridges, and implant abutments. In addition, ceramics can be color-matched to the patient's natural teeth, making them a popular choice for aesthetic restorations. One of the main advantages of ceramics over metals is their ability to promote osseointegration. Unlike metals, ceramics are bioinert, meaning they do not elicit a significant immune response from the body. This allows for the formation of a strong bond between the implant and the surrounding bone, promoting osseointegration and ensuring long-term stability. However, one of the main challenges with ceramics is their brittle nature, which can make them prone to fracture or chipping under certain conditions. To address this issue, researchers have developed new ceramic materials, such as yttria-stabilized zirconia, which have improved fracture toughness and strength. In summary, ceramics are a highly biocompatible and aesthetically pleasing option for dental implants, providing excellent strength and wear resistance. While their brittle nature remains a challenge, ongoing research is focused on developing new ceramic materials and manufacturing techniques to improve their mechanical properties and enhance their performance in dental applications.

I.19.3 Polymers

Polymers are a class of biomaterials that have gained significant attention in recent years for their potential use in dental implants. Polymers are highly versatile materials that can be engineered to exhibit a wide range of mechanical, chemical, and biological properties, making them an attractive

option for implant applications. One of the main advantages of polymers is their flexibility, which can reduce the risk of stress shielding and implant failure. In addition, polymers are highly biocompatible and can be engineered to degrade over time, promoting tissue regeneration and repair. This is particularly useful in cases where a temporary implant is required, such as in periodontal or bone tissue engineering applications. However, one of the main challenges with polymers is their low strength and wear resistance compared to metals and ceramics. To address this issue, researchers have developed polymer-ceramic composites, which combine the mechanical properties of ceramics with the biocompatibility and flexibility of polymers. These composites have shown promise in a range of dental applications, including implant abutments and bone regeneration scaffolds. Overall, polymers are a promising option for dental implants, providing excellent biocompatibility and flexibility. While their low strength and wear resistance remain a challenge, ongoing research into polymer-ceramic composites and other advanced materials is aimed at overcoming these limitations and developing more effective implant materials.

I.19.4 Composites

Composites are another class of biomaterials used in dental implants, which are typically composed of a combination of two or more materials, such as ceramics and polymers. Dental composites have been used for decades in restorative dentistry, such as in fillings and veneers, and their use in implants is gaining popularity due to their favorable mechanical properties and aesthetics. One of the main advantages of composite materials is their ability to be customized to match the mechanical properties of natural teeth. Composites can be engineered to exhibit a range of strength, stiffness, and wear resistance, making them suitable for a variety of implant applications. In addition, composite materials can be color-matched to the patient's natural teeth, providing an aesthetically pleasing option for implant restorations. However, one of the main challenges with

composites is their potential for wear and degradation over time. To address this issue, researchers have developed new composite materials, such as fiber-reinforced composites, which have improved mechanical properties and wear resistance. Overall, composites are a promising option for dental implants, providing excellent customization and aesthetic properties. While their wear resistance and potential for degradation remain a challenge, ongoing research is focused on developing new composite materials and manufacturing techniques to overcome these limitations and enhance their performance in dental applications. Various biomaterials classes are shown in **Figure I.29**.

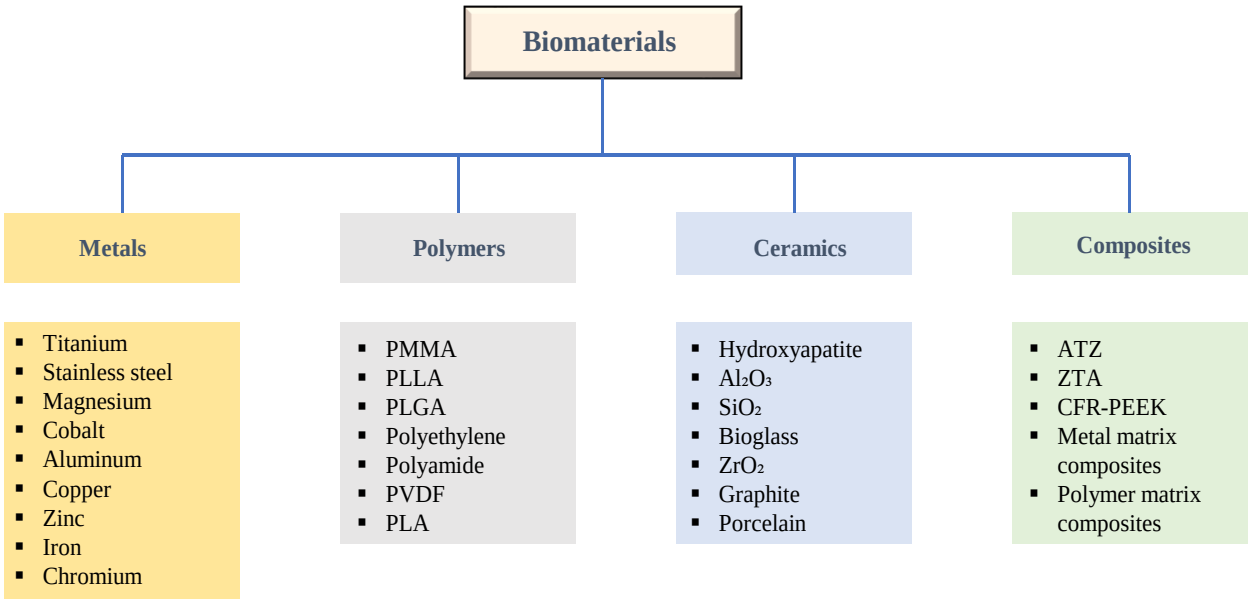

Figure I.29 *Biomaterials classes.*

I.20 Manufacturing of biomaterials

The manufacturing of biomaterials for dental implants is a critical process that involves the creation of materials with specific mechanical, chemical, and biological properties. There are various methods used for the manufacturing of biomaterials, including traditional methods such as casting, machining, and powder metallurgy, as well as newer methods such as 3D printing (**Figure I.30)** and electrospinning. The selection of the manufacturing method depends on several factors,

including the material properties, the intended application, and the desired final product. For instance, traditional methods like casting and machining are well-suited for producing large, complex structures such as implant bodies, while newer techniques like 3D printing are ideal for creating intricate geometries and customized designs. During the manufacturing process, it is essential to ensure the quality and consistency of the materials produced. This involves rigorous quality control measures, such as testing the materials for mechanical strength, biocompatibility, and chemical composition, as well as ensuring that the materials are free from defects and impurities. In summary, the manufacturing of biomaterials for dental implants is a complex process that requires careful consideration of the material properties, intended application, and regulatory standards. With advances in manufacturing techniques and quality control measures, biomaterials can be produced with greater precision and consistency, leading to improved patient outcomes and greater success rates for dental implants.

I.20.1 Selective laser melting (SLM)

Selective laser melting (SLM) is a type of additive manufacturing technique that can be used for the fabrication of dental implants. This process involves the use of a high-powered laser to selectively melt and fuse layers of metallic powder to create a three-dimensional (3D) structure. During the SLM process, a computer-aided design (CAD) model is first created to define the desired geometry of the implant. The CAD model is then converted into a series of digital slices, which are used to control the laser beam as it fuses successive layers of metallic powder together. The final product is a fully dense implant with excellent mechanical properties and precise geometries. One of the main advantages of SLM is its ability to create complex geometries with high accuracy and precision. This technique allows for the production of customized implants that are specific to each patient's unique anatomy. Additionally, SLM produces implants with a uniform, homogenous structure, reducing the risk of defects or weak spots that can compromise

implant performance. Another benefit of SLM is its ability to produce implants with a controlled microstructure. By adjusting the processing parameters, the microstructure of the implant can be optimized for specific mechanical properties, such as strength, stiffness, and wear resistance. Overall, SLM is a promising manufacturing technique for dental implants, offering precise control over implant geometry and microstructure. While the cost of SLM-produced implants is currently higher than traditional methods, ongoing research and development are focused on reducing costs and expanding the range of materials that can be used in SLM.

I.20.2 Laser surface alloying (LSA)

Laser surface alloying (LSA) is a surface modification technique that can be used to improve the mechanical, chemical, and biological properties of biomaterials for dental implants. This process involves the use of a high-powered laser to melt and fuse a thin layer of alloying material onto the surface of the implant. During LSA, a laser beam is directed at the surface of the implant, melting the surface layer and allowing the alloying material to diffuse into the underlying substrate. This results in a modified surface layer with improved wear resistance, corrosion resistance, and biocompatibility. One of the main advantages of LSA is its ability to improve the wear resistance of the implant surface. By adding a layer of wear-resistant material, LSA can increase the lifespan of the implant and reduce the risk of failure due to wear and tear. LSA can also improve the biocompatibility of the implant surface by altering its chemical composition. For example, the addition of titanium or other biocompatible elements can enhance the ability of the implant to integrate with surrounding tissue and reduce the risk of rejection. Overall, LSA is a promising technique for improving the surface properties of biomaterials for dental implants. While LSA can be more expensive than traditional surface modification techniques, ongoing research and development are focused on optimizing the process and reducing costs. Additionally, LSA can be

combined with other surface modification techniques to produce implants with tailored properties that meet the specific needs of individual patients.

I.20.3 Selective laser sintering (SLS)

Selective laser sintering (SLS) is another type of additive manufacturing technique that can be used for the fabrication of biomaterials for dental implants. This process involves the use of a high-powered laser to selectively fuse layers of powdered material together to create a three-dimensional (3D) structure. During the SLS process, a computer-aided design (CAD) model is first created to define the desired geometry of the implant. The CAD model is then converted into a series of digital slices, which are used to control the laser beam as it fuses successive layers of powdered material together. The final product is a fully dense implant with excellent mechanical properties and precise geometries. One of the advantages of SLS is its ability to produce implants with a high degree of precision and accuracy. This technique allows for the production of customized implants that are specific to each patient's unique anatomy. Additionally, SLS can produce implants with a uniform, homogenous structure, reducing the risk of defects or weak spots that can compromise implant performance. Another benefit of SLS is its ability to produce implants from a variety of materials, including metals, ceramics, and polymers. This allows for a range of properties to be tailored to specific patient needs, such as strength, stiffness, and biocompatibility. Overall, SLS is a promising manufacturing technique for dental implants, offering precise control over implant geometry and microstructure. While the cost of SLS-produced implants is currently higher than traditional methods, ongoing research and development are focused on reducing costs and expanding the range of materials that can be used in SLS.

I.20.4 Metal injection molding (MIM)

Metal injection molding (MIM) is a manufacturing technique that is widely used for the production of metal-based biomaterials for dental implants. This process involves the injection of a mixture of metal powder and binder into a mold, which is then subjected to heat and pressure to form a solid metal implant. During MIM, metal powders are first mixed with a thermoplastic binder to create a feedstock. The feedstock is then injected into a mold, which is typically made of metal or ceramic, using a high-pressure injection molding machine. Once the mold is filled, it is heated to remove the binder and sinter the metal particles together to form a solid metal implant. One of the advantages of MIM is its ability to produce complex geometries with high precision and accuracy. This allows for the creation of customized implants with complex shapes that are specific to each patient's unique anatomy. Additionally, MIM allows for the production of implants with excellent mechanical properties, including high strength and wear resistance. Another benefit of MIM is its ability to produce large quantities of implants with consistent quality and reproducibility. This makes MIM an attractive option for mass production of dental implants, as it can significantly reduce production time and costs compared to traditional machining or casting methods. However, MIM also has some limitations, such as the restricted range of materials that can be used and the need for post-processing to remove residual binder and achieve the desired microstructure. Despite these limitations, MIM is a promising manufacturing technique for dental implants, offering high precision and efficiency in the production of metal-based biomaterials.

I.20.5 Functionally graded material (FGM)

Functionally graded materials (FGMs) are a relatively new class of biomaterials that have attracted attention for their potential application in dental implants. FGMs are characterized by a gradual transition in material properties from one end of the implant to the other, resulting in a continuous variation in the properties of the implant. This gradient in properties can be tailored to match the

mechanical, physical, and biological requirements of the implant and the surrounding tissue. The manufacturing process for FGMs involves depositing layers of different materials onto a substrate using advanced additive manufacturing techniques such as 3D printing. By varying the composition and structure of the deposited layers, FGMs can be designed to exhibit specific properties such as high strength, good biocompatibility, and controlled degradation rates. In dental implants, FGMs can be used to create implants with a gradient in mechanical properties, allowing for a better distribution of stress and strain across the implant and reducing the risk of implant failure. FGMs can also be designed to have a graded surface chemistry, which can improve the implant's ability to bond with surrounding bone and promote osseointegration. Overall, FGMs represent a promising area of research for the development of advanced biomaterials for dental implants. The ability to tailor the material properties of implants to match the specific needs of each patient can lead to improved implant success rates and better clinical outcomes.

I.21 Nanodentistry

Nanodentistry is a field of dentistry that involves the use of nanotechnology to develop and improve dental materials and procedures. Nanotechnology involves the manipulation and control of matter at the nanoscale level, typically between 1 and 100 nanometers in size. This technology can be used to modify the properties of dental materials and devices, leading to improved biocompatibility, mechanical strength, and durability. One application of nanodentistry is the development of nanocomposites for dental restorations. These composites incorporate nanoparticles of materials such as silica, titanium dioxide, or calcium phosphate to enhance the mechanical properties and biocompatibility of the composite material. Nanoparticles can also be used to enhance the antimicrobial properties of dental materials, reducing the risk of bacterial infections and decay. Another application of nanodentistry is the development of nanorobots, or nanobots, that can be used for a variety of dental procedures. These tiny robots can be designed to

perform tasks such as repairing damaged tissue, detecting and removing plaque, and delivering medications or therapeutic agents to specific sites in the mouth. Nanodentistry also holds promise for the development of improved imaging and diagnostic tools for dental care. Nanoparticles can be used to enhance the contrast of dental x-rays and other imaging techniques, leading to more accurate diagnosis and treatment planning. While still in the early stages of development, nanodentistry has the potential to revolutionize the field of dentistry, leading to improved materials, procedures, and outcomes for patients.

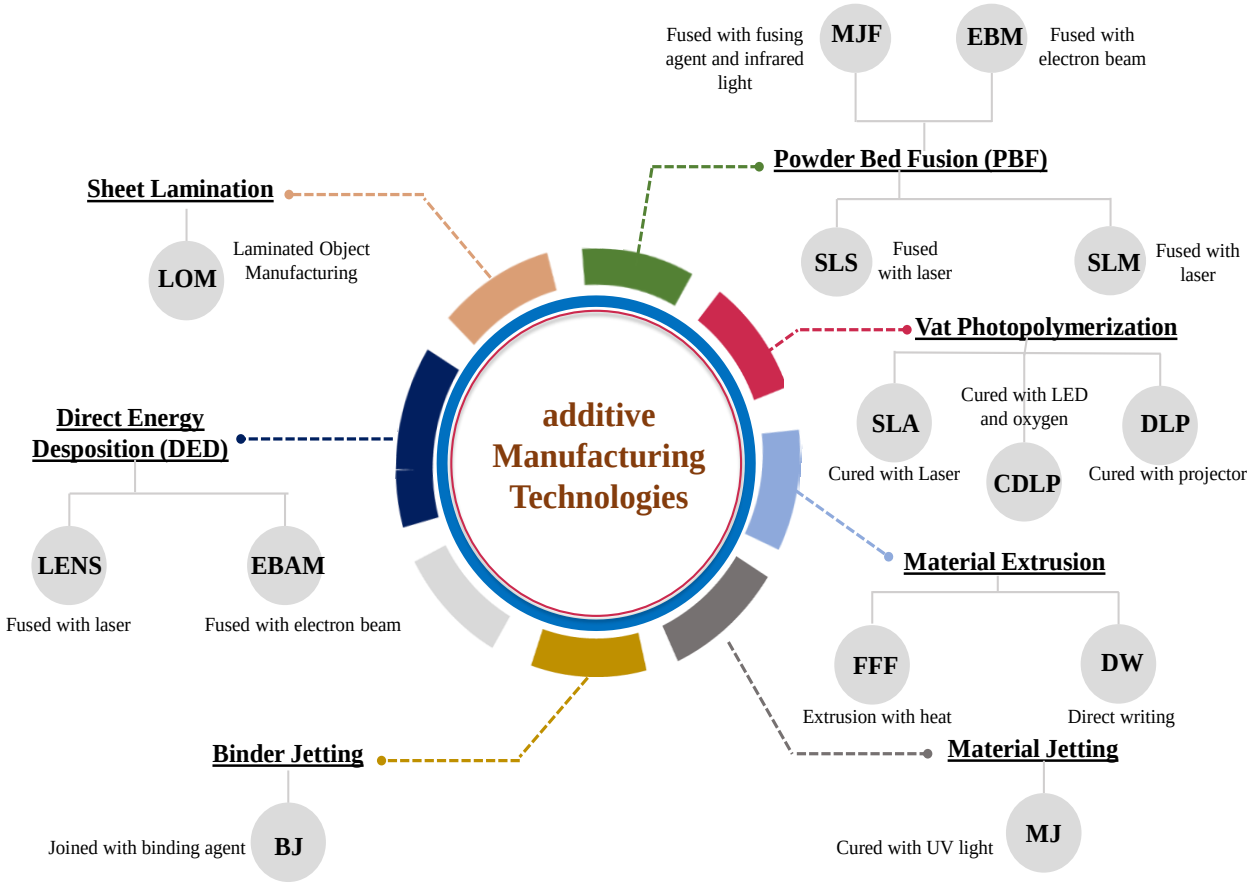

Figure I.30 *Additive Manufacturing Processes.*

Chapter II Literature Review

The finite element method is an advanced and popular tool for computational analysis that solves mathematical (differential) equations in engineering. This numerical technique is widely used in biomechanics with the aid of specific software. One of the axes where the finite element tool is being used is in the field of dental implants (to analyze stresses, strains, and displacements at the level of the bone, implant, and its components). There are several procedures (Figure 1) before moving on to FE analysis, including scanning and imaging (CT scan), reconstructing the 3D parts of the bone and implant, meshing, loading and boundary conditions. Researchers and engineers are currently studying the biomechanical influence of many factors that can impact implant and bone in a vitro approach using the FE technique, such as implant diameter, implant length, implant thread, implant shape (tapered or cylindrical), implant material, loading magnitude and directions, abutment-implant connection type, osseointegration and bone remodeling process. The results obtained from the finite element analysis (stress/strain) can help researchers to evaluate the behavior of bone and implant, and determine the mechanical strength of the implant, abutment, and prosthesis. This review aims to study the use of FEA in the field of dental implants and to provide a deep understanding through the analysis of recent studies presented in detail.

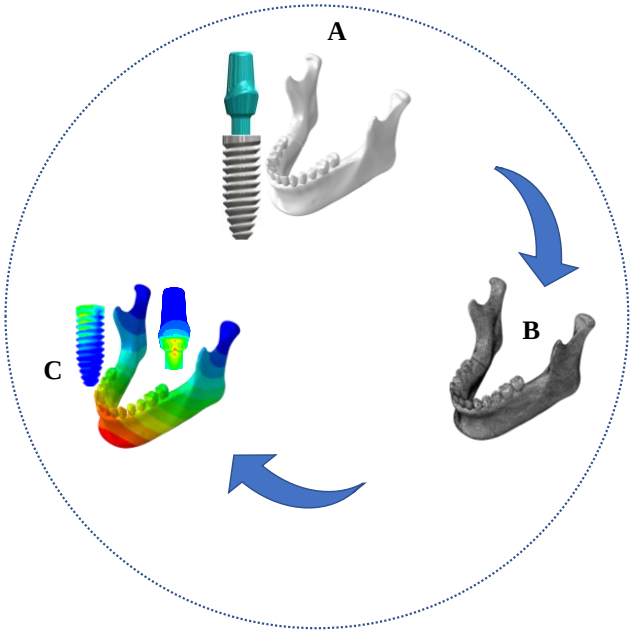

Figure II.1 *Main steps for numerical simulation. (A) reconstruct the 3D model; (B) meshing and boundary conditions; (C) analyze and extract results.*

II.1 Modeling of mandible bone and implants

The mandible bone can be modeled from medical images using various imaging techniques such as X-ray imaging, computed tomography (CT), magnetic resonance imaging (MRI), and ultrasound imaging. These techniques play an important role in describing the bone quality (bone density), determining fractures and multi-scale bone characterization. Medical images of bone from different scans can be segmented to reconstruct bone surface mesh using dedicated software that offers many segmentation features and algorithms and can eventually generate an STL (standard stereo-lithography) file, which is a uniform mesh with many triangles. For example, the CT scan can generate medical images with a DICOM file (Digital Imaging and Communications in Medicine). These datasets can be analyzed for segmentation with various software (free open-source software or even paid commercial software). One of the most common software packages for this kind of job is MimicsTM, and the final shape can be exported for another process to create the solid part with the use of computer-aided design

(CAD) software, such as Solidworks. Some studies have simply created the bone as solid on a mesoscale simply to facilitate the analysis. The implant can be modeled with the same process, but in most cases, it can be reconstructed using the direct method with CAD package software. Some manufacturers provide information with details about implant design. Thence, the process of reconstructing the bone and the implant requires high skill using numerical methods.

II.2 Methodology for the review

The outline of the review was chosen through a clear strategy represented by many questions, which are explained as follows:

- Dental implant design and materials
- Bone properties
- Finite element parameters (including loading, boundary conditions, mesh element type and FEA software)

II.2.1 Search strategy

An electronic search was carried out using Science Direct and Springer databases, with the following keywords: “dental implant finite element analysis”, “dental implant FEA”, “dental implant FE”, and “dental implant computational analysis”. The year was chosen in the search between 2019 and 2022 (prior to July 4, 2022).

II.2.2 Study selection

All papers related to oral surgery and finite element analysis were collected from many scientific journals, especially papers whose title are related to dental implants. Papers containing only an abstract or on a single page were not collected.

II.2.3 Inclusion and Exclusion Criteria

Exclusion criteria were reviews, conference proceedings, orthodontic implants, zygomatic implants, and no FE application. Inclusion criteria were full manuscripts in indexed journals that are related to the finite element method and dental implants, and that are assigned to report one of the following conditions: implant design, bone properties, mesh and boundary conditions. A full review was done manually for the selected references. The accessed papers have been studied and divided in the results section into studies regarding implant design and materials, studies regarding bone properties, studies regarding finite element parameters, studies regarding the mechanostat theory, and studies regarding bone remodeling algorithms. To maintain clarity, they are discussed in sections that match the above-mentioned categories.

II.3 Results

II.3.1 Study selection

The flowchart of the review is shown in **Figure II.2.** Among the obtained results, 102 papers were initially selected. 21 studies were excluded because they did not meet the inclusion criteria. In the end, a total of 81 studies were reviewed.

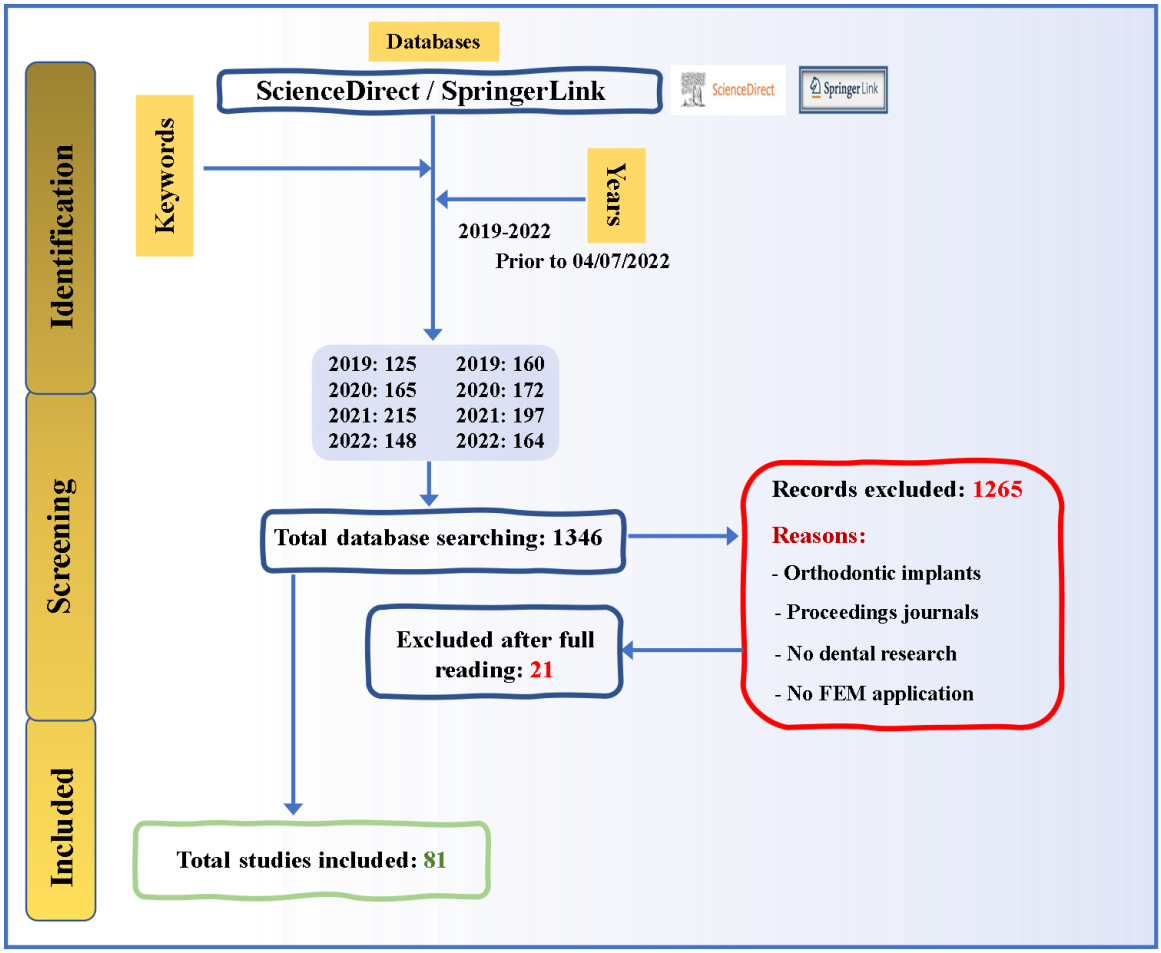

Figure II.2 *The flowchart of this review.*

II.3.2 Relevant Data of Included Studies Regarding Implants design and materials

Based on the results listed in **Table *II.1*** Dental implants' primary characteristics..Most of the manuscripts used titanium material for the dental implant in their studies. Six research studies used zirconia material. Only one study used coated materials and FGM, and the other two used PEEK-Ti composite and CFR-PEEK as the implant material. Regarding the length and diameters of implants, there is a wide range of dimensions. There are no fixed standard dimensions in this regard. Six papers in which the implant diameter is not specified. The minimum diameter was 2 mm and the maximum diameter was 6mm, so the implant diameters in the included studies had a mean SD of 4.2mm. The most common diameter among the

selected studies is 3.5 mm (14 studies) and 4.5 mm (13 studies). Regarding the length, 7 papers in which the implant diameter is not specified. The minimum length was 4 mm and the maximum length was 15 mm. The most common length among the selected studies is 13 mm. Regarding implant shape, the most common shape was the tapered shape. About the connection type between implant and abutment, the internal connection was the most used in the selected references. 17 papers in which the type of connection is not specified. The most used CAD software is Solidworks.

Table II.1 Dental implants' primary characteristics.

Author year reference	Geometric characteristic		Software used	Implant Type	Abutment Connection	Material
	Diameter D (mm)	Length L (mm)				
Park et al. (2022) [71]	4, 4.5, 5	7	/	Cylindrical	Internal	Titanium
Jafari et al. (2022) [72]	4	12	SolidWorks	Cylindrical	Internal	Titanium/FGM/Ha coated Ti
Dayrell et al. (2022) [73]	3.75	13	Rhinoceros	Cylindrical	Morse taper	Titanium
Chang et al. (2022) [74]	3.5	11	Creo Parametric	Tapered	Internal	Titanium
Xie et al. (2022) [75]	3.5	10	3-Matic	Tapered	one piece	Titanium/Titanium-zirconia
Zupancic et al. (2022) [76]	4.1	4,6,8	Medtool	Cylindrical	/	Titanium
Huang et al. (2022) [77]	4.2	10	SolidWorks	Tapered	Internal	Titanium
Chen et al. (2022) [78]	3.3,4.5,4.8	6,8	/	Cylindrical	Internal	Titanium
Sun et al. (2022) [79]	4.3	11	/	Tapered	Morse taper	Titanium
Patil et al. (2022) [80]	2.5,3,3.5,4	12	3-Matic	Cylindrical	/	Titanium
Yu et al. (2022) [81]	4.3	10	SolidWorks	Tapered	one piece	Titanium
Armentia et al. (2022) [82]	4.5,5.5	13	/	Tapered/ Cylindrical	Internal/External	Titanium

Author year reference	Geometric characteristic		Software used	Implant Type	Abutment Connection	Material
	Diameter D (mm)	Length L (mm)				
Mohamed et al. (2022) [83]	/	/	SolidWorks	Cylindrical	External	Titanium
Mohammadi et Selahi (2022) [84]	4	12.95	Catia	Tapered	Internal	Titanium
Zupancic et al. (2022) [85]	4.1	4,6,8	Medtool	Cylindrical	/	Titanium
Liu et al. (2022) [86]	4	6,10	SolidWorks	Cylindrical	/	Titanium
Cheng et al. (2022) [87]	3.75	10	Pro/ENGINEER Wildfire	Tapered	Internal	Titanium
Bassi-Junior et al. (2021) [88]	3.75	13	SolidWorks	Cylindrical	/	Titanium
Ausiello et al. (2021) [89]	4.2	9	Rhinoceros	Tapered	/	Titanium
Lee et al. (2021) [90]	3.5,4,4.5	10	Mimics	Tapered	Internal/External	Titanium
Silva et al. (2021) [91]	4	7	Rhinoceros/ SolidWorks	Tapered	External	Titanium
Fabris et al. (2021) [92]	3.5	15	SolidWorks	Cylindrical	one piece	Zirconia
Jafariandehkordi et al. (2021) [93]	4	10	Autodesk Inventor	Cylindrical	Internal	Titanium
Chen et al. (2021) [94]	4.3	10	SolidWorks	Cylindrical	Internal	Titanium
Liu et al. (2021) [95]	3.6,4.5	8,10	SolidWorks	Cylindrical	Internal	Titanium/PEEK-Ti
Cantó-Navés et al. (2021) [96]	4.20	11.50	SolidWorks	Tapered	Internal	Titanium
Lee et al. (2021) [97]	3.5,4,4.5	10	3-Matic	Tapered	Internal/External	Titanium
Gibreel et al. (2021) [98]	3.75	11	SolidWorks	Tapered	Internal	Titanium
Kul et al. (2021) [99]	3.5,5.5	8,12	SolidWorks	Tapered	Internal	Titanium
Honório et al. (2021) [100]	3.75	11.5	SolidWorks	Tapered	Internal	Titanium
Lemos et al. (2021) [101]	4	10	Rhinoceros/ SolidWorks	Tapered	Internal/External	Titanium

Author year reference	Geometric characteristic		Software used	Implant Type	Abutment Connection	Material
	Diameter D (mm)	Length L (mm)				
Patil et al. (2021) [102]	3.5	12	SolidWorks	Tapered	/	Titanium
Darwich et al. (2021) [103]	4	13	SolidWorks	/	/	Titanium
Giner et al. (2021) [104]	4.3	11	SolidWorks	/	Internal	Titanium
Borges et al. (2021) [105]	2,3.75	10	SolidWorks	Tapered	Morse taper/ External	Titanium
Lee et al. (2021) [106]	4.5	10	/	Tapered	Internal	Titanium
Sato et al. (2021) [107]	3.75	13	/	Tapered	/	Titanium
Mourya et al. (2021) [108]	4.2	10	Ansys	Tapered	Internal	Titanium/CFR-PEEK
Oyar et al. (2021) [109]	4	13	Rhinoceros	Tapered	Internal	Titanium
Ercal et al. (2021) [110]	4.1	7	SolidWorks	Tapered	Internal	Titanium
da Rocha et al. (2021) [111]	4.1	6	SolidWorks	Cylindrical	External	Titanium
Zincir et Parlar (2021) [112]	3.5,4,4.5	11.5	Rhinoceros	Tapered	Internal	Titanium
Manafi et al. (2021) [113]	4	8,10,12	/	Tapered	External	Titanium
Pirmoradian et al. (2020) [114]	4.1	8.5,10 11.5,13	Catia	Cylindrical	one piece	Titanium
Chakraborty et al. (2020) [115]	4	13	SolidWorks	Tapered	Internal	Titanium
Alaqeely et al. (2020) [116]	4.1	10	3-Matic	Cylindrical	/	Titanium
Valera-Jiménez et al. (2020) [117]	3,3.5,4.3	10,13	SolidWorks	Tapered	Internal	Titanium
Kayabasi (2020) [118]	/	/	/	Cylindrical	Internal	Titanium
Wu et al. (2020) [119]	4	11.5	SolidWorks	Tapered	Internal	Titanium
Jin et al. (2020) [120]	4	11.5	Abaqus	Cylindrical	one piece	Titanium

Author year reference	Geometric characteristic		Software used	Implant Type	Abutment Connection	Material
	Diameter D (mm)	Length L (mm)				
Bayata et al. (2020) [121]	3.5;4;4.5;5	13	SolidWorks	Cylindrical	Internal	Titanium
Moreira et Francischone (2020) [122]	2.9,3.5	11.5	SolidWorks	Tapered	Morse taper	Titanium
Dantas et al. (2020) [123]	5	8.6	SolidWorks	Cylindrical	/	Zirconia
de Souza Rendohl et al. (2020) [124]	4.3,5	5	Rhinoceros	Cylindrical	Internal	Titanium
Bachiri et al. (2020) [125]	4.1	14	SolidWorks	Cylindrical	Internal	Titanium
Ayali et al. (2020) [126]	/	10,13	Rhinoceros	Tapered	Internal	Titanium
Zhong et al. (2020) [127]	4.6	12	SolidWorks	Tapered	Morse taper	Titanium
Niroomand et Arabbeiki (2020) [128]	4.1	/	Ansys	Cylindrical	one piece	Titanium
Stocchero et al. (2020) [129]	3.6	6	SolidWorks	Cylindrical	/	Titanium
Morita et al. (2020) [130]	3.8	11	/	Cylindrical	External	Titanium
Araki et al. (2020) [131]	4	6,8,10	SolidWorks	Cylindrical	Internal	
Shash et al. (2020) [132]	4	11	Autodesk Inventor	Tapered	Internal	Zirconia
Brune et al. (2019) [133]	5	12	Rhinoceros	Cylindrical	Morse taper	Titanium
Chatterjee et al. (2019) [134]	4	9,10,11	SolidWorks	Cylindrical	Morse taper	Titanium
Jung et al. (2019) [135]	5	11	Visual-Mesh	Tapered	Internal/External	Titanium
Azcarate-Velázquez et al. (2019) [136]	4	13	/	Tapered	Internal	Titanium
Demenko et al. (2019) [137]	3.3-5.4	4.5-8.5	/	Cylindrical	one piece	Titanium

Author year reference	Geometric characteristic		Software used	Implant Type	Abutment Connection	Material
	Diameter D (mm)	Length L (mm)				
Chang et al. (2019) [138]	3.5,4.5,5.5	11	Avizo 3D	Tapered	Internal	Titanium
Aslam et al. (2019) [139]	4.5	11	Creo Parametric	Cylindrical	Internal	Titanium
Berger et al. (2019) [140]	4.1	/	ANSYS DesignModeler	Cylindrical	external	Titanium
Kasani et al. (2019) [141]	3.7	13	SolidWorks	/	/	Titanium
Lee et al. (2019) [142]	/	7	3-Matic	Cylindrical	Internal/External	Titanium
Bulaqi et al. (2019) [143]	/	/	SolidWorks	Cylindrical	Internal	Titanium
Petris et al. (2019) [144]	3.75	7	SolidWorks	Tapered	Morse taper	Titanium
de la Rosa Castolo et al. (2019) [145]	0.5-6	13	/	Cylindrical	Internal	Titanium
Mello et al. (2019) [146]	4.1	10	Rhinoceros/ SolidWorks	Cylindrical	/	Titanium
Cheng et al. (2019) [147]	5	/	Pro/Engineer	Tapered	one piece	Zirconia
Sharanraj et al. (2019) [148]	/	10	Catia	Tapered	/	Zirconia
Dávila et al. (2019) [149]	4.5	/	/	Tapered	/	Titanium
Li et al. (2019) [150]	4.1,4.3	11,12	Catia	Tapered/ Cylindrical	Internal	Titanium
Dhatrak et al. (2019) [151]	3.5	15	/	Tapered	/	Titanium

II.3.3 Relevant Data of Included Studies Regarding bone properties

Table *II.2* details the main properties of the mandible bone investigated in the included manuscripts. In view of **Table *II.2***, most studies treated bone as an isotropic material, while six papers analyzed it as an orthotropic material. All studies used 3D models. Young's modulus, the most common among studies for cortical bone, is 13.7 GPa and for cancellous bone, it is 1.37

GPa. The rest of the research used different values or used formulas related to bone density and HU (Hounsfield units) based on CT scans. The one thing certain among all the studies is that the cortical bone was much stiffer compared to the cancellous bone.

Table II.2 Bone properties.

references	**model**	**Young's modulus (GPa)**		**Bone type**
		Cortical bone	**Cancellous bone**	
[71]	3D	13.7	1.3	Isotropic
[72][73][74][77][94][98][103][105][106][108][109] [110][113][114][122][124][133][135][140][141][143][142][145][146][149]	3D	13.7	1.37	Isotropic
[75][99][138]	3D	14	1.37	Isotropic
[76][85][121]	3D	13.7	13.7	Isotropic
[80]	3D	13.6	13.6	Isotropic
[81]	3D	14	1.40	Isotropic
[83]	3D	13.7	7.93	Isotropic
[86][111]	3D	E_x=12.6 Ey=12.6 Ez=19.4	E_x=1.148 Ey=0.210 Ez=1.148	Orthotropic
[87]	3D	13.7	1.85	Isotropic
[89][136]	3D	13.7	5.5	Isotropic
[90][97]	3D	13.7	3.5	Isotropic
[91][101]	3D	13.7	1.10	Isotropic
[92]	3D	E_x=19.5 Ey=13.6 Ez=10.2	E_x=0.38 Ey=0.38 Ez=0.38	Orthotropic
[93]	3D	13.7	0.24	Isotropic
[95]	3D	13.4	1.37	Isotropic
[96]	3D	15	0.5	Isotropic
[102]	3D	13.6	13.6	Isotropic
[107][115][127][134]	3D	Using equation related to	Using equation related to density and HU	Isotropic

references	model	Young's modulus (GPa)		Bone type
		Cortical bone	Cancellous bone	
		density and HU		
[112]	3D	13	5.5	Isotropic
[116]	3D	18	0.7	Isotropic
[117]	3D	13.7	0.5	Isotropic
[118]	3D	20.5	2.16	Isotropic
[119]	3D	14.8	1.48	Isotropic
[120]	3D	13.7	0.95	Isotropic
[123]	3D	13.7	0.7	Isotropic
[125]	3D	14.7	1.37	Isotropic
[126]	3D	13.7	1.85	Isotropic
[128]	3D	13	1.37	Isotropic
[129]	3D	14	0.62	Isotropic
[132]	3D	E_x=9600 Ey=9600 Ez=17800	E_x=0.144 Ey=0.99 Ez=0.344	Orthotropic
[137]	3D	13.7	0.69	Isotropic
[139]	3D	E_x=12.6 Ey=12.6 Ez=19.4	E_x=1.15 Ey=0.210 Ez=1.15	Orthotropic
[144]	3D	14	1	Isotropic
[147]	3D	13	0.345	Isotropic
[151]	3D	22.8	1.148	Isotropic
[151]	3D	E_x=12.7 Ey=17.9 Ez=22.8	E_x=0.210 Ey=1.148 Ez=1.148	Orthotropic

II.3.4 Relevant Data of Included Studies Regarding FE parameters

Table *II.3* details the main parameters used in all reviewed manuscripts. 24 studies used 10-node tetrahedral as an element type, while 12 studies used 4-node tetrahedral. Only three studies

used hexahedral elements, the rest used tetrahedral but did not specify if they were linear or quadratic. Regarding the software employed (with different versions), 32 studies used Ansys software, 17 studies used Abaqus, 4 studies used COMSOL, 3 studies used Algor Fempro, and two studies used MECHANICAL FINDER. Two other studies used Femap, and the rest of the studies used different software. Regarding the contact between bone and implant, most of the studies treat the bone-implant interface as 100% osseointegrated. The bonded feature was used for this purpose. Five studies used no full osseointegration; they used friction contact (a friction coefficient of 0.3 is the most used). Regarding the loading conditions, most studies used a combination of loading, 48 studies used oblique loading, and 40 papers used vertical loading (axial loading). 33 studies used 100 N as the magnitude of loading (either axial or oblique).

Table II.3 FE parameters.

References	Mesh element	FEA software	Loading conditions	Contact bone-implant
[71]	4-node tetrahedral	Abaqus	Vertical: 50 N Oblique: 200 N	-
[72]	10-node tetrahedral	Ansys	Oblique: 102 N	Bonded
[73]	10-node tetrahedral	Ansys	Vertical: 100 N, 300 N	Bonded
[74]	-	Ansys	Oblique: 300 N	Bonded
[75]	4-node tetrahedral	MSC Marc/Mentat	Oblique: 150 N	Bonded
[76][85]	10-node tetrahedral	Abaqus	Vertical: 100 N Oblique: 100 N	Bonded
[77]	4-node tetrahedral	SolidWorks	Vertical: 50 N, 300 N	Bonded
[80]	4-node tetrahedral	Ansys	Vertical: 100 N	Bonded
[81]	4-node tetrahedral	Abaqus	Oblique: 300 N	Bonded
[86]	10-node tetrahedral	Abaqus	Oblique: 110 N	Bonded
[87]	10-node tetrahedral	Ansys	Oblique: 200 N	Bonded
[89]	tetrahedral	Ansys	Oblique: 350 N	Bonded
[90]	tetrahedral	Abaqus	Vertical: 100 N Oblique: 200 N	Bonded
[91]	tetrahedral	Ansys	Vertical: 300 N, 800 N	Bonded

References	Mesh element	FEA software	Loading conditions	Contact bone-implant
[92]	tetrahedral	COMSOL	Oblique: 100 N	Bonded
[93]	10-node tetrahedral	COMSOL	Pressure: 1.117 MPa	Bonded
[94]	tetrahedral	Ansys	Oblique: 400 N	Bonded
[95]	hexahedral and tetrahedral	Ansys	Vertical: 100 N Oblique: 100 N	Bonded
[96]	10-node tetrahedral	Ansys	Vertical: 300 N	Bonded
[97]	tetrahedral	Abaqus	Vertical: 200 N Oblique: 100 N	Bonded
[98]	tetrahedral	Ansys	Vertical: 100 N Oblique: 100 N	Bonded
[99]	10-node tetrahedral	Ansys	Vertical: 365 N Oblique: 200 N	Bonded
[101]	tetrahedral	FEMAP	Vertical: 200 N Oblique: 100 N	Bonded
[102]	tetrahedral	Ansys	Vertical: 100 N	Bonded
[103]	4-node tetrahedral	Ansys	Vertical: 200 N	Bonded
[105]	-	Ansys	Vertical: 150 N Oblique: 100 N	Bonded
[106]	tetrahedral	Ansys	Oblique: 150 N	Bonded
[107]	4-node tetrahedral	MECHANICAL FINDER	Oblique: 63.8 N	Bonded
[108]	10-node tetrahedral	Ansys	Vertical: 1000 N Oblique: 500 N	Bonded
[109]	tetrahedral	Algor Fempro	Oblique: 200 N	Bonded
[110]	10-node tetrahedral	Autodesk Nastran	Vertical: 200 N Oblique: 100 N	Bonded
[111]	10-node tetrahedral	Abaqus	Oblique: 23 N	Bonded
[112]	tetrahedral	Algor Fempro	Vertical: 250 N Oblique: 250 N	-
[113]	10-node tetrahedral	Abaqus	Vertical: 700 N	Bonded
[114]	10-node tetrahedral	Abaqus	Oblique: 180 N	Bonded
[115]	10-node tetrahedral	Ansys	Vertical: 200 N	Bonded
[116]	tetrahedral	Ansys	Torque: 25N.cm	friction coefficient 0.3

References	Mesh element	FEA software	Loading conditions	Contact bone-implant
			Force: 1KN	
[117]	-	COMSOL	Oblique: 300 N	Bonded
[118]	tetrahedral	Ansys	Vertical: 114.6 N horizontal: 23.4 N horizontal: 17.1 N	Bonded friction coefficient 0 friction coefficient 0.3
[119]	10-node tetrahedral	Ansys	Vertical: 100 N	Bonded
[120]	tetrahedral	Abaqus	Oblique: 150 N	Bonded
[121]	10-node tetrahedral	Ansys	Oblique: 100 N	frictional
[122]	10-node tetrahedral	Ansys	Vertical: 100 N Oblique: 100 N	Bonded
[123]	tetrahedral	COMSOL	Oblique: 100 N	Bonded
[124]	10-node tetrahedral	Ansys	Vertical: 150 N	Bonded
[125]	4-node tetrahedral	Abaqus	-	Bonded
[126]	tetrahedral	Algor Fempro	Vertical: 100 N	Bonded
[127]	4-node tetrahedral	Abaqus	Muscles forces Oblique: 100 N	Bonded
[128]	10-node tetrahedral	Ansys	Oblique: 100 N	Bonded
[129]	-	VOXELCON	Oblique: 150 N	Bonded
[130]	10-node tetrahedral	MECHANICAL FINDER	Vertical: 120 N Oblique: 120 N	-
[131]	tetrahedral	SolidWorks	Oblique: 100 N	Bonded
[132]	tetrahedral	Ansys	Oblique: 118.2 N	Bonded
[133]	-	Ansys	Vertical: 100 N	Bonded
[134]	10-node tetrahedral	Ansys	Vertical: 100 N	friction coefficient 0.4
[135]	tetrahedral	Visual-Crash	Oblique: 100 N	Bonded
[136]	4-node tetrahedral	Abaqus	Vertical: 400 N Oblique: 400 N	Bonded
[137]	hexahedral	Ansys	Oblique: 118.2 N	Bonded
[138]	-	Ansys	Oblique: 100 N	-
[139]	tetrahedral	Ansys	Vertical: 200 N to 800 N Oblique: 50 N to 150 N	Bonded
[140]	10-node tetrahedral	Ansys	Vertical: 135 N	Bonded

References	Mesh element	FEA software	Loading conditions	Contact bone-implant
			Oblique: 135 N	
[141]	tetrahedral	Ansys	Vertical: 50 N, 100 N, 150 N	Bonded
[142]	4-node tetrahedral	Abaqus	Vertical: 200 N Oblique: 200 N	Bonded
[143]	tetrahedral	Abaqus	Torque: 35 N.cm	Bonded
[144]	10-node tetrahedral	Ansys	Oblique: 250 N	Bonded
[145]	tetrahedral	-	Vertical: 63 N	Bonded
[146]	tetrahedral	Femap	Vertical: 400 N Oblique: 200 N	Bonded
[147]	-	Ansys/LS-DYNA	Vertical: 100 N horizontal: 25 N horizontal: 17 N	friction coefficient 0.3
[148]	tetrahedral	Ansys	Vertical: 50 N to 300 N	Bonded
[149]	4-node tetrahedral	COMET	Vertical: 100 N	Bonded
[150]	hexahedral	Abaqus	Torque: 35 N.cm Oblique: 20 to 200 N	Bonded
[151]	10-node tetrahedral	Abaqus	Vertical: 100 N Oblique: 100 N	Bonded

II.3.5 Relevant data of included studies regarding bone remodeling algorithm

Bone remodeling is a complex mechanism, many factors can influence it such as the mechanical loading (forces). Studies have shown that mechanical stress/strain can affect the cell's stability, these forces result in adaptive changes in bone structure (bone homeostasis). Numerous mathematical models to estimate cell and bone density changes can be found in the literature. Park et al. [71] have evaluated the impact of bone remodeling with certain biomechanical conditions (implant diameter: 4, 4.5, 5 mm) under a biting force of 50 N in 150 days of bone remodeling. They have used FE software (ABAQUS) with UMAT subroutine and they simulated the evolution of bone properties around the implant using the following formulas:

$$w(x^i) = \frac{1}{2}\sigma(x^i) : \varepsilon(x^i) \qquad (1)$$

w: the strain energy density

i osteocyte i at its location *xi*

σ: the stress tensor

ε: the strain tensor

Table II.4 Different parameters used in bone remodeling algorithm and FE model [71].

Parameters	**Description**	**Numerical values**
x^i	Location of osteocyte i	calculated
w	strain energy density	calculated
ψ	mechanical signals	calculated
$C(n_0, \mu^i)$	model parametric function depending on the number of considered osteocytes and sensitivity of osteocyte	calculated
W_0	threshold value of the mechanical signal	0.002 J/g
μ^i	sensitivity of osteocyte	1.0
n_i	number of cell	n_0 = 13,300 osteocytes $n_1(t = 0)$ = 15 osteoclasts $n_2(t = 0)$ = 15 osteoclasts
g_{ij}	factors produced by the cell i that regulate the formation of cell j	calculated
A_i, B_i, γ	model parameters that regulate the production of cells	A_1=1.6 B_1= -0.49 γ_1= 16.67 g/J A_2=-1.6 B_2= 0.6 γ_2= 33.37 g/J
α_i	cells production rate	α_1= 3 osteoclasts/day α_2= 4 osteoblasts/day
β_i	cells removal rate	β_1= 0.2 osteoclasts/day β_2= 0.02 osteoblasts/day
m	mass of bone	calculated
ρ	apparent density of bone	calculated
k_i, K_i	normalized activities	k_1,K_1=0.0024 osteoclasts/day k_2,K_2=0.000017 osteoclasts/day

N_i	numbers of actively resorbing/forming bone cells	calculated
E_0	young's modulus of perfect bone without porosity	3.137 GPa
ρ_L	density of perfect bone without porosity	1,200 kg/m^3
δ_s , δ_c	constants describing young's modulus evolution	δ_s=2.5 δ_c=3.2

Jafari et al. [72] have also examined bone remodeling using a specific algorithm and finite element method around three different implant materials (Titanium, titanium with hydroxyapatite coating, and radial functionally graded materials). They have evaluated the final bone configuration (Young's modulus of bones). They used a mathematical model (with bone density function):

$$\frac{d\rho}{dt} = A(S-k)$$

ρ: apparent bone density

A: the remodeling rate constant

k: the reference (homeostatic) stimulus of the intact bone

S: the stimulus

$$S(x,y,z,t) = \frac{u(x,y,z,t)}{\rho(x,y,z,t)}$$

u: the strain energy density

S is a scaler function of the position vector components and time.

The differential equation of bone remodeling of bone tissue was used as follows:

$$\frac{d\rho}{dt} = \begin{cases} A(S-(1+\delta)k) & S > (1+\delta)k \\ 0 & \text{if} \quad (1-\delta)k \le S \le (1+\delta)k \\ A(S-(1-\delta)k) & S < (1-\delta)k \end{cases}$$

The average Young's modulus of each bone was calculated in every remodeling stage by the following formulas:

For cancellous bone:

$$E = 2349\rho^{2.15}$$

For cortical bone:

$$E = 24000\rho - 23.930$$

Their results showed that radial FGM implants generate the highest remodeling stimulus and bone density, during the remodeling process the bone density was increased around the implant. Regarding overload-induced bone resorption, the stress values were within the safe range (lazy zone).

II.3.6 Finite element studies and mechanostat theory

Mechanostat theory is a good criterion that can be used with finite element analysis (strain analysis in bone tissue) to describe the behavior of the bone. Xie et al. [75] have studied the effects of the materials on fixed partial dentures supported by two endosseous implants (a diameter of 3.5 mm and a length of 10 mm) with titanium, zirconia, and titanium-zirconia materials. The strain in bone tissue was analyzed. They have found that the strains in the spongious bone for all models were below the physiological upper limit of 3000 micro-strain (based on mechanostat theory). Liu et al. [86] have evaluated the effect of bone quality with short (6 mm) and standard implants (10 mm) with an all-on-four design. The stress/strain analysis was performed using maximum principal stress and strain. In their study, they empathized that the volume of elements with strains of over 3000 micro-strains (με) in bone was counted for the risk of overload, according to Frost's mechanostat theory. Silva et al. [91] have examined the biomechanical behavior of 3-unit implant-supported prostheses under

parafunctional forces. They have used microstrain analysis criteria to evaluate bone tissue and the risk of resorption scale by mechanostat theory. Fabris et al. [92] have used von Mises equivalent strain to compare it with mechanostat strain levels. Jafariandehkordi et al. [93] have evaluated the implant design parameters (Young's modulus, length, radius) based on mechanostat theory by equivalent strain analysis. They have highlighted that if the strains in the bone tissue exceed 25,000 με, the bone fracture will occur. Lee et al. [97] have studied the effect of implant diameter, abutment connection type, and bone density on the stability of the implant and bone. They have analyzed the principal strain to evaluate the bone behavior based on mechanostat theory (strain levels). Moreira et al. [122] have interpreted the results based on the mechanostat theory without describing the bone state. Dantas et al. [123] have compared results with mechanostat theory levels by calculating the octahedral shear strain values in root-analog and screw implants. They have found that root-analog implants can be a promising solution for dental implant options. Lee et al. [142] have evaluated the stability of the bones (cortical and cancellous), and the volume fractions according to strain levels of bone remodeling were estimated using the mechanostat theory. De la Rosa et al. [145] have examined the biomechanical performance of different bar-IOD designs by analyzing the stress and strain distribution on the bone with secondary stability. The mechanostat theory was taken into account as bone damage criteria.

These studies used mechanostat theory as a basis to describe the behavior of bone under mechanical loading. A reliable technique that is frequently employed in the field of biomechanics is the application of this theory (mechanostat theory or frost theory) with the use of the finite element method.

Finite element analysis involves several processes, including collecting data, 3D modeling (models reconstruction) models, mesh setting, boundary conditions, and loading. These procedures are performed with certain software, requiring expertise and skills.

II.4 Conclusion

All reviewed manuscripts in this chapter have certain limitations. The bone was considered isotropic and solid in most of the data analyzed in this review. The interior structure of bone tissue is porous and exhibits an anisotropic characteristic. The muscles, lips, and tongue forces were not applied in the computational analysis. The majority of studies are focused on the macro-level (or mesoscale), and there is a lack of data about the bone remodeling process using finite element analysis and implanted algorithms. It can be said that there is no established standard for performing finite element analyses in the dental implantology field. To acquire trustworthy FEA findings, it is necessary to use data from CT scans by using techniques to obtain the non-homogeneous and anisotropic properties. Nevertheless, finite element analysis is an effective tool to predict stress and strain in bone tissue and dental implant components as well as describe such phenomena broadly in the biomechanics field.

Chapter III Finite element analyses of porous dental implant designs based on 3D printing concept

III.1 Introduction

Titanium (Ti) and its alloys are biocompatible materials that are largely used in dental implant systems. Dense dental Ti implants exhibit excessive stiffness and mismatch with the surrounding bone thus causing stress shielding, aseptic loosening and implant failure [152][153]. Implant stability is divided into primary stability (mechanical stability) and secondary stability (osseointegration). The principle of osseointegration depends on the primary stability which is influenced by implant design, bone quality, and surgical protocol [154]. To attain long-term osseointegration and to maximize the implant life, researchers are working on designs of implants to find suitable ones. During mastication forces after implantation, appropriate stresses should be transferred to the surrounding bone but due to the dense metallic implants and stiffness mismatch between implant and bone, a very low level of stresses are transferred to the bone and major load is carried by the implant which may cause stress shielding and bone resorption [153][155][156]. To overcome the aforementioned problems, research has found that the application of porous implants might inhibit the effect of stress shielding to ensure the implant's longevity [157][158] [159]and increase the possibility of bone ingrowth[160]. Studies showed that porous implants show reduced stiffness which effectively stresses transfer to the bone and facilitate bone ingrowth [161][[162] [163][164].

Currently, additive manufacturing (3D printing) techniques have great potential in the biomedical industry, especially to manufacture complex designs of implants [165] [166][167]. Moreover, this technology can be used to customize implants for specific patient conditions, because it provides great control of porosity, micro surface roughness, making complex profiles [168][169][170]. 3D printing increased the potential in the field of implants due to quick production, the desired shape and fabrication bioinspired design [171][172][173].

The bone tissue has a complex behavior, consisting of organic components (such as collagen) which provide tensile properties and inorganic components (calcium, phosphorus) which are responsible for compression strength and stiffness [174]. Mandible consists of cortical bone which surrounds cancellous bone, the cortical bone has dense structures. However, the cancellous bone has a highly porous structure. Bone is classified on the mechanical properties such as Young's modulus, the thickness of the outer layer (cortical bone) and density [175]. Osteoporotic bone is a disease in elderly patients that decreases bone density [176]. Bone has the capability to continuously remodel itself through the activities of different cells, which include bone resorption by osteoclasts and bone formation by osteoblasts [177]. Wolff [178] defined a relationship between bone remodeling and the direction of loading via a process called mechanotransduction. Frost HM [179] redefined Wolff's law as the mechanostat hypothesis which is based on the level of strains [180]. Several approaches have been proposed in this concern [181][182][183][184]. Finite element analysis (FEA) is a well-known tool in the field of implants, it can easily predict the biomechanical behavior of implants and bones under various biomechanics conditions. Stress and strain analysis of the bone healing, bone-implant interface [185] [186] and implant design [187] has been the subject of multiple FEA studies [188][189][190][191][192][193][194][195][196][197][198][199]. Huang et al. [200] used FE analysis to investigate the effect of implant neck and cortical bone thickness on primary and secondary stability, they used four commercial implants of different sizes. Results showed that implant neck design has a role in micromotion and stress concentration in cortical bone. Ausiello et al. [89] numerically analyzed the effect of neck geometry of three implants of dense titanium with different angle platforms under a combined compressive and shear load on strain in the bone. The results showed that the straight neck produces more strain compared to the two other neck configurations. Jeng et al. [201] established the effect of implant neck wall thickness on

bone and implant component using nonlinear finite element analysis, they used three different implant sizes (diameters 4, 5, and 6 mm) of titanium grade 4 with three implant neck wall thicknesses of 0.45, 0.50, and 1.00 mm. They reported that increasing implant neck thickness can significantly decrease bone strain. Marcián et al. [202] studied the state of the bone under different loading conditions on fully osseointegrated and partially-integrated implants based on two approaches, the mechanostat hypothesis and tensile/compression yield strains. Results showed that dense trabecular architecture leads to an increased strain in alveolar bone, and non axial loading produce higher strain than axial loading. Mehboob et al. [203] established the effect of implant type and porosity on patient's bone and studies the state of the bone based on mechanostat hypothesis and by using FEA. They concluded that the highly porous implants in weak bone produce very strain intensity, and the dense titanium produce very low strain intensity.

This study aims to investigate the effect of implant neck design and porosity of mono-piece implant on secondary stability in healthy bone type III and the osteoporotic bone under different loading. The failure criteria and mechanostat hypothesis were used to examine the behavior and the state of the bone.

III.2 Materials and Methods

III.2.1 Construction of 3D models

A simplified section of mandible bone was constructed in NURBS (non-uniform rational basis spline) CAD (computer-aided design) software Rhinoceros 3D v6.0. 3D models of bone quality, implant design and implant porosity were also constructed.

III.2.1.1 Modeling of bone heterogeneity

Patients have different bone qualities which depend on age, everyday activity and food intake. Therefore heterogeneity in mandible bone is considered to construct 3D finite element models of the bones. Two types of bones are considered; healthy bone and osteoporotic bone. The model of bone type III (healthy bone) was constructed, the cortical bone is modeled around the cancellous bone with a thickness of 1.5 mm. Similarly, osteoporotic cortical bone also envelops the osteoporotic cancellous bone, which has lower Young's modulus to mimic lower bone density (**Figure III.1.a**). The height of the bone was 27 mm and the width was 10 mm.

III.2.1.2 Design of implant neck

Various types of implant designs are available commercially. Therefore, different implant designs are modeled to investigate their effect on bone. A typical mono-piece straight implant (one-piece) is selected for modeling in SolidWorks 2020. 3D models of three implants were created with the same dimensions (3 mm × 15 mm) as shown in **Figure III.1.b.** Three angles of the implant neck were designed as 0°, 10°, 15° which are named implant A, implant B and implant C, respectively. All components were assembled in SolidWorks with the consideration that dental implants were fully osseointegrated with the bone.

III.2.1.3 Designs of implant porosity

Conventional Ti alloy dense implants with various designs are used to replace defective teeth. Therefore, a dense Ti alloy implant and two porous implants were modeled to investigate their influence on the surrounding bone. Two states of porosity of Ti (63% porous and 77% porous) in addition to the bulk Ti alloy (Ti-6Al-4V), based on previous study [203] are illustrated in **Figure III.1.c**. The effective Young's moduli are used to mimic the porosity of the

dental implants to save the computational time and convergence of the simulations. Details of implant dimensions are shown in **Figure III.1.d**.

III.2.2 Mesh, loading and boundary conditions

All models are imported in the finite element (FE) software ABAQUS v6.20. All components are meshed with tetrahedral elements (C3D10), as shown in **Figure III.2.a** Five different mesh sizes (0.1, 0.2, 0.3, 0.4 and 0.5 mm) were used to investigate the accuracy of the results. It was determined that models with a size of 0.2 mm mesh size produce adequate accurate results, this determines the mesh size, total number of tetrahedral elements and nodes as listed in **Table III.1**. The regions interested are meshed with 0.2 mm mesh size, the rest ranged between 1 mm and 0.3 mm. The aspect ratio was less than 3 to ensure a good mesh quality. The total numbers of elements and nodes of all models meshes are reported in **Table III.1**.

Table III.1 *Total numbers of nodes and elements used in this study.*

Implants	**Cases**	**Number of nodes**	**Number of elements**
Implant A	(0° platform)	125995	84425
Implant B	(10° platform)	128604	86213
Implant C	(15° platform)	128833	86385

All materials simulated in this study are considered isotropic, homogeneous, and linearly elastic. **Table III.2** summarizes the properties of the materials used in this study.

Table III.2 *Properties of the materials.*

Components	Materials	Young Modulus (GPa)	Poisson's Ratio (ν)	References
Mandibular Bone	Healthy cortical bone	13.7	0.3	[141][101]
	Healthy cancellous bone	1.37		
	Osteoporotic Cortical bone	8.71		
	Osteoporotic cancellous bone	0.465	0.2	
Implant	Bulk titanium alloy (Ti-6Al-4V)	114	0.3	[203]
	77% porous implant	18	0.3	
	63% porous implant	9	0.3	

The following two occlusal forces are chosen in this study:

- 200 N is applied in the corono-apical direction (along the implant axis, named axial loading).
- 150 N is applied in the buccolingual direction (perpendicular to the implant axis, named buccolingual loading) [202].

The bottom surfaces of the bone are fixed in all axes, a bonded contact was used between bone-bone and bone-implant (fully osseointegrated), as shown in **Figure III.2.b**.

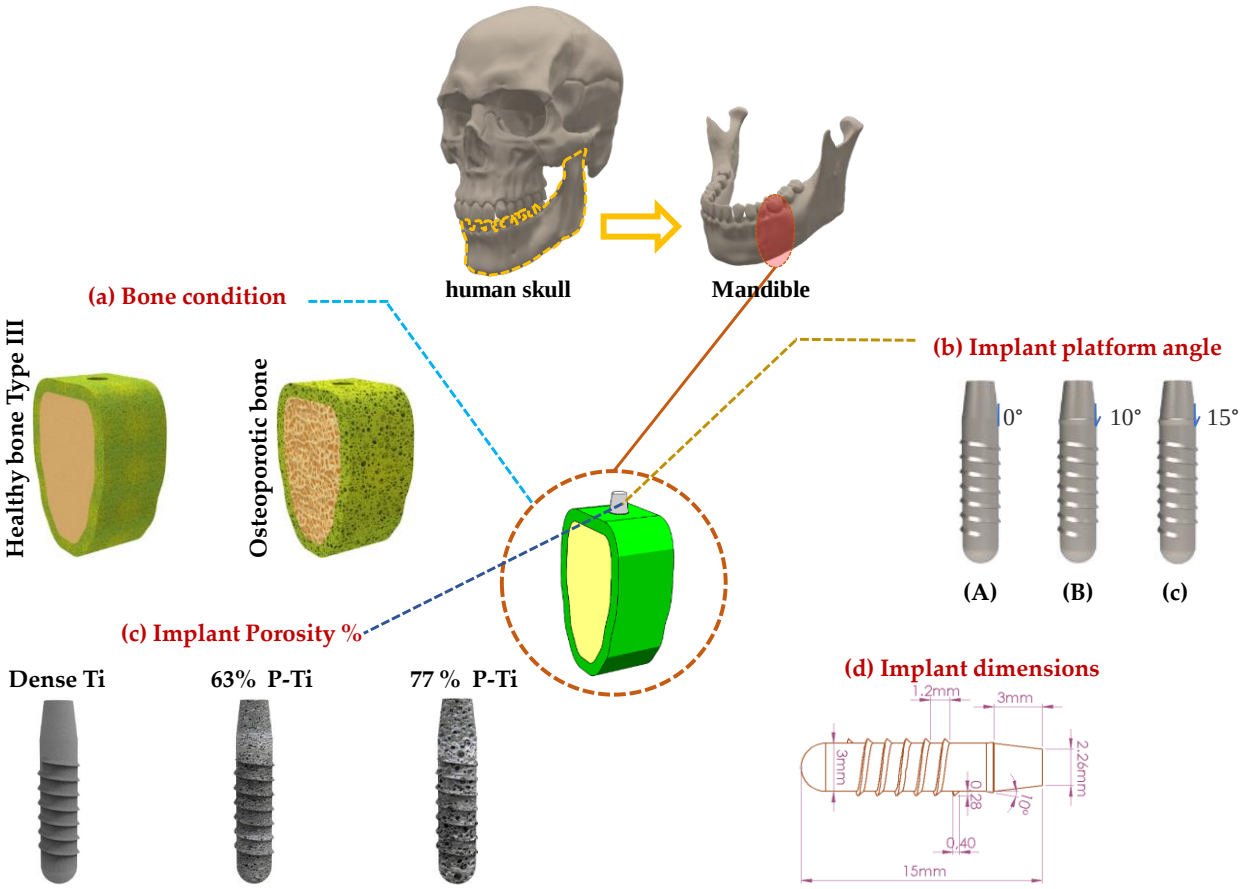

Figure III.1 *3D geometric models; (a) mandibular bone section, (b) neck platform angle, (c) implant porosity and (d) dimensions of the implant.*

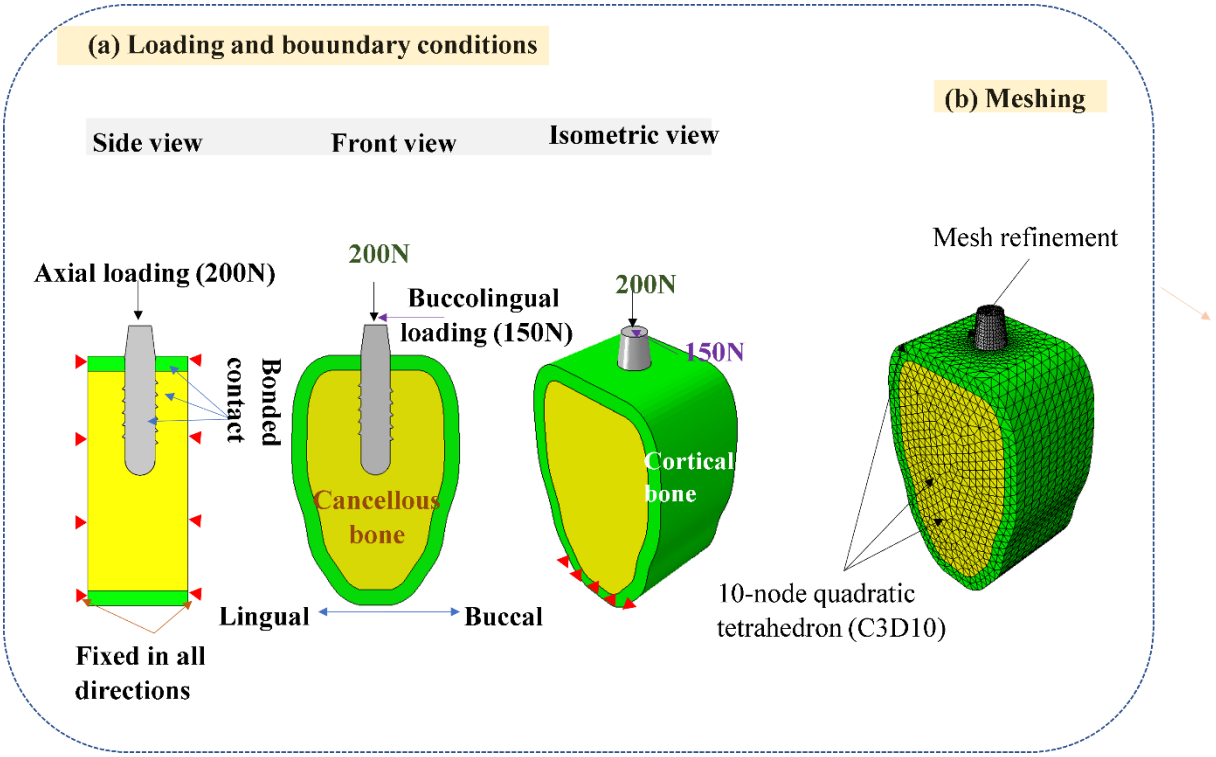

Figure III.2 *(a) Loading and boundary conditions and (b) 3D finite element mesh.*

III.3 Results

III.3.1 Von Mises stress in cortical bone

The von Mises stresses are investigated because it provides a more accurate state of the stress [193], it is commonly utilized in three-dimensional stress studies. The von Mises stress is referred to as equivalent stress and it is defined in terms of the principal stresses by **equation (1)** [204]. **Fig. 3** and **Fig. 4** show equivalent stress distribution in the cortical bone under axial and buccolingual loading respectively. The maximum von Mises stresses acting in cortical bone are reported in **Table 3**.

$$\sigma_e = \sqrt{\frac{1}{2}\left[(\sigma_1-\sigma_2)^2+(\sigma_2-\sigma_3)^2+(\sigma_3-\sigma_1)^2\right]} \qquad (1)$$

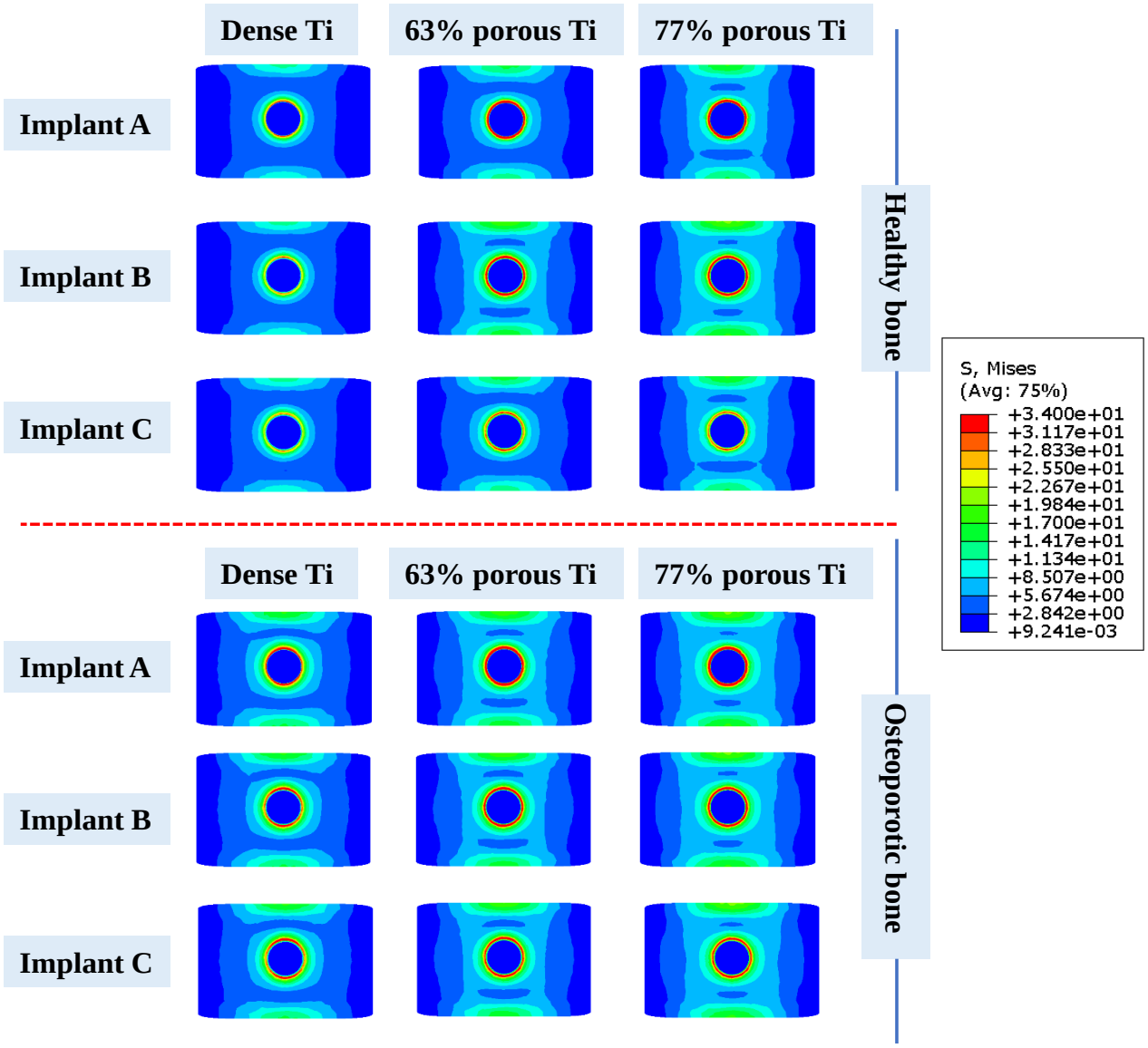

Figure III.3 *Von Mises stress distribution (in MPa) in the cortical bone under axial loading.*

It could be observed that results obtained for the cortical bone when applying buccolingual load were significantly greater than those obtained when the applied load was axial. **Figure III.3** and **Figure III.4** show that the stress distribution was higher in the cervical line at the implant-bone interface for all cases, this region has always been subject to more stress. The results indicated that maximum equivalent stress under axial loading was observed in the osteoporotic bone with a value of 74.8 MPa, and minimum stress reaching a value of 30.1 MPa in the healthy bone. Under buccolingual loading, the maximum von Mises stress was noticed in

the healthy bone with 304 MPa and the minimum stress in the osteoporotic bone with a value of 77 MPa. Overall, the reduction of stress in the bone under axial loading was due to an improvement in bone quality.

It was also observed that the design of the implant neck had an important effect on the distribution of stress at the cervical line of the cortical bone, as the angle of the implant neck changes the stress decreases which means that a straight neck generates great stress in both cases for the healthy and osteoporotic bone.

From the results, it was noticed that the stresses in the case of porous (77% and 63% porous Ti) implants are higher than those of the bulk Ti. Under axial loading, the maximum value of bone stress was 74.8 MPa and it was obtained in the osteoporotic bone with the 77% porous Ti. However, the lowest bone stress was obtained in the healthy bone with Bulk Ti implant reaching a value of 30.1 MPa. This increase is more noticeable in the case of osteoporotic bone and implant C. Under buccolingual loading, the maximum stress value (304 MPa) was obtained with the 77% porous Ti implant in the healthy bone. The minimum values (77 MPa) were observed for the Bulk Ti implant in the osteoporotic bone. Titanium's porosity percentage affects the variations of the stress in the cortical bone, due to different mechanical properties of the implants which mean the lower Young's modulus, the greater stress was observed in all cases. The yield stress *of human cortical bone was determined to be between 50-200* MPa [205]. Under axial loading, the stresses are less than the yield stress, but in the case of buccolingual loading in the porous implants the values are greater than the yield stress, this may cause mini-fracture of the bone.

III.3.2 Von Mises stress in cancellous bone

The distribution of stress is studied at the level of the cancellous bone because it has a major contribution to the process of bone remodeling. **Figure III.5** show the stress distribution under axial and buccolingual loading, maximum stresses are reported in **Table III.4** Under axial loading, higher stresses were observed in osteoporotic bone compared to the healthy bone. On the contrary, in the case of buccolingual loading, the stresses in osteoporotic bone are lower compared to healthy bone. Under axial loading, the maximum stress value (8.98 MPa) was obtained in the healthy bone, and the lowest value was observed in the case of osteoporotic bone with a value of 3.15 MPa in healthy and osteoporotic bone. It can be observed from the obtained results that the neck of the implant did not affect significantly the peak stress in the cancellous bone. On the other hand, the implant's porosity has a distinct effect. Stresses were higher in the case of porous implants than the bulk Ti, increasing the porosity of the implants led to producing more stress, this is what was achieved in previous studies [206]. Stresses under axial loading are much lower compared to the stresses generated under buccolingual loading. The strength of cancellous bone ranges from 0.1 to 16 MPa [207], and understanding the fracture of cancellous bone with implant systems requires an understanding of the yield and failure properties of cancellous bone.

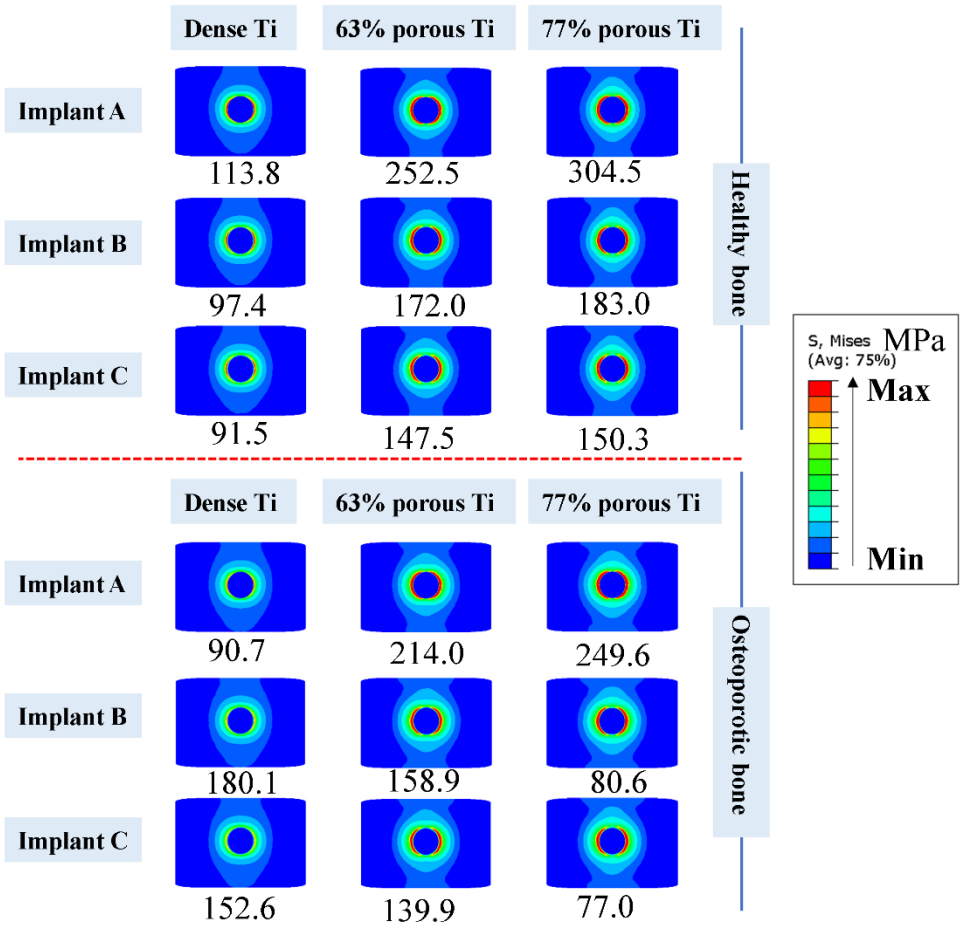

Figure III.4 *Von Mises stress distribution (in MPa) in the cortical bone under Buccolingual loading.*

Table III.3 *Maximum von Mises stress in cortical bone in MPa.*

	Osteoporotic bone			Healthy Bone type III		
	77% porous Ti	63% porous Ti	Bulk Ti	77% porous Ti	63% porous Ti	Bulk Ti
	Under axial loading 200N					
Implant A (0° platform)	74.8	61.5	42.8	65.1	58.7	35.7
Implant B (10° platform)	49.3	49.0	40.3	43.0	43.6	34.8

Implant C (15° platform)	41.0	39.3	38.6	35.2	33.3	30.1
	Under Buccolingual loading 150N					
Implant A (0° platform)	249.6	214.0	90.7	304.5	252.5	113.8
Implant B (10° platform)	180.1	158.9	80.6	183.0	172.0	97.4
Implant C (15° platform)	152.6	139.9	77.0	150.3	147.5	91.5

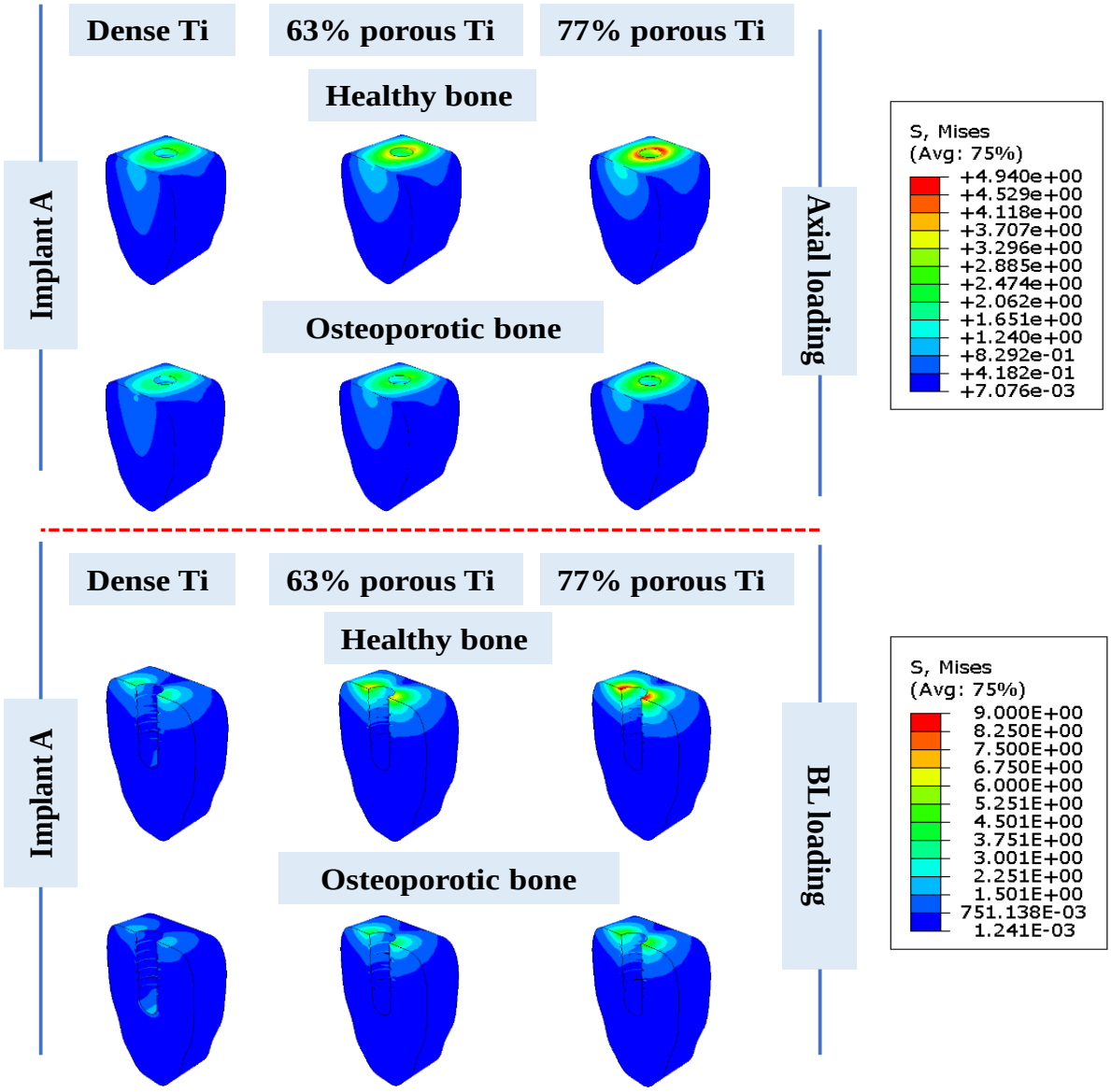

Figure III.5 *Von Mises stress distribution in cancellous bone in MPa under axial and buccolingual loading.*

Table III.4 *Maximum von Mises stress in cancellous bone in MPa.*

	Osteoporotic bone			Healthy Bone type III		
	77% porous Ti	63% porous Ti	Bulk Ti	77% porous Ti	63% porous Ti	Bulk Ti
	Under axial loading					
Implant A (0° platform)	3.24	2.78	2.42	4.94	4.12	3.17

Implant B (10° platform)	3.17	2.71	2.42	4.86	4.04	3.15
Implant C (15° platform)	3.15	2.68	2.41	4.84	4.02	3.15
			Under Buccolingual loading			
Implant A (0° platform)	5.28	4.06	1.99	8.98	7.18	3.61
Implant B (10° platform)	5.27	4.03	1.99	8.98	7.14	3.55
Implant C (15° platform)	5.26	3.98	1.96	8.98	7.09	3.55

III.3.3 Strains in cancellous bone

III.3.3.1 Principal strain: failure criteria

To explore the biomechanical response of the cancellous bone, principals' strains were analyzed because it has special meaning in failure prediction for isotropic materials. **Table III.5** lists the principal strain values obtained from the analyses. The maximum principal strain is generally tensile, and the minimum principal strain is compressive. The bone yield strains are 7300 με in compression and 6500 με in tension [208][209]. Based on the principal strain failure criterion we can study the risk of bone failure at the bone-implant interface by comparing the principals' strains with the yield strains of the cancellous bone. Depending on the obtained results, the principal strains were much higher in the osteoporotic bone compared to the healthy bone. In addition, it was observed that the buccolingual loading generates more strains than the axial loading. The maximum value of the first principal strain was 10190 με and the third principal strain was -10123 με, and this was obtained in case of osteoporotic bone under buccolingual loading. Under axial loading, the minimum value of the first principal strain was 1845 με and for third principal strain reach a value of -2391 με, it was observed in the healthy bone. However, there is no significant difference in peak strains between the three implant neck designs (A, B, C), but it should be mentioned that the implant surface porosity effect was clearly observed. A reduction in principal strains in cancellous bone was consistently observed when

implant porosity was increased. Under axial loading, the principal strains obtained were below the bone yield strains (6500 με, -7300 με). Contrarily, under buccolingual loading with the porous Ti in the osteoporotic bone the values were above the bone yield strains, as shown the comparison in **Figure III.6**. Under BL loading, in healthy bone with 77% porous Ti, the values of the principals strains converge to the limit (6500 με, -7300 με). The lowers principals' strains were noticed with the Bulk Ti compared to the porous Ti in the healthy bone under the both loading.

Table III.5 *Principals micro-strain in cancellous bone (με).*

		Osteoporotic bone			**Healthy Bone type III**		
		77% porous Ti	**63% porous Ti**	**Bulk Ti**	**77% porous Ti**	**63% porous Ti**	**Bulk Ti**
		Under axial loading					
Implant A (0° platform)	Max	5027	4674	4422	2184	2063	1898
	Min	-5104	-4208	-3372	-3112	- 2453	-1572
Implant B (10°platform)	Max	4656	4570	4654	2105	1982	1845
	Min	-5007	-4193	-3387	-3058	-2389	-1579
Implant C (15°platform)	Max	4666	4593	4323	2095	1960	1869
	Min	-5003	-4188	-3389	-3042	-2377	-1580
		Under Buccolingual loading					
Implant A (0° platform)	Max	9949	7440	3942	6264	4907	2416
	Min	-10160	-7617	-4306	-6375	-5007	-2532
Implant B (10°platform)	Max	10190	7590	3878	6386	5008	2419
	Min	-10200	-7606	-4109	-6395	-5002	-2416
Implant C (15°platform)	Max	9964	7351	3758	6322	4891	2335
	Min	-10123	-7530	-3764	-6353	-4955	-2391

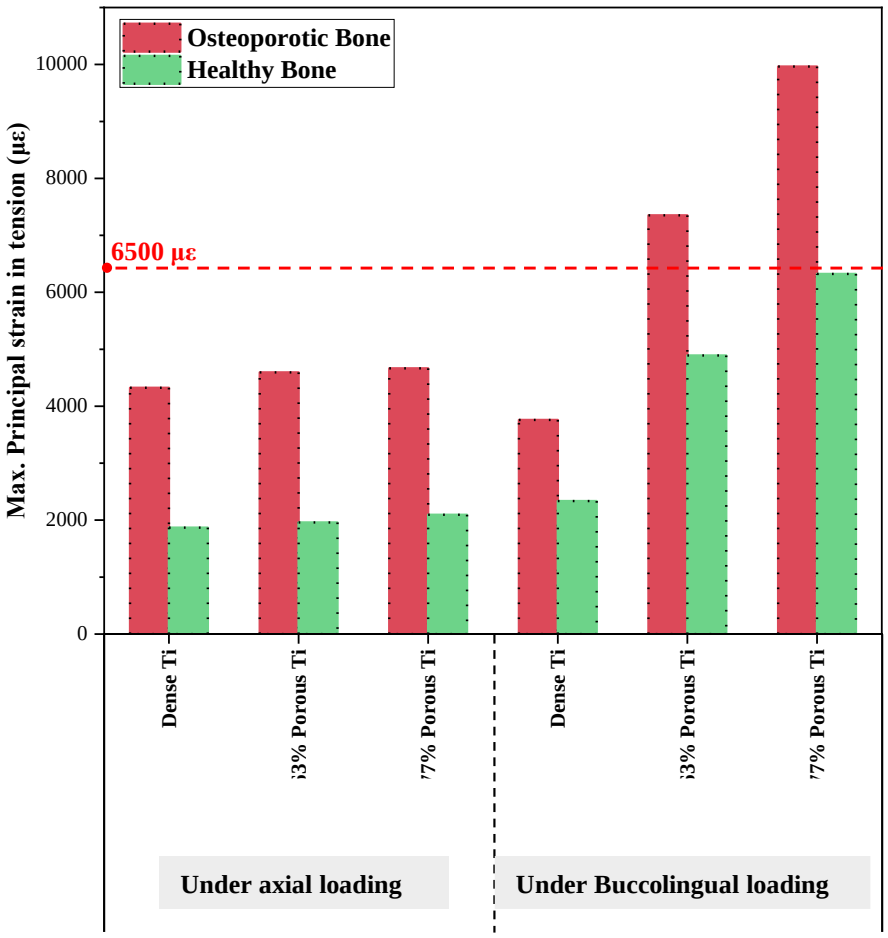
Osteoporotic Bone
Healthy Bone
Max. Principal strain in tension (με)
10000
8000
6000
4000
2000
0
6500 με
Dense Ti
Under axial loading
Under Buccolingual loading

(a)

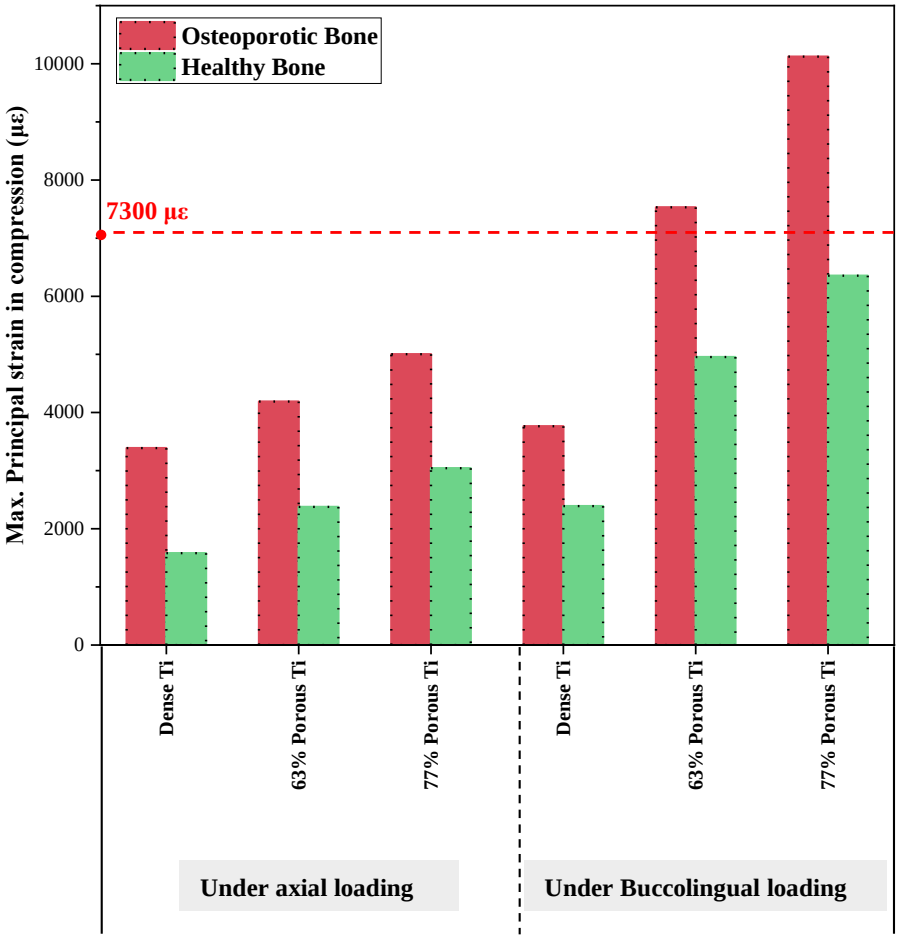

(b)

Figure III.6 *Histograms show the comparison in principals' strains; (a) in tension and (b) in compression.*

III.3.3.2 Strain intensity: mechanostat hypothesis

Another approach for analyzing the response of cancellous bone under biomechanics conditions is the use of the mechanostat hypothesis which categorizes bone behavior according to the intensity of the strain [210].

Figure III.7 exhibits the concept of the mechanostat hypothesis and indicates the different thresholds for bone behavior. According to the mechanostat hypothesis, effective strain below 1000 με cause disuse atrophy, the strain between 1000–1500 με represent adapted state which

means bone homeostasis is maintained, the strain between 1500-3000 με cause the physiological overload state which indicates an increase in bone mass, above 3000 με leads to bone damage, and above 25000 με leads to catastrophic fracture [15]. Strain intensity was calculated by the following formula (Equation 2) [204]:

$$\varepsilon_i = \frac{1}{\sqrt{2}(1+\nu)}\sqrt{(\varepsilon_1-\varepsilon_2)^2+(\varepsilon_2-\varepsilon_3)^2+(\varepsilon_3-\varepsilon_1)^2} \qquad (2)$$

Table III.6 *Strain intensity in cancellous bone.*

	Osteoporotic bone			**Healthy Bone type III**		
	77% porous Ti	**63% porous Ti**	**Bulk Ti**	**77% porous Ti**	**63% porous Ti**	**Bulk Ti**
	Under axial loading					
Implant A (0° platform)	2690	2064	1570	1668	1 198	687
Implant B (10° platform)	2654	2050	1490	1662	1180	687
Implant C (15° platform)	2644	2034	1519	1651	1175	684
	Under Buccolingual loading					
Implant A (0° platform)	5000	3738	2012	3432	2606	1307
Implant B (10° platform)	4950	3726	2016	3450	2560	1306
	4928	3682	2008	3442	2544	1302

Implant C (15° platform)	

Results indicate that the strain intensity is higher in the case of osteoporotic bone compared to the healthy bone. The maximum value of strain intensity was 5000 με and it was obtained under buccolingual loading in the osteoporotic bone, and the lowest strain intensity was obtained under axial loading in the healthy bone with 687 με. It was observed that the buccolingual loading produces higher strain intensity than the axial loading Under axial loading, it was noticed that the strain intensity was below 3000 με in the osteoporotic and healthy bone. We also noticed that when the implant neck is changed, the strain intensity does not alter significantly. The obtained data show that implant porosity has a significant impact on strain intensity. Under axial loading, The maximum value of strain intensity was 2690 με in osteoporotic bone with 77% porous Ti, and the lower value (687 με) in healthy bone with the bulk Ti. Under BL loading, the strain intensity is higher than 3000 με with 77% and 63% porous Ti in the osteoporotic bone. Likewise, we can also observe this comparison in the case of healthy bone with the 77% porous Ti implant. This analysis confirms what has been achieved in the previous section where the principals' strains were examined. **Figure III.8** represents a comparison in strain intensities based on the mechanostat hypothesis in cancellous for various porous Ti. In the case of dense pure titanium under axial loading in the healthy bone, the values of strain intensity are lower compared to 1000 με which is the limit of the atrophy stage. Instead, in the case of osteoporosis the strain intensity range between 1000-1500 με, this is the interval of the adaptive state. Therefore, bulk dense titanium can cause stress-shielding in the healthy bone with much less strain intensity. Nevertheless, it can improve the performance of bone in the case of osteoporosis.

III.3.4 Influence of bone quality

The change of bone quality is expressed as a variation in the young modulus. It was observed that bone quality has a clear effect on the distribution of stresses and strains so that the strain intensity of the bone was reduced with the improvement of bone quality. Based on mechanostat hypothesis, the bone remodeling in the case of osteoporosis behaves differently than it does in healthy bone.

III.3.5 Influence of implant neck design

In order to study the influence of implant design on implant-bone interface, three different neck implants were designed. Maximum von Mises stress in cortical bone was found with implant A compared to implant B and C, this indicates that the shape of the implant neck influences the stress distribution, and an implant with a straight neck produce more stress on the marginal bone. In addition, no significant difference was observed at the level of the cancellous bone when the implant neck was changed.

III.3.6 Influence of implant stiffness

Regardless of implant neck design or bone quality, decreasing the stiffness of the implants increased the amount of stress and strain in the bone. In comparison to Bulk Ti, porous Ti implants of varied stiffness produce more strain and stress. Based on the mechanical stimuli, porous Ti implants provide a distinct biomechanical environment in the surrounding bone, and dense Ti implants may cause atrophy or stress-shielding because they transfer less stress in the bone.

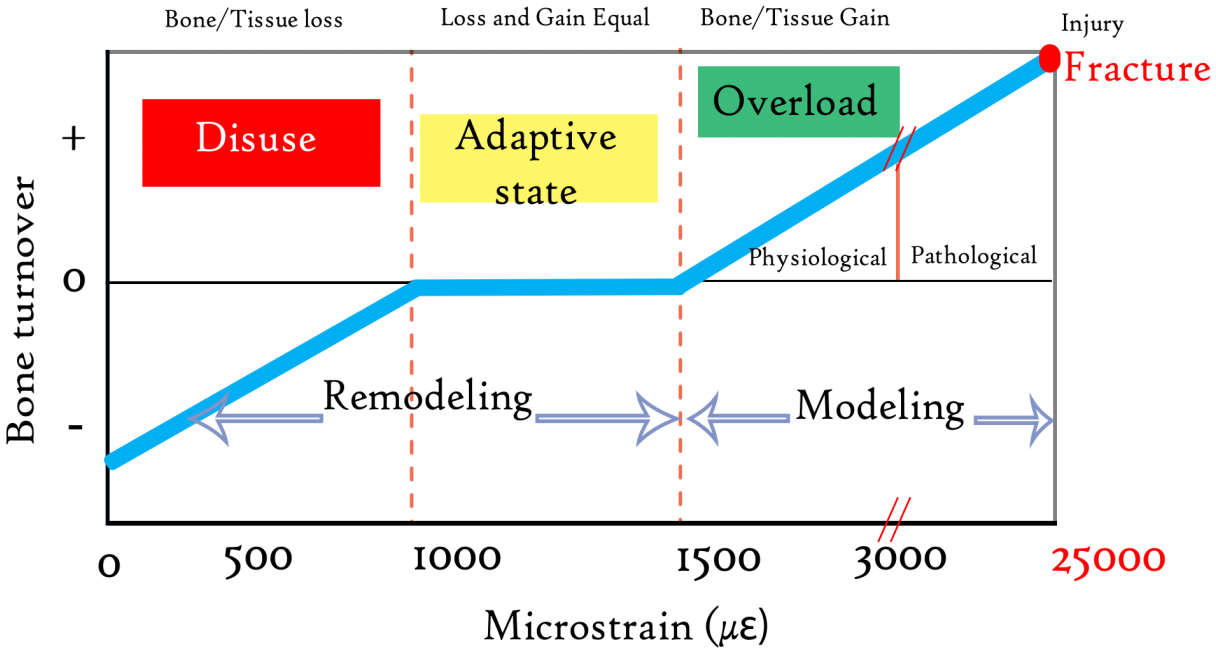

Figure III.7 *Concept of mechanostat hypothesis* [211].

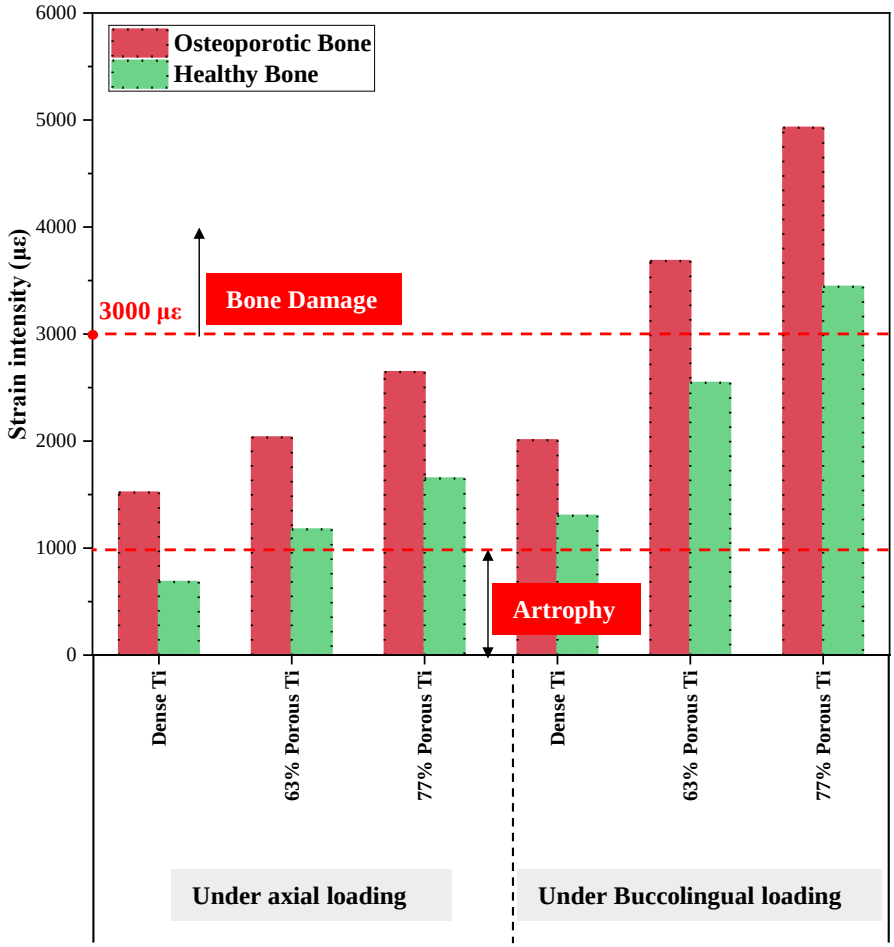

Figure III.8 *Histogram shows a comparison in strain intensities based on mechanostat hypothesis in cancellous bone for porous Ti and bulk implants under different loading and bone conditions.*

III.4 Discussion

Ti and its alloys are widely used in the fields of implants due to their high biocompatibility. However, dense forms of Ti may have several disadvantages, such as insufficient osseointegration capacity, and stress shielding due to the high Young's modulus [212]. Porous Ti has been developed to be a promising alternative to bulk Ti for dental implant applications [213].

The present study examines the effect of bone quality, implant neck design, and the surface porosity of implant under certain biomechanics conditions (loading) to have enough knowledge of bone behavior. The results indicate that the stress was higher in osteoporotic bone compared to healthy bone. Osteoporosis can develop fractures and make the bone more fragile leading to bone loss or secondary osteoporosis [214]. It is necessary to have much knowledge of the cortical bone thickness, density, and bone health conditions, due to their role on the stress distribution pattern. It is therefore essential to take into account that a straight implant neck is not the preferred choice to achieve an osseointegration environment at the bone-implant interface because it can deteriorate the load dissipation in the bone tissue [89].

The results of this study showed that the neck design of the implant influences cortical bone-implant contact at the cervical region. Thus, stress increasing can lead to implant mobility and bone fracture in case stress exceeds yield stress. This may lead to bone loss or forming a pocket that allows bacteria colonialization [215] then the bone cannot be repaired by bone grafting. Conversely, the design of the neck did not affect the distribution of stress at the level of the cancellous bone

This study showed that the stress was lower in cancellous bone compared to cortical bone, due to the variation in stiffness, cortical bone is stiffer (have higher Young's modulus) than cancellous bone. This explains why it is a protective layer around the internal cavity. The principal strains were analyzed to compare them with the yield strains, based on yield criteria. The results show that compressive strain was high and that may lead to maintaining the integrity of a bone-implant interface. However, tensile strains may lead to stretching the bone. Results indicate that in the case of 77% porous Ti in the osteoporotic bone under buccolingual loading, the principal's strain was higher compared to yield strains, and that can lead to bone damage or fracture. The results reflect that porous Ti implants generate more strains than bulk Ti in cancellous bone. This means the principal strains were increased by increasing the porosity.

Strain intensity was calculated to study it with a mechanostat hypothesis, using this hypothesis is very common in research [203][210][202][216] to predict the functional response of the bone. The results show that low strains in cancellous bone for dense titanium (Bulk Ti) may result in bone atrophy especially under axial loading. In contrast, the higher strain may lead to microfractures in peri-implant bone [217] and subsequently implant failure. Reducing implant stiffness is of great importance for the bone remodeling process. Therefore, it can prevent stress shielding which affects the stability of the implant and induces bone resorption. In vitro [218], a study has reported the relationship between porous substrates with rough surfaces and cell adhesion which improve the process of osseointegration and prevent the phenomenon of stress-shielding, this has also been proven in an animal experimental study [219]. It is critical to take into consideration that low Young's modulus can cause bone damage when strain exceeds 3000 με, based on the mechanostat hypothesis, and this is what was confirmed using yield strains intervals.

The results showed that stress and strain under buccolingual are higher than axial loading. The reason is that load that may represent the lateral loading produces more shear forces. Non-axial loads (in linguo-buccal or mesio-distal direction) are most destructive compared to axial loads. It is necessary to design dental implants based on bone conditions to attain fully osseointegration at the peri-implant bone and inhibit stress shielding. Additive manufacturing will be a better option to produce porous implants for their mechanical adapted properties.

It's important to note that the study has some limitations, the behavior of the bone cannot act as isotropic and homogenous. Moreover, porous cancellous bone and porous implants were simplified by solid models to save the computational cost. The role of the gums and the effects of forces applied by oral cavity muscles were not considered. The simplification of the models in this study allows us to do an approximate analysis. Thus, the findings of the study should be supported by more clinical trials.

III.5 Conclusion

This study concludes that the effect of bone quality, neck platform configurations and implant porosity is more pronounced. The biomechanical response of healthy bone and osteoporotic bone is different. In the case of osteoporosis, the bone is maintained with dense titanium. Instead, in the case of healthy bone, the strain generated with dense bulk titanium may lead to bone atrophy. Straight's implant design is not the preferred option for the cortical bone.

1. The greater the angle of the neck, the less stress on the cortical bone.
2. The lower the porosity of the implant, the better the behavior in relation to bone stress/strain in osteoporotic bone under axial loading.

3. The higher the porosity of the implant, the better the behavior in relation to bone stress/strain in healthy bone.
4. The better the bone quality, the less bone stress.
5. Very low and very high porosities of implants cause bone resorption and microfracture, respectively, thus optimal implants are suggested for healthy and osteoporotic bones.

The porous titanium fabricated via 3D printing techniques (additive manufacturing) can be a good alternative to reduce stress-shielding and for bone remodeling. Additive manufacturing technology allows us to improve the mechanical properties of porous titanium, due to its advantages on surface modification, control design of pores structures. The results of this study need more investigations including animal trials to validate simulated results.

Chapter IV Concept of functionally graded materials (FGM) For Dental Implants

IV.1 Introduction

Dental implants made of titanium alloys (Ti) are one of the most reliable alternatives to replace defective teeth due to their excellent biomechanical properties [220]. Conventional implants are made of dense titanium that is fabricated as solid structures, thus exhibiting 5-10 folds higher stiffness than bone [221]. This high mismatch of implant stiffness and bone may cause stress shielding, aseptic loosening, and bone resorption [222]. Therefore, studies have explored the use of porous titanium to reduce the stiffness of implants and mimic the bone properties [223] to overcome the aforementioned complications. Moreover, bone remodeling around implants is influenced by many factors, such as implant material and design [224], implant surface[225], and bone quality [136]. Higher stiffness implants take more load and transfer fewer stresses and strains to the surrounding bone. The amount of strain in surrounding bone determines the remodeling process under occlusal loads [107], and this was proved by Wolff's Law [178].

Frost [180] described the mechanostat theory as a change in strain level and corresponding changes in bone density. Bone density is a measurement that is frequently used to assess clinical findings in bone health. Each person may have different bone densities. Some elderly people have osteoporosis, which causes a decrease in bone density. Also, bone density varies in different age groups, genders, and diseases. Furthermore, several methods in biology have been used to examine complex physical phenomena such as thermal damage and the temperature in living tissue with laser irradiation [226][227]. *Laser therapy has been proposed to reduce clinical markers of peri-implant tissue inflammation* [228]. Many techniques of thermal therapy and heat treatment have been considered one of the best existing alternatives for modern clinical treatments [229–234]

To overcome the aforementioned complications, researchers have been working to develop new materials and bioinspired designs of structures using additive manufacturing (3D printing) to obtain mechanical properties well compatible with bone tissue [235] [236]. Low stiffness additively manufactured porous implants are promising alternatives to mimic the properties to meet biomechanical clinical needs. To attain excellent performance of such implants, the use of functionally graded designs and multi-objective optimization is necessary for optimal design and to further reduce the possibility of complications [237][238]. All these efforts and contributions have resulted in significant advancements in the field of orthopedic and dental implants.

To simulate different bone densities, the designs of implants, and various mechanical loads, several researchers have demonstrated the great success of computer methods in evaluating implant performance [189,202,239–242]. Jafari et al. [72] have studied the influence of implant materials (functionally graded material (FGM), hydroxyapatite (HA)-coated and Ti) on bone remodeling. Their findings concluded that the most promising model is the radial FGM dental implant, and the second-most preferable choice is the HA-coated dental implant compared to the dense titanium. Ghaziani et al. [243] have examined the effect of FGM with titanium/Hydroxyapatite fixtures on bone remodeling around osseointegrated trans-femoral prostheses. The results showed that using a radial FGM with low-stiffness material in the outer layer and less metal composition significantly improved bone remodeling. Despite the numerous studies [115,244,245] that investigated the bone quality and implant materials, few papers have evaluated the effect of FGM porous Ti implants on surrounding bone strains.

In this study, different bone densities (0.6, 0.7, 0.8, 0.9 and 1 g/cm^3) with various designs of implants, including FGM Ti (axial and radial), conical and cylindrical implants, were simulated

under an axial load of 200N to mimic the masticatory force. The mechanostat theory was used to evaluate bone behavior. The levels of stress and strain were analyzed using mechanostat theory in different cases and suitable designs of implants were suggested according to the bone density.

IV.2 Materials and Methods

IV.2.1 Construction of three-dimensional models

A section of mandible bone with a height of 22 mm was designed in the NURBS (non-uniform rational basis spline) CAD (computer-aided design) software Rhinoceros 3D v4.0 (NURBS Modeling for Windows, Seattle, WA, USA). The cancellous bone is surrounded by a 1.5 mm layer of cortical bone to mimic the real bone (Type III Bone [175]). Five conditions of bone density (0.6, 0.7, 0.8, 0.9 and 1 g/cm^3) were used as shown in **Figure IV.1.a.** Three-dimensional solid models of two implants (conical and cylindrical) were created using Solidworks 2020 (Dassault Systèmes, Vélizy-Villacoublay, France). The implant and abutment were considered as mono-piece (single piece), with a height of 18 mm and a diameter of 4 mm. The geometry and dimensions of the dental implants are shown in **Figure IV.1.b.**

IV.2.2 Designs of FGM dental implants

Figure IV.1.b.displays four FGM implant designs in addition to the conventional implant. Two configurations were created using Abaqus software v6.14 (Dassault Systèmes, Vélizy-Villacoublay, France) with the partitioning cells method. FGM implants were graded in axial and radial directions, which were axially functionally graded material (FGM A) and radiallly functionally graded material (FGM R). In these designs, implants were divided into four equal sections in axial and radial directions for FGM A and FGM R, respectively. The implant has a length of 14 mm, making each section 3.5 mm vertically for FGM A. The implant has a diameter

of 4 mm, for FGM R, each section was modelled with a thickness of 1 mm. The threads are included in the external section. In all configurations, each section represents different porous titanium with different Young's modulus (53 GPa, 31 GPa, 18 GPa, and 9 GPa, listed in **Table 1**). The FGM A implant was designed with two combinations, the one with the highest stiffness at the top section and the least at the bottom section, and vice versa. FGM A-53 has a Young's modulus of 53 GPa on the top section and 9 GPa on the bottom section, as shown in **Figure IV.1.b.** Similarly, FGM A-9 A has a reverse sequence (9 GPa on the top and 53 GPa on the bottom). The FGM R implant also has two combinations. FGM R-53 is a radial functionally graded material with a Young's modulus of 53 GPa on the implant's outer section and 9 GPa on the implant's inner section. In reverse order, the same goes for FGM R-9 (9 GPa on the outside section and 53 GPa on the internal section). The first part of our simulations was to evaluate the effect of the conventional implant with conical and cylindrical shapes on all bone densities and the second part was to examine the impact of FGM implants on the strain distribution in the bone densities (0.9 and 1 g/cm^3) adversely affected (bone loss) by conventional implants.

IV.2.3 Properties of materials used in simulations

All materials used in this study were considered isotropic, homogeneous, and linearly elastic. Carter and Hayes [246] investigated the relationship between nominal modulus and apparent density in the cancellous bone as shown in **Eq. 1**. The below equation was used to calculate different Young's moduli for different bone densities of the cancellous bone [247].

$$E = C\rho^3 \qquad (1)$$

Where E is the nominal Young's modulus in MPa, C is 3790 MPa·cm^9/g^3 and ρ is the bone density in g/cm^3. Five values of bone density were chosen in this study (0.6, 0.7, 0.8, 0.9, 1

g/cm^3). All the materials properties used in the finite element simulations were taken from the literature, as shown in **Table IV.1**.

Table IV.1 *Properties of the materials.*

Components	Materials	Young's Modulus (GPa)	Poisson's Ratio ν	References
Mandibular Bone	Cortical bone	13.7	0.3	[141]
	Cancellous bone	0.818 (with 0.6 g/cm^3)	0.3	
		1.30 (with 0.7 g/cm^3)		
		1.940 (with 0.8 g/cm^3)		
		2.762 (with 0.9 g/cm^3)		
		3.790 (with 1 g/cm^3)		
Crown	Feldspathic porcelain	82.8	0.33	[185]
Implant	Dense Titanium (Ti-6Al-4V)	114	0.3	[192] [203]
	Porous Ti (30 %)	53.84	0.3	
	Porous Ti (47.3 %)	31.49	0.3	
	Porous Ti (62.8 %)	18.33	0.3	
	Porous Ti (77.6 %)	9.11	0.3	

IV.2.4 Mesh, loading, and boundary conditions

All models were imported into ABAQUS v6.14 (Dassault Systèmes, Vélizy-Villacoublay, France) to run the simulations. The interfaces between bone and implant were considered perfectly bonded (fully osseointegrated) [72]. An axial load of 200 N was applied on the top of the implant as shown in **Figure IV.2**. The intensity of 200 N was chosen as a mean of vertical masticatory force [115][248]. The bottom surfaces of the bone were fixed in all axes.

The bone-implant interface was refined with tetrahedral elements of type C3D10, and the regions away from the contacting area were meshed by coarser elements, as shown in **Figure**

IV.2. A mesh convergence analysis was carried out to ensure that the FE model's prediction accuracy was unaffected by the mesh element size. The element sizes for cortical bone, cancellous bone, and the implant were 0.06 mm, 0.08 mm, and 0.2 mm, respectively. An aspect ratio of less than 3 was verified to improve mesh quality and ensure the accuracy of the results.

1.1.Mechanostat hypothesis

According to Frost's [180] mechanostat theory, the remodeling response of bones depends on the level of strain exerted. The mechanostat theory identifies five main ranges of strain and bone remodeling accordingly [15]:

- Bone atrophy *for* $\varepsilon_{oct} < 1000\mu\varepsilon$
- Bone homeostasis *for* $1000\mu\varepsilon < \varepsilon_{oct} < 1500\mu\varepsilon$
- Bone gain *for* $1500\mu\varepsilon < \varepsilon_{oct} < 3000\mu\varepsilon$
- Bone damage *for* $\varepsilon_{oct} > 3000\mu\varepsilon$
- Bone fracture *for* $\varepsilon_{oct} > 25000\mu\varepsilon$

Where ε_{oct} is the octahedral shear (equivalent) strain, representing the most appropriate strain for the mechanostat theory [249], which was calculated by **Eq. 2**.

$$\varepsilon_{oct} = \frac{2}{3}\sqrt{(\varepsilon_1 - \varepsilon_2)^2 + (\varepsilon_2 - \varepsilon_3)^2 + (\varepsilon_3 - \varepsilon_1)^2}$$

Where ε_{oct} is the octahedral shear strain, ε_1, ε_2 and ε_3 are the principal strains in x, y, and z directions.

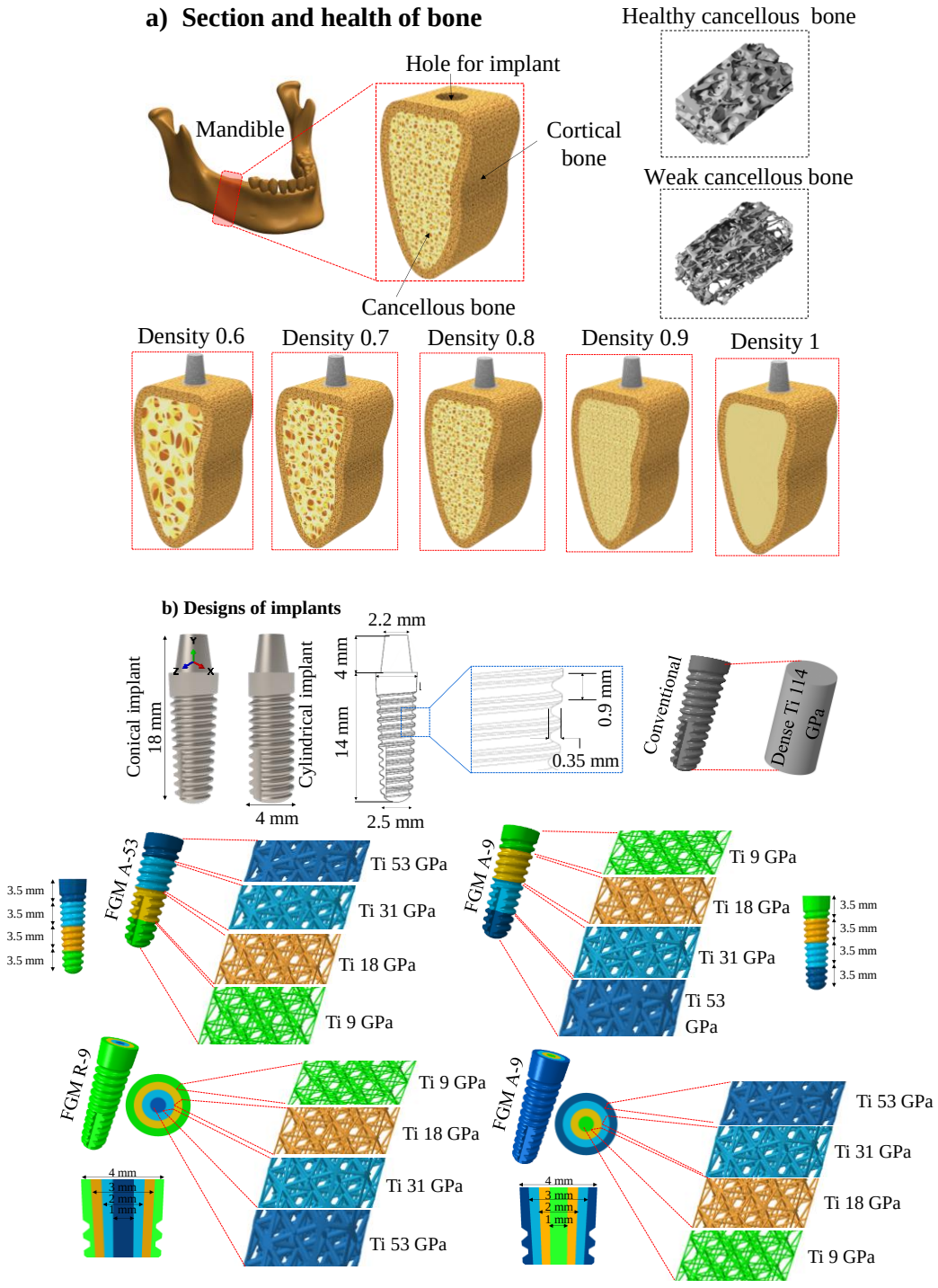

Figure IV.1 *Construction of finite element models; (a) section and health of bone, (b) designs of implants.*

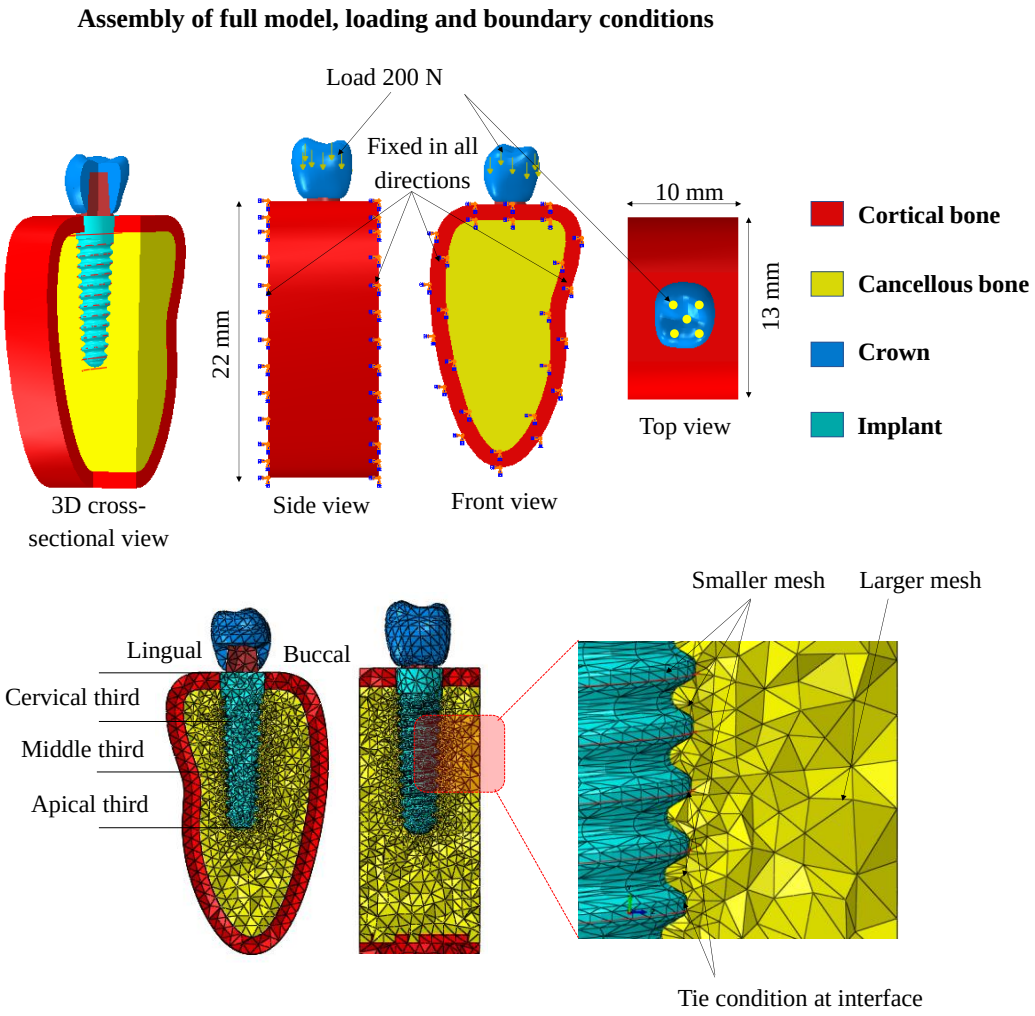

Figure IV.2 *Assembly, loading, and boundary conditions.*

IV.3 Results

Finite element models of different bone densities were simulated when different types of implants were inserted into bones. The results are presented to estimate the levels of displacements (μm: micrometer), strain (με: microstrain), and stresses (MPa: Megapascal) in different bone densities.

IV.3.1 Effect of implant design on bone density

IV.3.1.1 Displacements in cancellous bone

The displacement patterns of all cases are illustrated in **Figure IV.3**. The maximum displacement was found at the interface between bone and implant. The highest values were found to be concentrated at the adjacent cortical bone on top, and then gradually decreased to the apical region in cancellous bone. The maximum value of displacement was 6.05 µm and it was observed with the conical implant when the bone density was 0.6 g/cm^3. In contrast, the lowest value of 2.07 µm was observed when bone density was 1 g/cm^3. As the bone density increased, a reduction in the displacement was observed. The cylindrical implant followed the same pattern, with no significant differences, as shown in **Figure IV.4.**

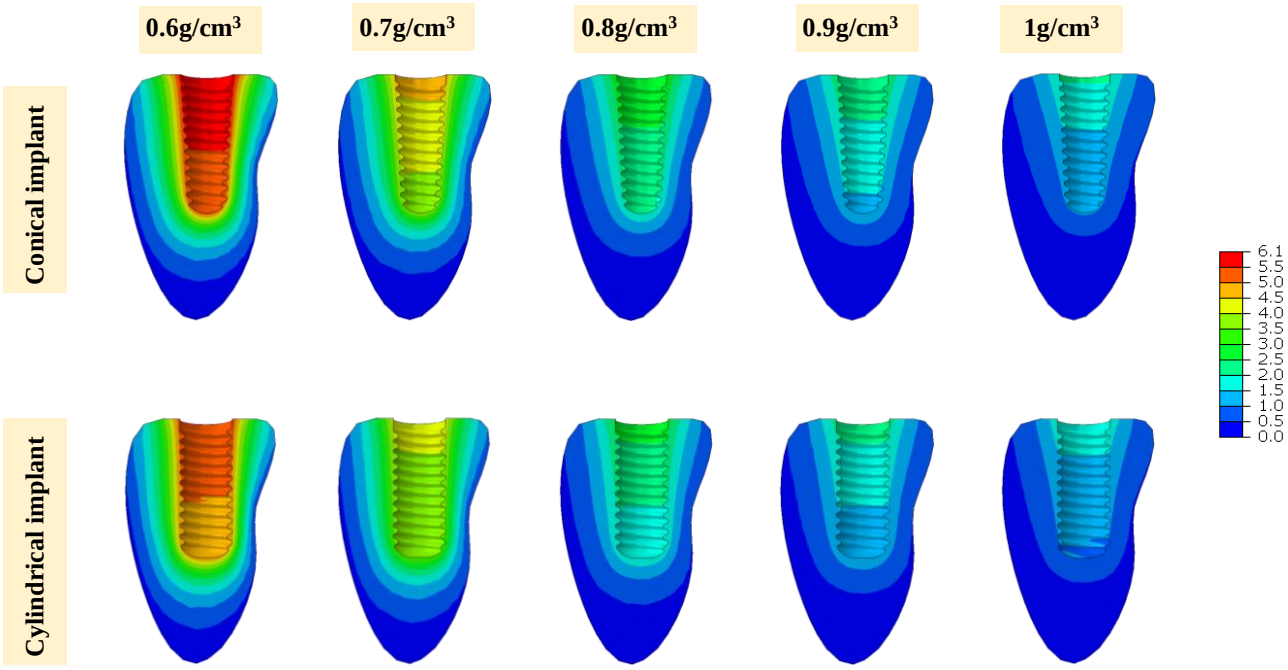

Figure IV.3 *Displacement distribution (µm) induced by conical and cylindrical implants in cancellous bone with different bone densities.*

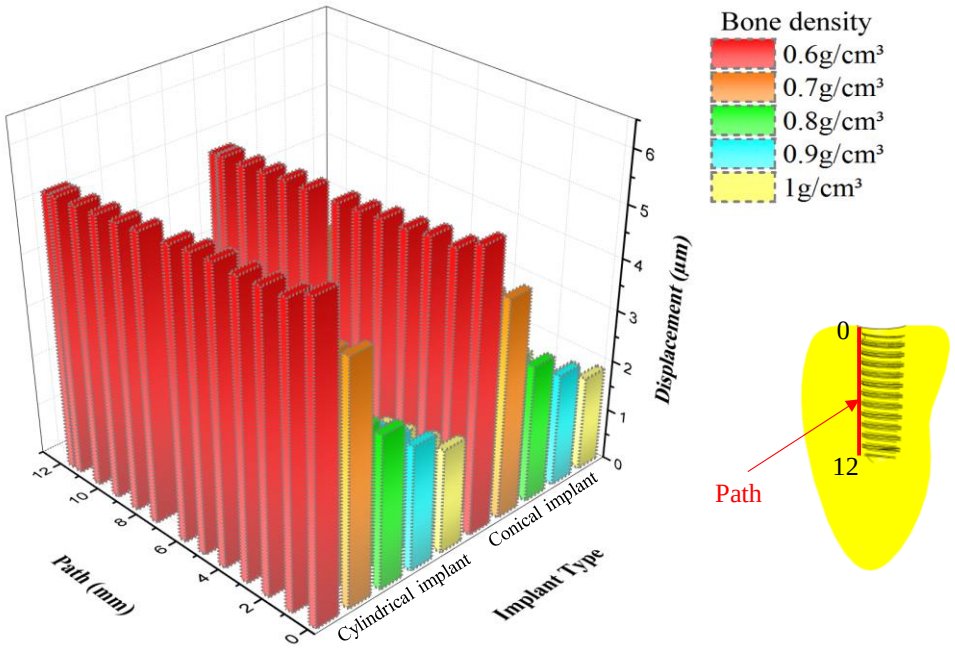

Figure IV.4 *Maximum displacement (μm) from the cervical region to the apical region.*

IV.3.1.2 Strains in cancellous bone

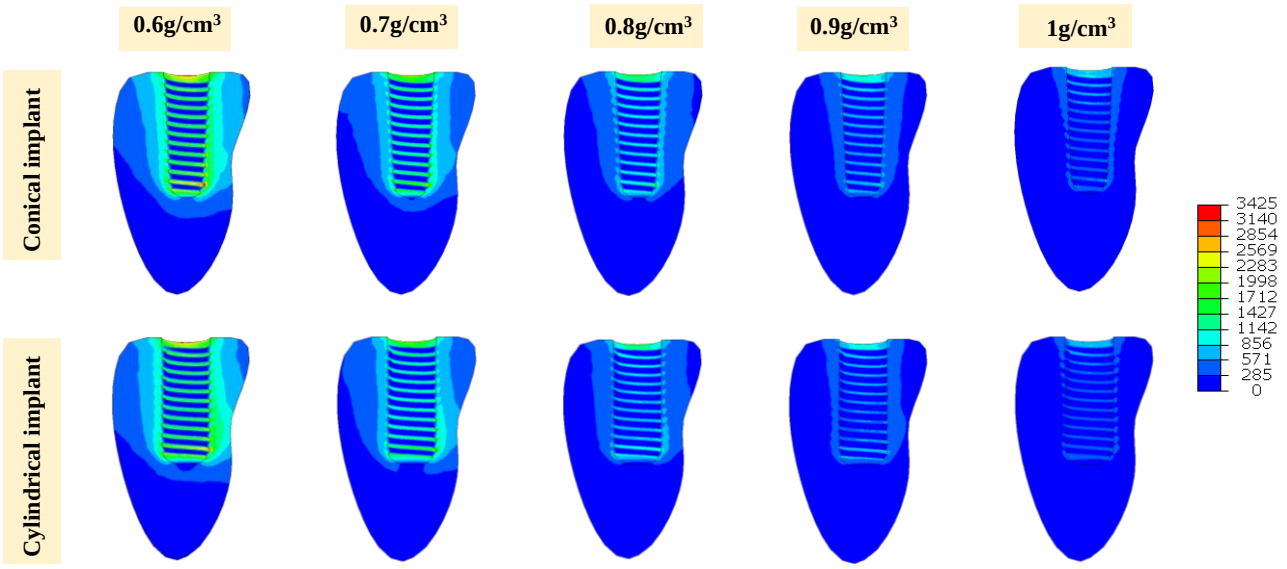

Figure IV.5 *Contour plots showing the first principal strains induced by conical and cylindrical implants with bone density variation.*

Bone remodeling is regulated by the level of strains in the surrounding bone. **Figure IV.5** shows the maximum principal strain in the cancellous bone under an axial load of 200 N. It was

observed that the maximum principal strain was concentrated at the top of the interface between cortical and cancellous bone. The highest strain concentrations were found in the conical implant with the lowest bone density of 0.6 g/cm^3. It was also observed that the implant design (conical or cylindrical implant) did not affect significantly the concentration of strains in the surrounding bone. The maximum value of octahedral shear strain was 3184 με and it was obtained with the conical implant when bone density was the lowest (0.6 g/cm^3). In contrast, the lowest value of 648 με was obtained in the cylindrical implant when the bone density was the highest (1 g/cm^3). These findings indicate that strains were increased by decreasing the bone density and vice versa. However, regardless of bone density, the implant type did not affect the peak strain significantly.

IV.3.1.3 Stresses in implants

Figure IV.6 shows the equivalent von Mises stress distribution in the implants. The peak stresses in all models were observed at the neck between the bone and implant interface. The highest von Mises stress was found with the highest bone density (1 g/cm^3) and the lowest stress was found with the lowest bone density (0.6 g/cm^3). Overall, the results showed that as bone density increased, the stress on implants also increased.

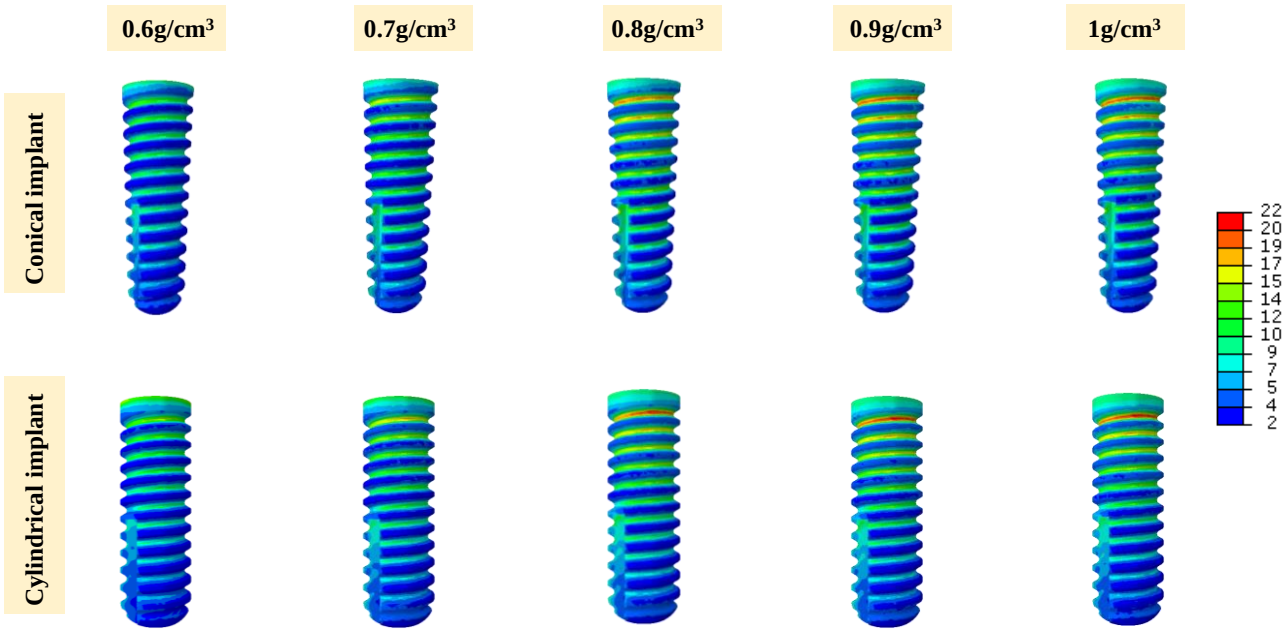

Figure IV.6 *Contour plots showing the von Mises stress (in MPa) in conical and cylindrical implants with bone density variation.*

Moreover, the stress was not significantly different between the two implant designs. **Figure IV.7** shows the bone state with a change in octahedral shear strain under different densities based on the mechanostat hypothesis when conical and cylindrical conventional implants were used. The lower the density of the bone, the higher the strain was generated. It was also noted that when the bone density of 0.6 g/cm^3 was simulated with conventional conical and cylindrical implants, the bone exhibited the highest strains, which is the damage state, and when the bone density was 0.7 and 0.8 g/cm^3, the bone homogeneity was maintained. Bone loss or atrophy state was observed when the bone density was higher (0.9 and 1 g/cm^3) in both conical and cylindrical conventional implants.

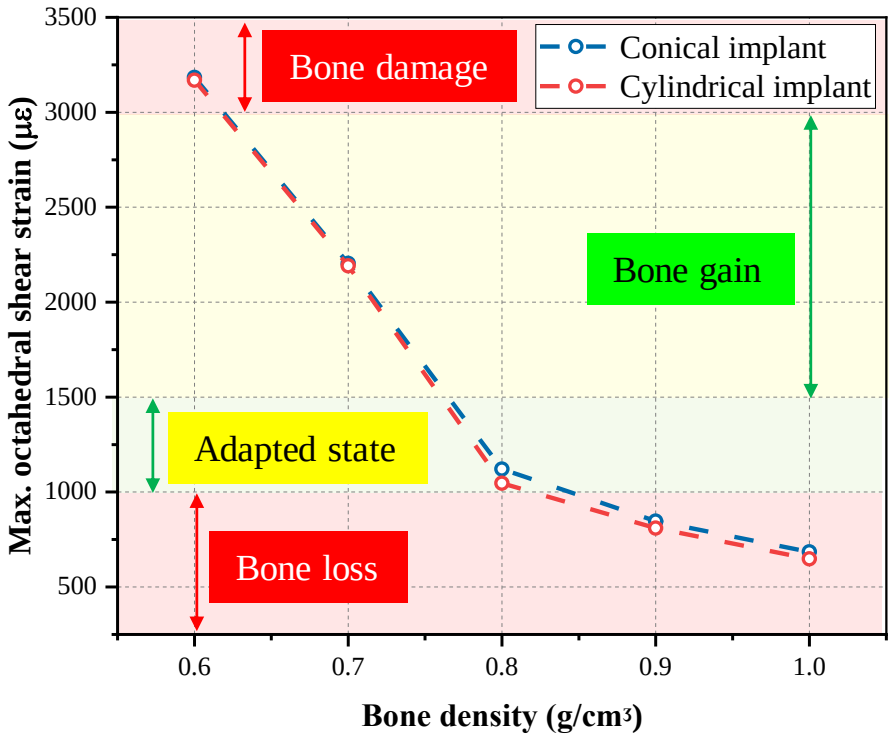

Figure IV.7 *Bone behavior with change in octahedral shear strain under different densities using conventional implants (based on mechanostat hypothesis).*

IV.3.2 Performance of FGM implants

IV.3.2.1 Stresses in implants

Figure IV.8 shows the stress distributions in the FGM conical implants with bone density of 0.9 g/cm^3 and 1 g/cm^3. The conical implant was chosen because it was noticed that there is no significant difference between the types of implants in terms of producing stress and strain at the bone-implant interfaces, and bone density of 0.9 g/cm^3 and 1 g/cm^3 were studied with FGM implants because bone atrophy was observed and stress-shielding may occur in these conditions. In all cases, the highest stress was concentrated at the top between the bone-implant interface and decreased towards the apical region. The maximum von Mises stresses in the FGM R-9 implant with bone density of 0.9 g/cm^3 and 1 g/cm^3 were 9.1 MPa and 7.56 MPa, respectively. In the FGM R-53 implant, the peak stresses were 28 MPa and 26.95 MPa for bone

density of 0.9 g/cm^3 and 1 g/cm^3, respectively. In the case of FGM A-9 with a bone density of 0.9 g/cm^3, the maximum stress was 13.5 MPa, and in the case of a bone density of 1 g/cm^3, the stress was 13.01 MPa. The maximum stress with implant FGM A-53 was 18.5 MPa with a bone density of 0.9 g/cm^3 and 17.88 MPa with a bone density of 1 g/cm^3. In conventional implants, the maximum stress values were 21.4 MPa and 23.5 MPa for bone density of 0.9 g/cm^3 and 1 g/cm^3, respectively. Almost the same pattern was followed in the case of FGM A-53, but with less distribution among the threads. The stresses were higher in the case of a bone density of 0.9 g/cm^3 compared to a bone density of 1 g/cm^3. Through these results, the different stress distribution at the level of implants with different materials may inevitably affect the production of strain at the bone level, which indicates that the implant material plays an important role in the bone remodeling process at different bone densities.

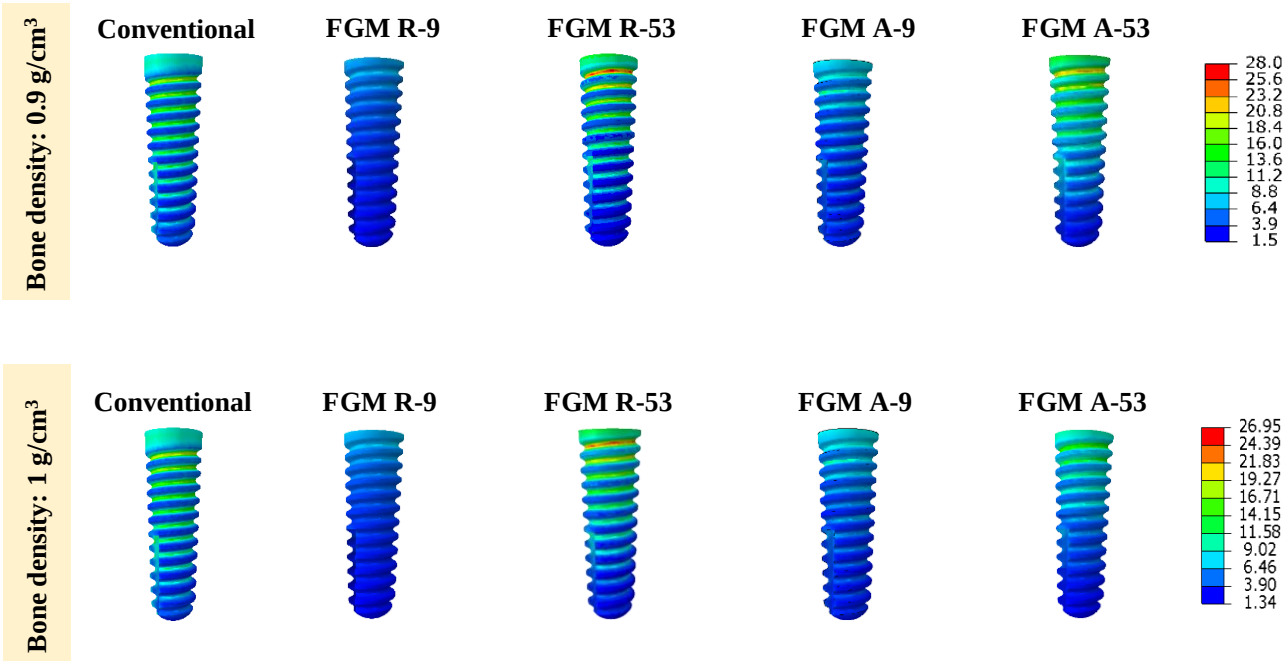

Figure IV.8 *Contour plots showing the von Mises stress (in MPa) in the different FGM conical implants.*

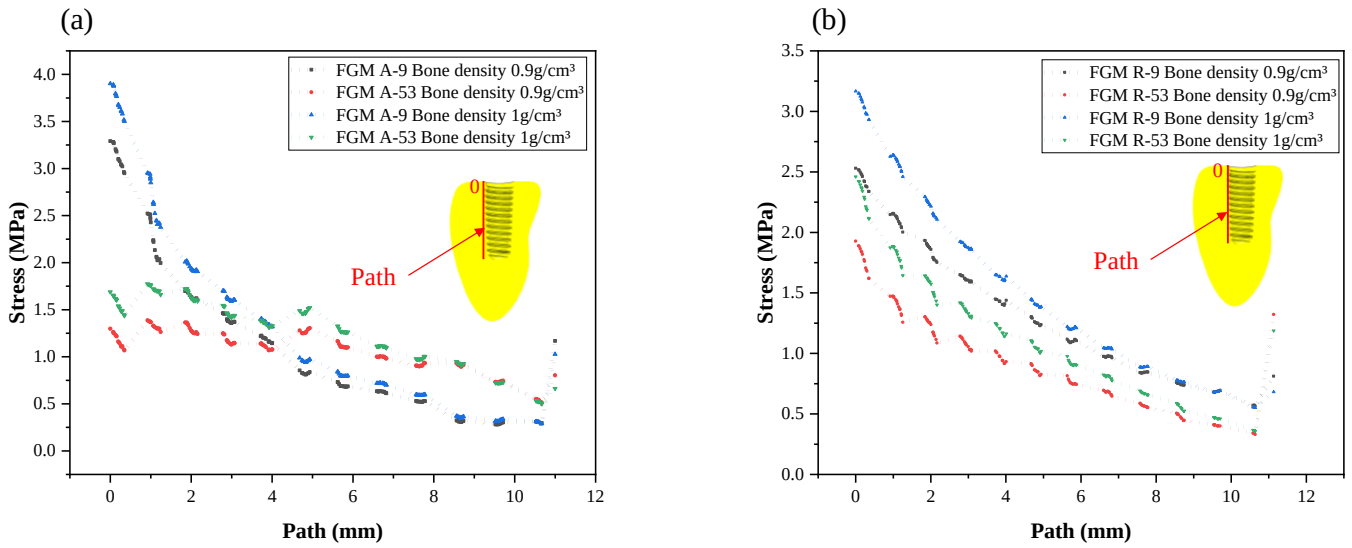

Figure IV.9 *Von Mises stress (in MPa) in cancellous bone by various FGM implants (in the axial path); a) axial FGM; b) Radial FGM.*

(a)

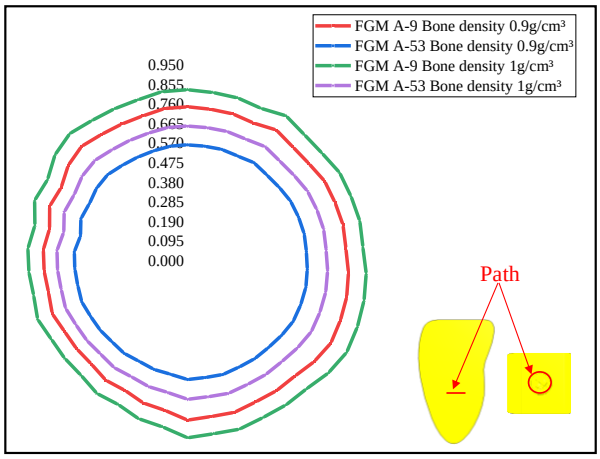

(b)

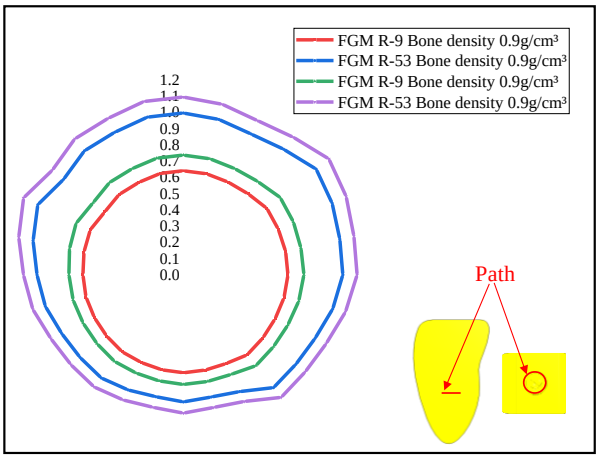

Figure IV.10 *Von Mises stress (in MPa) in the cervical region of cancellous bone by various FGM implants; a) axial FGM; b) Radial FGM.*

IV.3.2.2 Stresses in cancellous bone

Figure IV.9 depicts the distribution of stress along the axis of cancellous bone from the cervical to the apical region. The stress induced by axial and radial FGM implants varies from one region to another. It was highest in the cervical third and lowest in the apical third. FGM A-9, as shown in **Figure IV.9.a** transfers more stresses in the cervical third than FGM A-53. On the contrary, stress was higher in the middle third with FGM A-53 implants. Furthermore, when compared to axial FGM implants, the stress generated in cancellous bone by radial FGM implants (**Figure IV.9.b)** was approximately uniform along the axis. In all situations, the stress was greater in the case of 1 g/cm^3 bone density compared to 0.9 g/cm^3 bone density. **Figure IV.10** shows stress distribution in the apical region of the cancellous bone with different FGM implants. It was noticed that FGM A-9 and FGM R-53 transfer more stress to the apical third of the cancellous bone compared to other FGM implants.

IV.3.2.3 Strains in cancellous bone

Figure IV.11 shows the first principal strain distribution in cancellous bone with different FGM implants for bone density of 0.9 g/cm^3 and 1 g/cm^3. The maximum principal strains were observed at the top between the bone-implant interface in all models. Strains tend to decrease gradually away from the implant-bone interface. In the case of the conventional implant and FGM R-53, the strain was less distributed between the threads. On the contrary, the strain was more distributed in the cases of FGM R-9 and FGM A-9. The maximum principal strain (1298 με) was observed in FGM R-9 with a bone density of 0.9 g/cm^3, and the lower value (898 με) was seen in the case of a conventional implant with a bone density of 1 g/cm^3. It was observed that principal strains were higher in the case of FGM implants compared to conventional implant. This indicates that the stiffness of the implant is an important parameter for the generation of strain in the surrounding bone. When the strain is less, it means that fewer stresses are transferred to the bone, which may lead to stress-shielding phenomena or bone atrophy. It was also noted that the maximum principal strains were higher when bone density was 0.9 g/cm^3 compared to 1 g/cm^3.

Figure IV.12 shows the maximum octahedral shear strain in cancellous bone. The higher values were found in the case of the FGM R-53 implant (1275 με with 0.9 g/cm^3 and 1197 με with 1 g/cm^3). Conventional implants produced the lowest values (847 με with 0.9 g/cm^3 and 685 με with 1 g/cm^3). The maximum octahedral shear strains with a bone density of 1 g/cm^3 in FGM R-9 and FGM A-9 were 1036 με 1080 με, respectively. However, an increase in octahedral shear strain was observed in the case when the bone density was 0.9 g/cm^3 (1072 με for FGM R-9 and 1145 με for FGM A-9). The maximum strain (1071 με) for the FGM A-53 implant was found with a bone density of 0.9 g/cm^3, and a 986 με with a bone density of of 1 g/cm^3. It was noticed that FGM implants produce more octahedral shear strain compared to conventional

implants. Besides the bone density, the material and design of the implants are other major factors in producing strains at the implant-bone interface. As bone remodeling is directed by strains, bone homeostasis is maintained in almost all FGM implants.

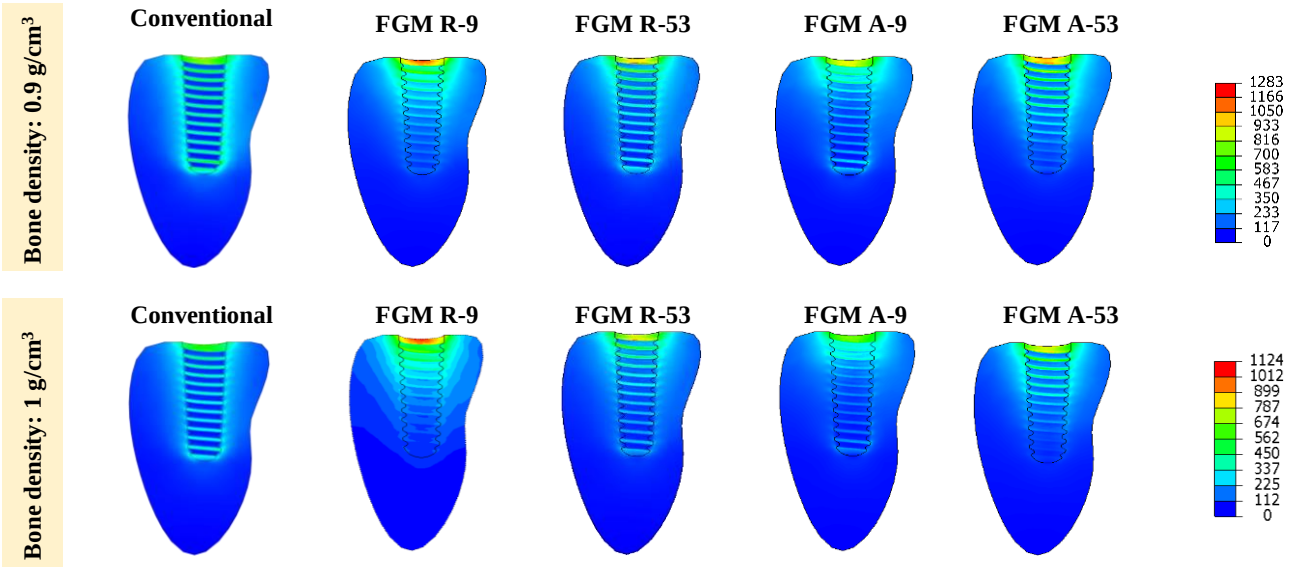

Figure IV.11 *Contour plots showing the first principal strain distribution in the cancellous bone with different FGM implants.*

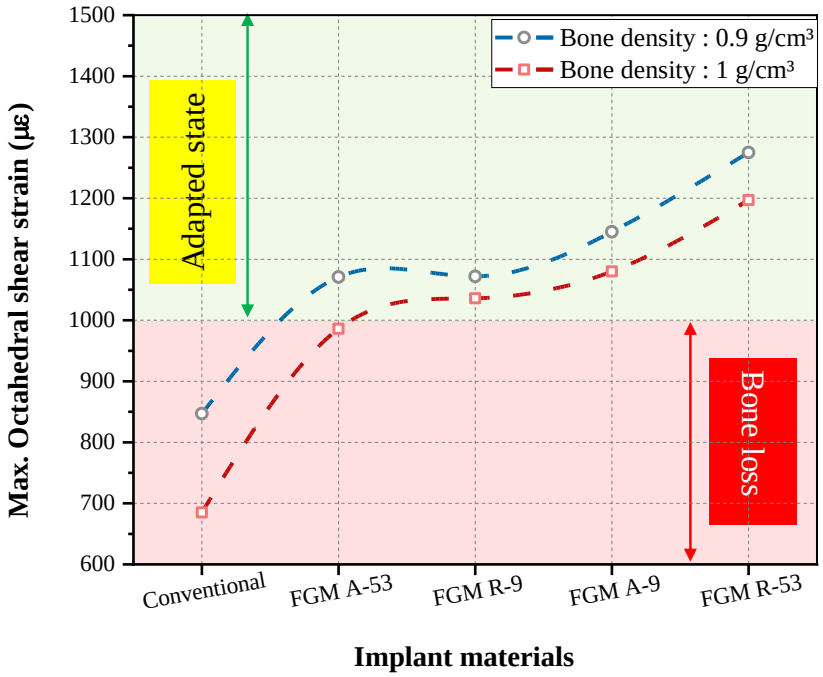

Figure IV.12 *Maximum octahedral shear strain in the cancellous bone under different implant materials.*

IV.4 Discussion

The long-term implant stability is contingent on favorable bone adaptation to maintain the osseointegration and bone remodeling process. Therefore, it is essential to evaluate how stress and strain in the surrounding bone affect the secondary stability. The current study was carried out to evaluate the effect of implant type on different bone densities under an axial load of 200 N. Five bone densities were chosen to explain how bone responds in a certain biomechanical environment. The mechanostat theory was used to compare the strains and their corresponding bone responses.It is well known that the amount of occlusal load transferred from the implant to the surrounding bone affects the surrounding bone density. **Figure IV.7** describes the bone responses with the obtained results of octahedral shear strains. The results indicated that there is no significant difference between the conical and cylindrical implants in terms of generating strains in all cases. However, implant design and bone density have a great influence on the generation of strains.

The bone density is determined and maintained by osteoblasts and osteoclasts cells on the surface of the bone. Researchers have assessed bone density by measuring bone mineral density (BMD) and indicated that the main risk factor of implant failure is bone density (quality and quantity) [250]. According to their studies, implants in the lower jaw (mandible) have a greater survival rate than those in the upper jaw (maxilla). This difference is thought to be mostly caused by bone density. In the present study, the results showed that the highest displacement (**Figure IV.3**) in cancellous bone was observed with the lowest bone density (0.6 g/cm^3). This indicates that the lowest bone density transmits the most micromotions when compared to denser bones. In the same condition, the bone was more prone to critically higher strains (**Figure IV.5**). This showed that the reduced density does not offer a favorable host environment for implants to

have a good prognosis. According to Frost's theory, different amounts of strains exert different responses to the bone remodelling process. **Figure IV.7** shows the lowest density (0.6 g/cm^3) bone exhibited the *damage behavior based on maximum octahedral shear strain.* It was observed from the obtained outputs that bone promotes bone resorption for a bone density of more than 0.8 g/cm^3. Bone loss and bone formation stay constant (adapted state) for a bone density of between 0.75 g/cm^3 and 0.8 g/cm^3. Bone mass and bone strength are increased (bone gain) for a bone density of between 0.65 g/cm^3 and 0.7 g/cm^3, due to the hormones and cytokines produced by the mechanical stimulus [251]. This difference in bone density gives us insight into how bone behaves biomechanically in producing strains. Several studies have used computational methods to describe the bone density based on mean Hounsfield unit (HU) values and computerized tomography (CT) scans [252], as well as to highlight the influence of mechanical stimulus using various bone remodeling algorithms [253][254]. Many techniques were performed in vivo to measure the strain at the bone-implant interface [255], and numerous FE studies looked at the impact of bone density as well [136][175].

Figure IV.9 displays the variations in von Mises stress along an axial distance for different FGM implants (axial and radial FGM). It was observed that the von Mises stresses were the highest at the top (cervical region), and the stress decreased gradually in the case of radial FGM (FGM-R) implants, in contrast to axial FGM (FGM-A) implants, where the stress path changed after 4 mm. By comparing the graph results, the low elastic modulus implant FGM A-9 produced more stresses in the cervical region and it transmitted the stresses to the apical region of cancellous bone as well (**Figure IV.10**). This indicates that FGM A-9 can prevent bone resorption in all zones. Since bone shows inhomogeneous structures in which functional gradients exist, an FGM implant possesses success. **Figure IV.12** reflects that FGM implants

generate more strains in surrounding bone compared to conventional implants. Because human bone is a porous functionally graded structure [256], FGM implants with micropores could mimic bone and improve bone density and ingrowth.

It has been studied [203] that porous titanium with low stiffness can avoid stress shielding, and this was confirmed in vivo tests [257][258] and pores can also facilitate bone ingrowth [259]. Many studies have recently used additive manufacturing techniques to fabricate porous and FGM implants [260][261] using additive manufacturing technologies [262]. Vivo studies [263–266] discovered that using 3D printed porous titanium improves osteogenic responses. Nowadays, additively manufactured functionally graded materials and designs present a class of new implants that can be used profusely in dental implants due to their excellent biomechanical performance.

The current study has a few limitations, such as the porous parts of the cancellous bone and implant porous were simplified by solid models to save computational cost. Moreover, the behavior of the bone may differ from actual behavior because cavity muscle forces were not considered. The simplifications in this study allowed us to do an approximate analysis. The future work will be extended to model porous implants, partial osseointegration cases, and bone remodeling processes by introducing a subroutine algorithm.

IV.5 Conclusion

To address the bone shielding issue, novel functionally graded material designs of dental implants were simulated with different bone densities.

This current study concluded that:

- Strain in bone increased with a decrease in cancellous bone density.

- The shape of the implant (conical and cylindrical) did not affect the distribution of stress and strain in the surrounding bone, significantly.
- Functionally graded materials of dental implants (FGM A-9, FGM A-53, FGM R-9, FGM R-53) produced appropriate levels of strains than the conventional implants. Thus, FGM implants ensure a better biomechanical environment for surrounding bone.
- Functionally graded implants solved the problem of bone loss using conventional implants and generated appropriate levels of strains in 0.9 and 1 g/cm^3 bone densities.
- The stiffness and the design of the FGM implant can be easily tailored by selecting appropriate porosity according to the patient's bone conditions, which can be the best choice for implant longevity.

The FGM porous Ti implants with low stiffness are a promising alternative to mimic the behavior of bone tissue and bone osteogenic responses compared to conventional implants (dense titanium). FGM titanium implants are the new designs of implants. Multiple designs of implants can be printed easily using additive manufacturing techniques. The porosity and location of dense material can be controlled to meet the clinical requirements of the patient. Such designs of implants have the potential to alleviate stress-shielding effects and bone atrophy due to their closeness to natural bone morphology. In addition, multi-objective optimization is necessary to improve the performance of the optimal implant design and reduce the possibility of oral complications.

Chapter V Mechanical Characteristics of Porous Ti Grade 5 using the Representative Volume Element (RVE) approach

V.1 Introduction

Layer-based additive manufacturing (AM) is a method for creating intricate three-dimensional physical items directly from three-dimensional computer-aided design (CAD) data. The inception of additive manufacturing goes back to 1980 with Dr. Hideo Kodama [267]. Additive Manufacturing (AM) also known as 3D printing, or rapid prototyping, or on-demand manufacturing, or digital fabrication, or desktop manufacturing, or solid freeform manufacturing, or layer manufacturing, or direct manufacturing technique. **Figure V.1** shows the basic staged involves in 3D printing [166]. A simple setup involves converting 3D model data into standard triangulate language format (STL), which is easy to print with additive manufacturing machine. AM has integrated numerous manufacturing techniques (powder bed fusion, directed energy deposition, material extrusion, binder jetting, curing, lamination etc.).

Recent years have seen a lot of interest in the powder bed fusion (PBF) technique because of its potential in the medical industry, notably with Ti-6Al-4V [268]. This method uses an energy source to selectively sinter or fuse a feedstock material made of fine powder into successive layers. Alternatively to using a laser beam (L-PBF) as the energy source, this technique also employs an electron beam (E-PBF), in which the kinetic energy of accelerated electrons is transformed into thermal energy upon impact with the powder bed. Commercially, this procedure is referred to as electron beam melting [269]. This method can meet the highest quality standards with appropriate conditions, such as good powder quality and well adjusted process parameters. However, when using L-PBF, a number of variables can affect the printibale structure., including hatch spacing (the distance between parallel laser passes), powder layer thickness, laser power, and laser scanning velocity [270].

Titanium and its alloys are widely used in orthopedic and dental implant fields because of their high biocompatibility. Porous titanium has been created using a variety of techniques, which can improve the fixation ability with the bone tissue. In addition, the stress-shielding phenomenon can occur due to the mismatch between stiffness of dense titanium and bone. Hence, porous titanium can prevent this phenomena. AM has great potential to solve this kind of problems of creating a porous surfaces. In an in vivo and vitro investigation [271][272], printibale porous titanium implants were examined, their architecture can affect the bone ingrowth into pore space. Studies showed that porous titanium with lower stiffness similar to bone can provide an excellent osseointegration by improving the early bone formation [273]. Therefore, porous titanium is a promising candidate for bone-tissue engineering applications.

Implants' porous architectures are mostly constructed from periodic arrays of representative volume elements (RVEs) [274]. Both mechanical properties and bone ingrowth depend on the RVEs' structure and size which are dependent on porosity and pore size as well. Porous structures reduced the elastic modulus with increasing the porosity, the strength will be very low, and the materials will have insufficient strength to replace natural host bones [275]. On the other hand, A porous construction with less porosity is likely to perform less biologically [276]. Typically, the mechanical and biological requirements are at odds. Therefore, it’s necessary to find optimal porous cellular to improve the mechanical and biological performances.

Periodic structures, sometimes referred to as lattice structures, include honeycombs and trusses and are composed of unit cells that are organized periodically to form a certain shape. Lattice structures have drawn a lot of interest due to their desirable properties, including superior specific strength and specific stiffness [277]. The repetition of a unit cell using a specific spatial pattern is the typical method for creating lattice structures, so the unit cell is the smallest

element. Complex porous lattice structures can be designed by computer- aided design (CAD) software and can be manufactured with additive manufacturing techniques because it's difficult to produce their complex architecture with conventional industrial techniques [278].

The study of mechanical performance of different lattice structures has been of interest to many researchers using finite element analysis (FEA) [192][279][280][281]. In this study, we selected five-unit cell as a representative strut-based unit (**Figure V.2)**, the cubic-cross (CC), the body-centered cubic (BCC), face-centered cubic (FCC), the octahedron (Octa), the octahedron-cross (Octa-c). Therefore, five lattice structure were modelled. The aim of this study is to verify the influence of the geometric properties of this unit cell such as strut diameter on the mechanical properties of the lattice structure using finite element method.

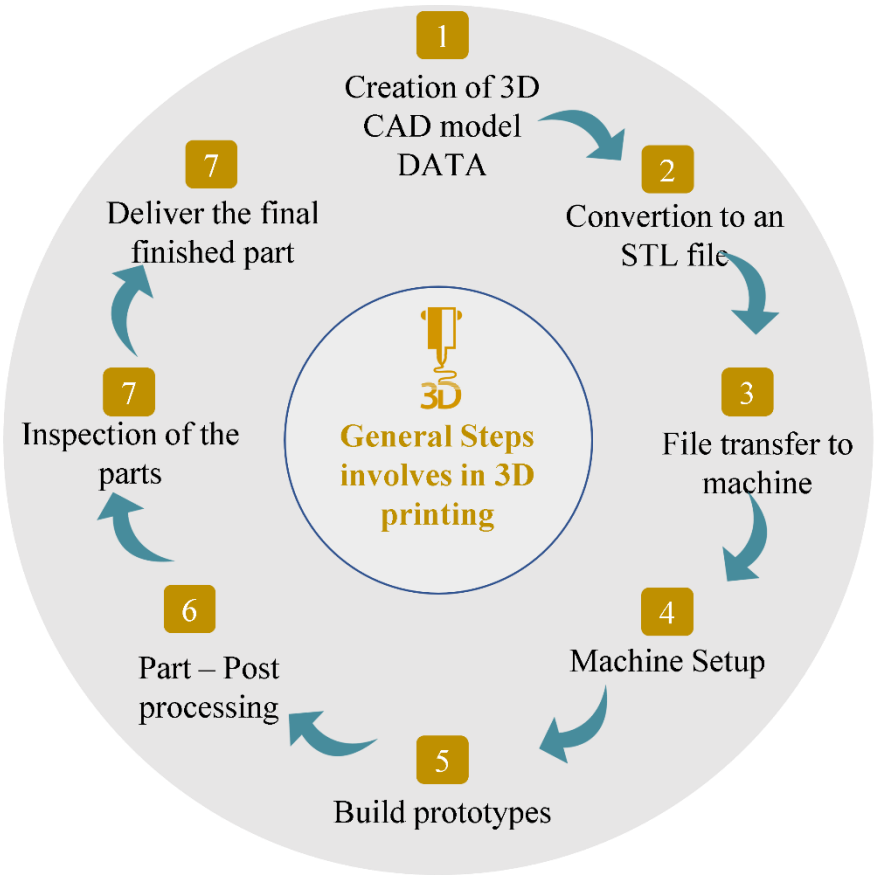

Figure V.1 *Main steps involves in 3D printing.*

V.2 Methodology

V.2.1 CAD modeling of unit cell and lattice structure design

A simple cubic unit type was used to design the units cell (**Figure V.2**). The unit cell is characterized by three parameters, the edge of the cube (L=1 mm), the internal strut diameter (SD in mm), and the pore size (Po). Five type of units cell were designed using Abaqus v6.20 software, the cubic-cross (CC), the body-centered cubic (BCC), face-centered cubic (FCC), the octahedron (Octa), the octahedron-cross (Octa-c). Three different strut diameters (SD) were chosen for this unit's cell, 0.1 mm, 0.2 mm and 0.3 mm, respectively. Five designs of 27-unit cells were modelled by using feature of linear repetition (3 × 3 × 3 lattice structure). **Figure V.3** shows the CAD modelling parameters of the selected scaffold (CC, BCC, FCC, Octa, Octa-C). The pore size of different lattices structure with different strut diameter (0.1 mm, 0.2 mm, 0.3 mm) are reported in **Table V.1**.

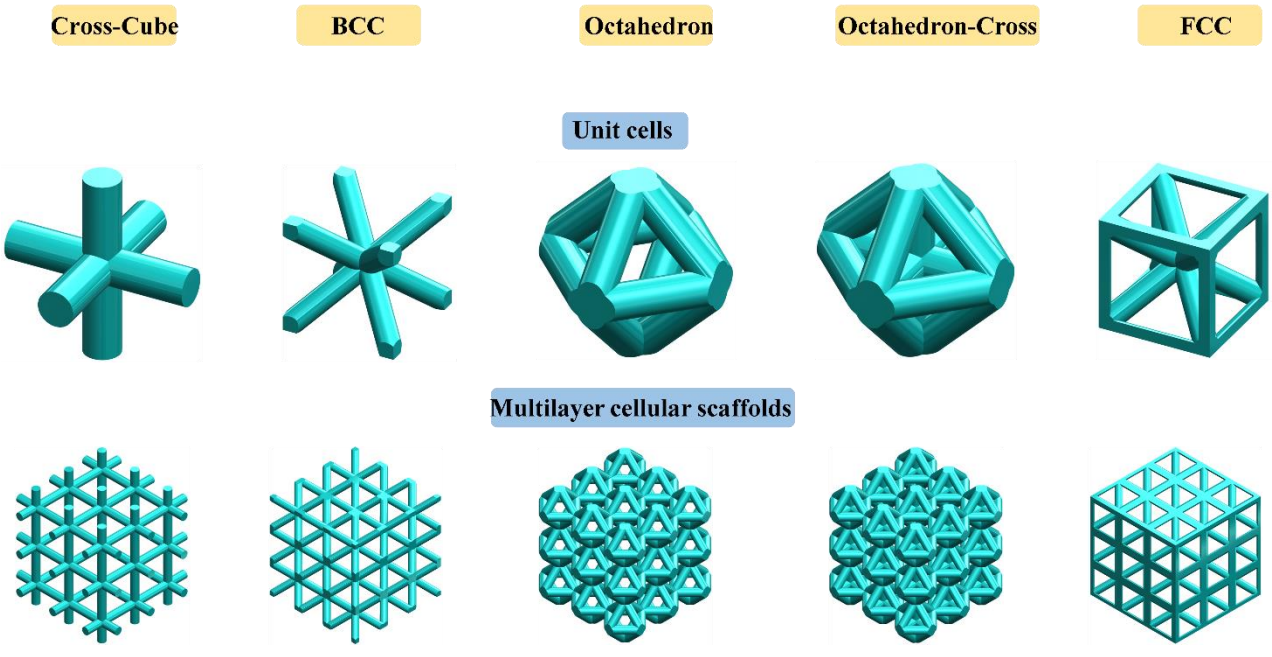

Figure V.2 *Different units cell and lattice structures ; the cubic-cross (CC), the body-centered cubic (BCC), face-centered cubic (FCC), the octahedron (Octa), the octahedron-cross (Octa-c).*

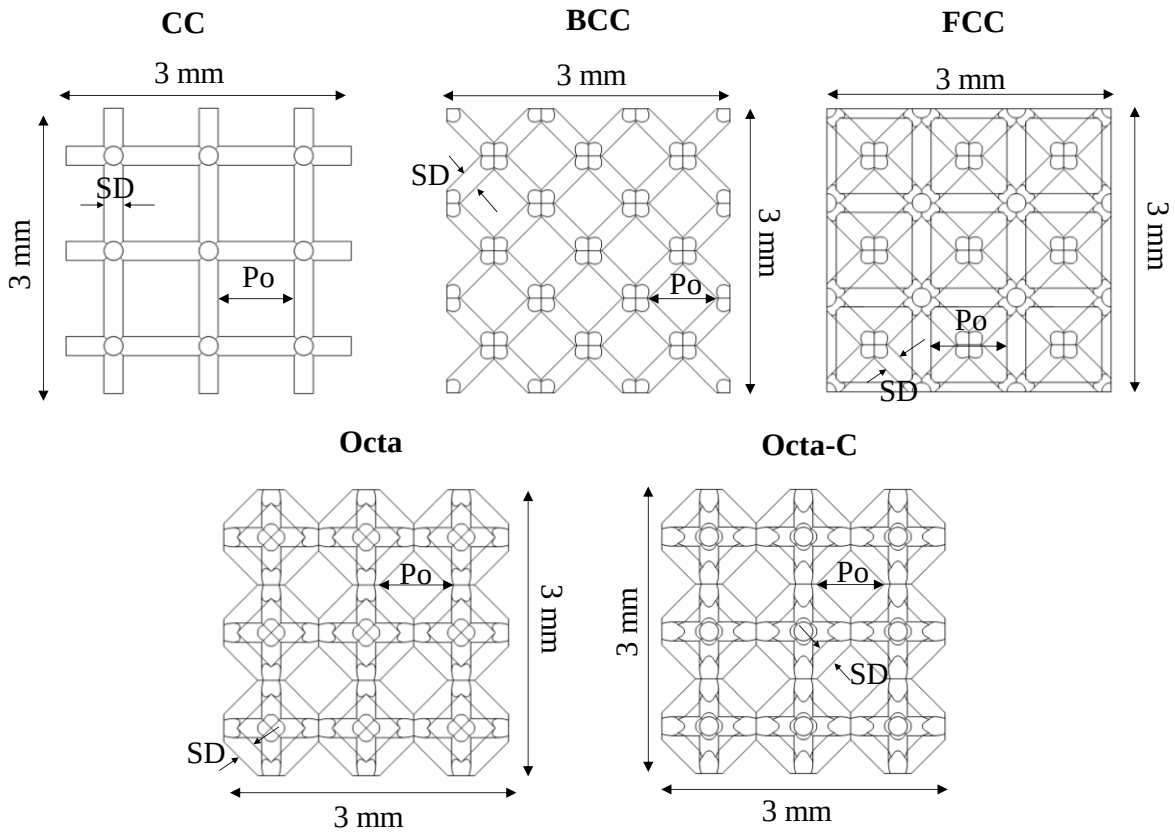

Figure V.3 *CAD modelling of porous structure.*

Table V.1 *Different lattice structures with their strut diameter, and pore size.*

	SD 0.1 mm	**SD 0.2 mm**	**SD 0.3mm**
	Pore size (Po)		
CC	900	800	700
BCC	859	717	575
FCC	900	800	700
Octa	859	717	575
Octa-C	859	717	575

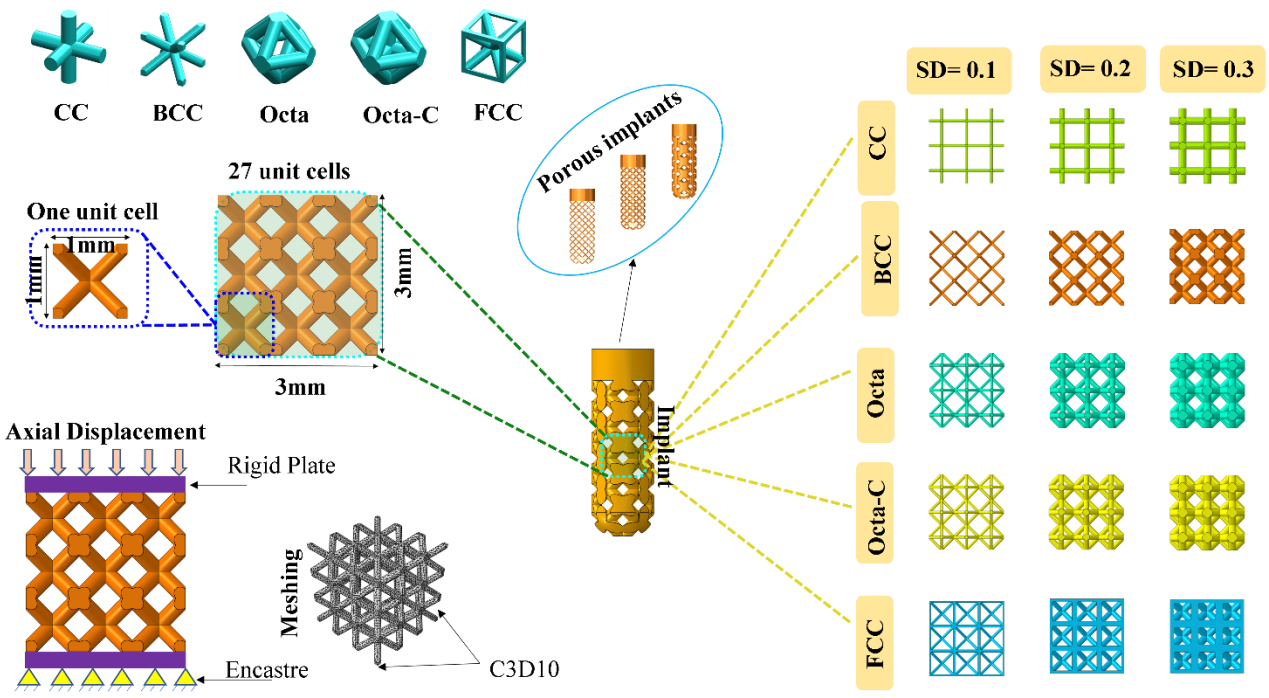

Figure V.4 *Finite element configuration of different models .*

V.2.2 Materials properties

The lattice structures of Ti-6Al-4V were investigated in this study. Ti-6Al-4V alloy is widey used in orthopaedic and dental applications for bone tissue engineering due to its advantageous mechanical properties and biocompatibility. To mesure the elastic and plastic properties, the the Johnson-Cook strength model has been used. The properties of titanium grade 5 (Ti-6Al-4V) used in this study are summarized in **Table V.2.**

Table V.2 *Properties of Ti-6Al-4V* [282].

Density ρ (kg/m^3)	Modulus of elasticity E (GPa)	Poisson's ratio ν	Intact strength constant A (MPa)	Strain hardening constant B (MPa)	Strain hardening exponent n	m	Strain rate constant C	Reference strain rate ξ (s^{-1})	melting temperature (K)	transition temperature (K)
4430	113.8	0.342	1098	1092	0.93	1.1	0.014	1	1878	715

V.3 Finite element parameters

In order to obtain mechanical properties, the latice structures were loaded under uniaxial compression. A quasi-static displacement loading of 0.5 mm was applied on the top of the scaffold. The bottom surfaces were fixed with zero displacements (translations and rotations), as shown in **Figure V.4**. The scaffold was meshed by C3D10 element with mesh seed size up to 0.08.

V.3.1 Post-processing

The following equation was used to determine the porosities:

$$p = \left(1 - \frac{V_p}{V_s}\right) \times 100\% \qquad (3)$$

where p, V_p, and V_s are the porosity of the porous model, volume of the scaffold (the porous structure) and volume of the solid (the cube), respectively.

Lattice structure's effective stress and strain are described as follows:

$$\sigma = \frac{F}{A_0} \qquad (4)$$

$$\text{Strain} = \varepsilon = \frac{\text{Displacement (mm)}}{\text{Initial height (mm)}} = \frac{\Delta l}{l_0} \qquad (5)$$

where F is the reaction force that was obtained on the scaffold's bottom surface and Δl is the displacement captured on the upper surface of the scaffold, l_0 and A0 are the initial length of the unit cell and the cross-section area, respectively. The displacements and reaction forces were extracted from the output field.

The effective Young's modulus (E_{eff}) was calculated from the ODB results (from the corresponding stress-strain curve) based on the Hooke's law:

$$E_{eff} = \frac{\sigma}{\varepsilon} \quad (6)$$

V.4 Results

V.4.1 Porosity of lattice structures

The equation (3) were used to determine the porosity pourcentage. The volumes of 27 unit cells were obtained (in mm^3) from Abaqus using material properties feature calculations. Results are reported in **Table V.3**. The varying of the strut sizes results in different porosity of the all lattice structures. The scaffold porosity decreased as the strut diameter was increased. The CC (cubic cross) lattice structure has the most porosity in comparison to the other lattice structures, which was followed by BCC structure. FCC and Octa-c have less porosity, as shown in **Figure V.5**. It could be observed that the greater porosity (97.78%) was with CC structure with strut diameter of 0.1 mm. The lowest porosity was with FCC structure (53.14%) with strut diameter of 0.3 mm. Generally, changing the type of lattice structures leads to different porosity. The diameter of the strut is the significant factor that changes the porosity.

Table V.3 *Porosity of different lattice structures with different strut diameter (SD).*

	Strut Diameter (SD in mm)		
	SD 0.1	**SD 0.2**	**SD 0.3**
	Porosity (%)		
CC	97,78	91,70	82,59
BCC	95,03	82,14	64,25
FCC	93,07	75,74	53,14
Octa	94,11	79,51	60,88

Octa-C	92,37	74,88	55,88

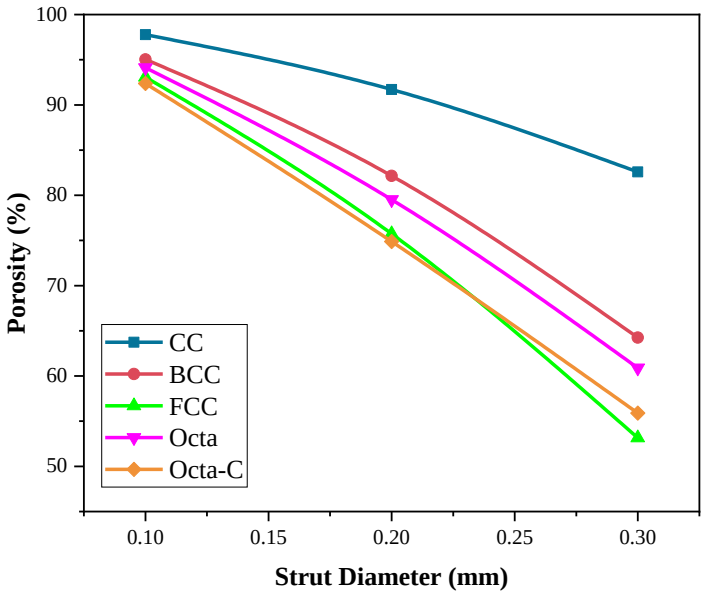

Figure V.5 *A graph of porosity decreasing as strut diameter increases in all diferent lattice structures.*

V.4.2 Compressive responses of lattice structures

Figure V.6 presents a summary of the effective stress-strain graphs of different structures obtained from compression test. **Figure V.6.a** depicts the stress-strain curve for CC lattice structure. It was observed that the CC 0.3 (with SD of 0.3 mm) has the highest magnitude and the CC 0.1 has the lowest magnitude. All data of effective Young's modulus and yiend strength are reported in **Table V.4**. It was noticed that the CC 0.3 has the highest stiffness and yield strength (8.87 GPa and 79 MPa, respectively) as compared to CC 0.2 (3.83 GPa, 34 MPa)) and CC 0.1 (522 MPa, 8.70 MPa). **Figure V.6.b** shows the stress-strain curve for BCC lattice structure. Similarly, so that when the lattice structure with a larger diameter (0.3 mm) means less porosity, the stiffness is high. BCC 0.3 effective elastic modulus and yield strength 59 MPa, 1.96 MPa, respectively.BCC 0.2 effective elastic modulus and yield strength 1.03 GPa, 25.72 MPa , respectively. BCC 0.1 effective elastic modulus and yield strength 5.32 GPa, 100.3 MPa,

respectively. **Figure V.6.c** shows the stress-strain curve for FCC lattice structure. Likewise, increasing the strut size increases the stiffness and strength of the lattice structure. FCC with strut size of 0.3 mm has the highest stiffness and effective yield strength (20.30 GPa, 255.82) MPa as compared to BCC 0.2 and BCC 0.1. In parallel, same oberservation was noticed with octa and octa-c lattice structures. Overally, an increase in stifness and effective yield strength is related to a decrease in porosity of the lattice structure.

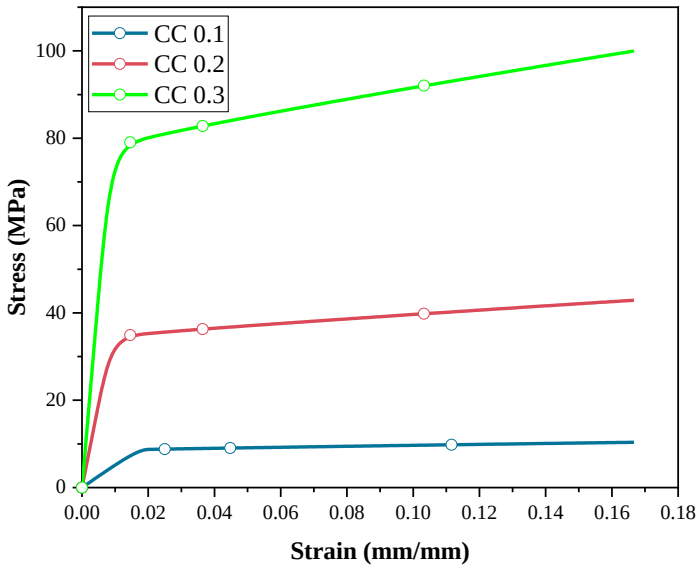

(a)

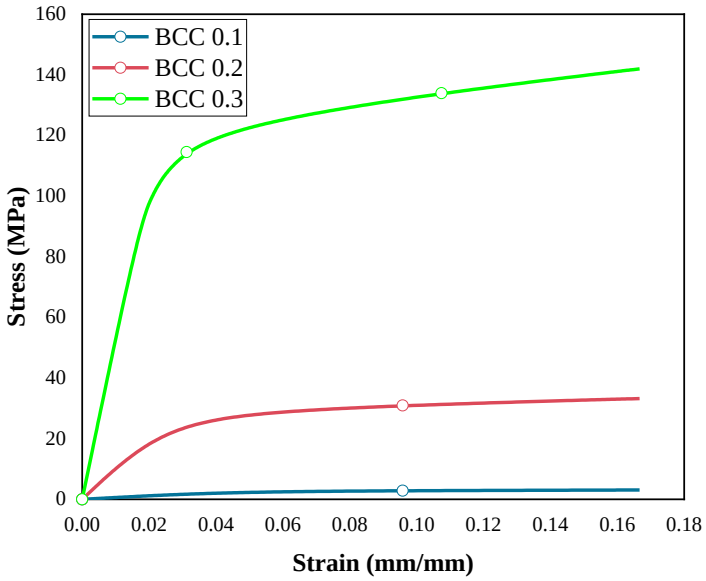

(b)

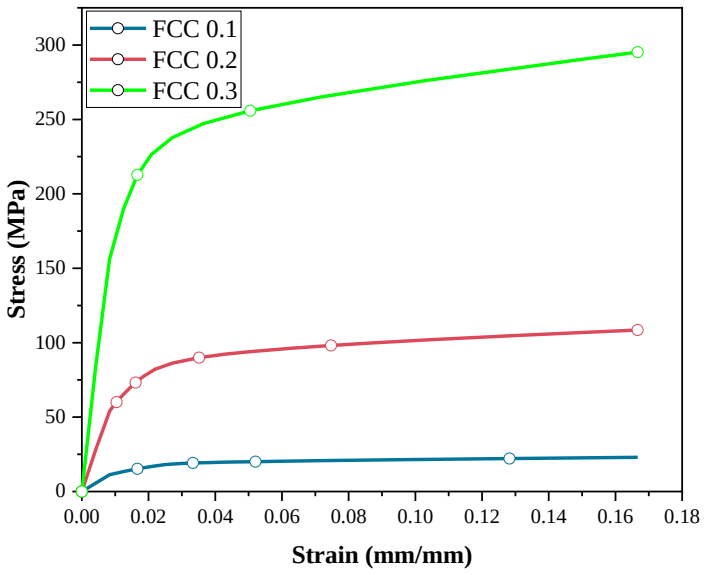

(c)

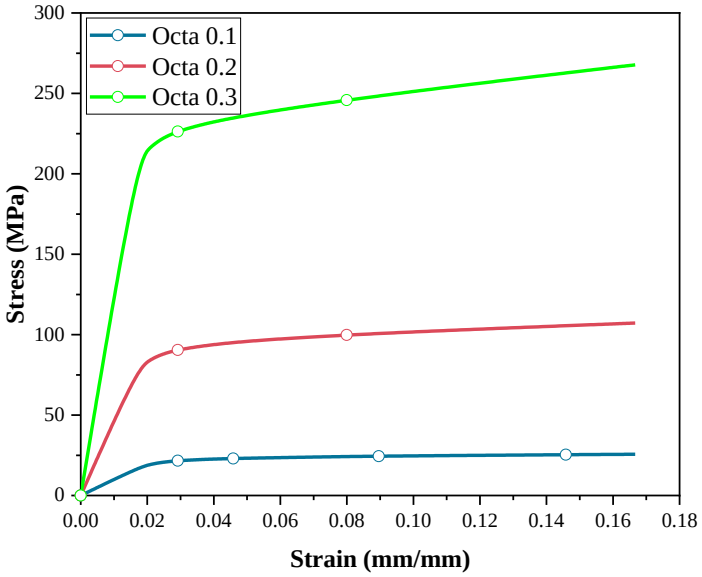

(d)

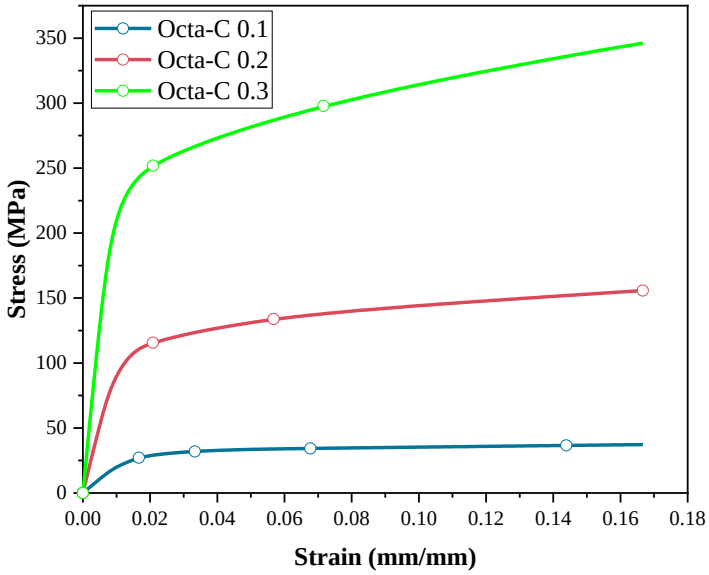

(e)

Figure V.6 *The effective stress-strain curves of different lattice structures; (a): CC, (b): BCC, (c): FCC, (d): Octa, (e): Octa-c.*

V.4.3 Comparison of lattice structures mechanical properties

Figure V.7 shows a comparison of the effective stress-strain curves of different lattice structures. Generally, CC and BCC curves are below of the rest lattice structures. Octa-c curves are above the rest of structures curve. The highest Young's modulus was observed with the

Octa-c (octa-c 0.3) lattice structure with a value of 26.77 GPa. The lowest stiffness was observed with BCC 0.1 (52 MPa). For a given strut diameter, the BCC cellular architectures provide the weakest stiffness and yield strengths. However, the FCC lattice structure provide moderate effective Young's moduli and yield strengths and the effective stress-strain curves are very close to those of the Octa lattice structure. The type of the unit cell and the strut diameter plays a major role in changing the stiffness and strength of the lattice structure, as shown in **Figure V.8**.

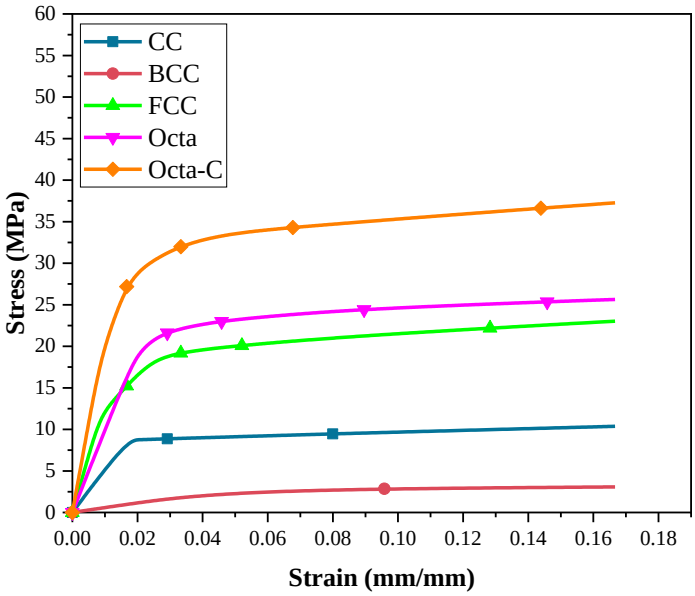

(a)

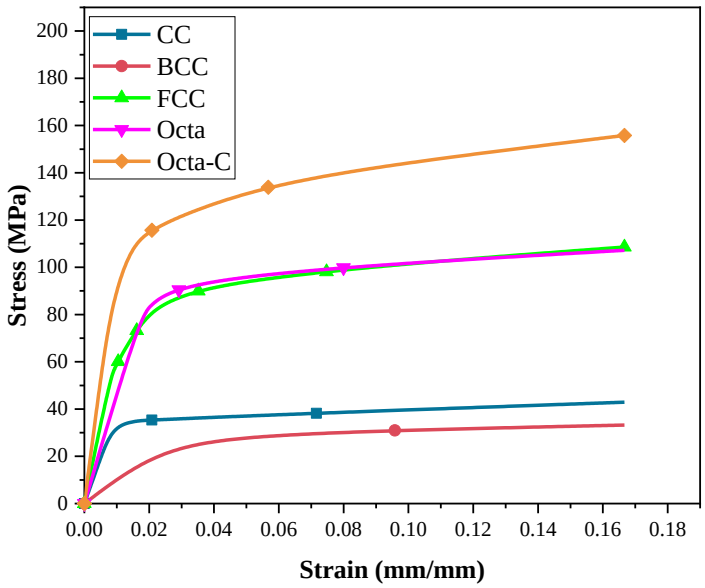

(b)

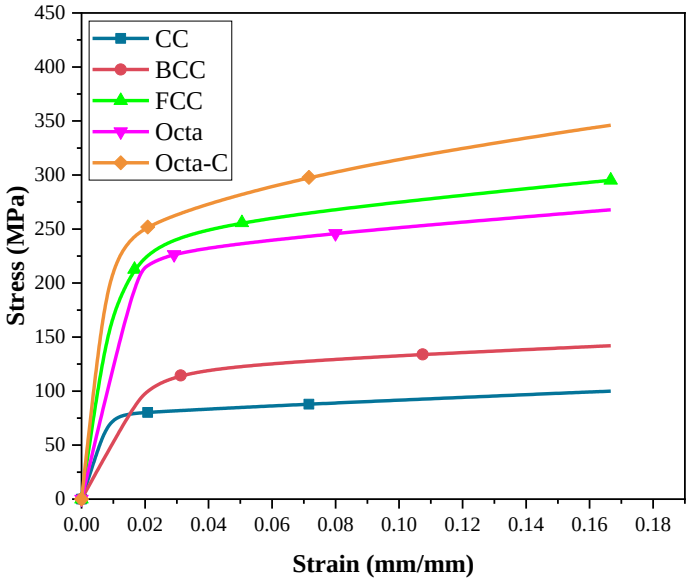

(c)

Figure V.7 *Comparison of effective stress-strain curves of different lattice structures; (a): with 0.1 mm strut diameter, (b): with 0.2 mm strut diameter (c): with 0.3 mm strut diameter.*

Table V.4 *Effective yield strength and Young's modulus of various lattice configurations.*

	Strut Diameter (SD)					
	SD 0.1		**SD 0.2**		**SD 0.3**	
	E_{eff} (GPa)	**σ_{eff} (MPa)**	**E_{eff} (GPa)**	**σ_{eff} (MPa)**	**E_{eff} (GPa)**	**σ_{eff} (MPa)**
CC	0.522	8.70	3.83	34	8.87	79
BCC	0.059	1.96	1.03	25.72	5.32	100.3
FCC	1.37	13.4	6.78	63.55	20.30	169.03
Octa	1.00	20	4.66	84.65	12.39	216.84
Octa-C	2.15	26.88	10.63	100	26.77	222.81

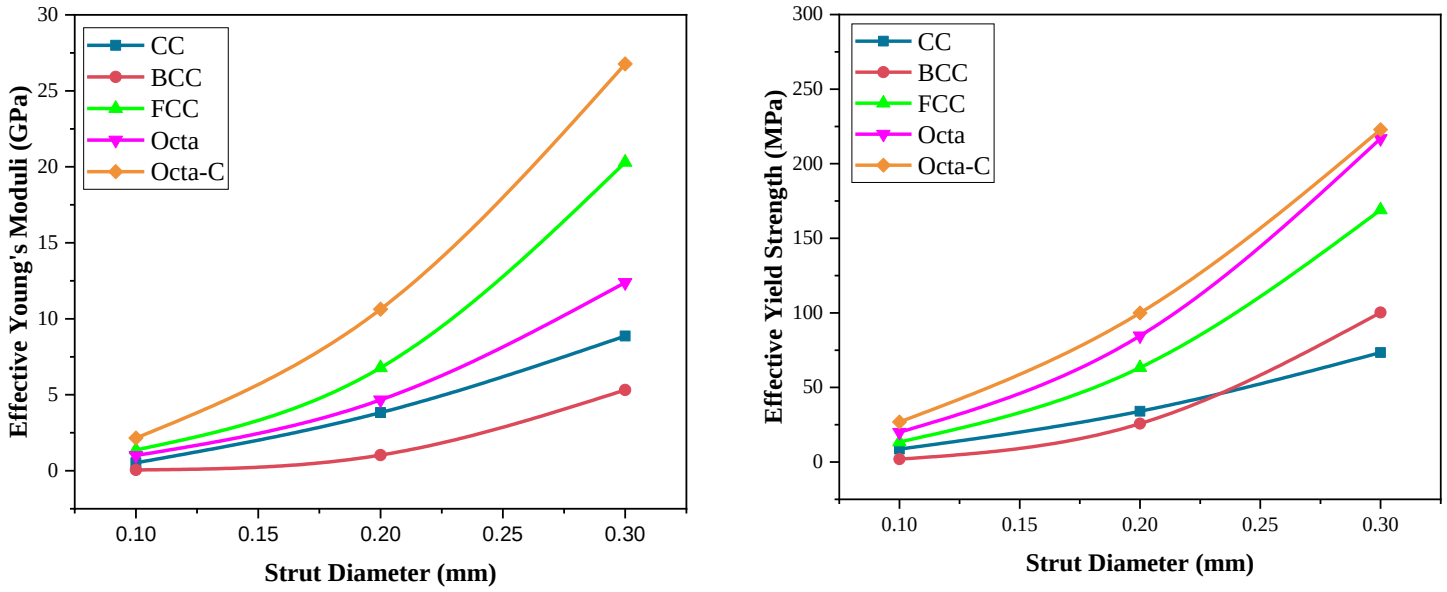

(a) (b)

Figure V.8 *Comparaison of different lattice structures design; (a):the effective Young's modulus, (b): the effective yield strength.*

V.4.4 Stiffness and pore size

The porous morphology (pore size) can provide a good environment for the ingrowth of natural bone.In this study, the strut diameter of different lattice structures were fixed (0.1 mm, 0.2 mm, 0.3 mm). Therefore, this geometrical parameter can affect the volume quantity of the structure and thus its porosity, as well as the pore size (Po). **Figure V.9** presents the effect of pore size on the Young's modulus of different lattice stucture. We note that the raising of pore size of the lattice structure increases the scaffold stiffness. It is clearly demonstrated that regardless of the pore size, the Octa-C structure has the greater Young's modulus. In addition, it could be obeserved that FCC and CC structures with same strut diameter have the same pore size. Likewise, the BCC, Octa and Octa-c have the same pore size. **Figure V.9** is devoted to showing that with the same strut diameter (SD) the lattice structure type has different stiffness than the other, and the larger the pore size, the lower the stiffness. **Figure V.9** is also intended to display a comparison between bone stiffness and lattice structures stiffness. To mimic the bone tissue,

scaffold stiffness need to be similar with those of natural bones. Cortical bone is stiffer than cancellous bone. Therefore, it need dense lattice structure. Cancellous tissue is characterized by its honeycomb-like structure. It could be observed from the graph illustrated in **Figure V.9** than lattice structures with larger pore size and lower strut diameter (means great porosity) can be a good choice for the cancellous bone, except the BCC 0.1 which has very low Young's modulus and yield strength. For cortical bone, the moderate pore size between 700 µm and 750 µm can be good option for its architecture, the Octa-c 0.2 or CC 0.2 with moderate stiffness (between 9 abd 12 GPa).

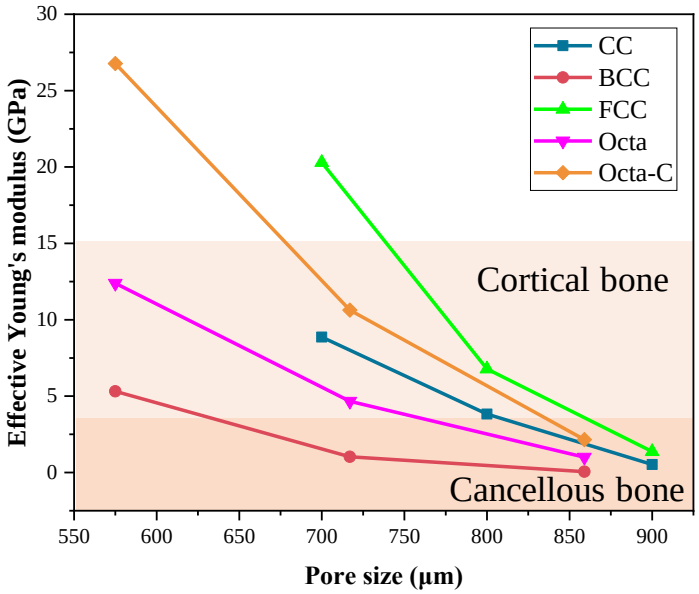

Figure V.9 *Effect of pore size on the lattice structure stiffness.*

V.5 Discussion

Due to their great biocompatibility, high specific strength, good corrosion and fatigue resistance, titanium and its alloys have been utilized extensively for many years as a solid implant material for the creation of biomedical implants. However, the significant mismatch in stiffness between bone tissue and conventional dental implants (made of dense titanium) can cause stress-

shielding. Therefore, researchers are working to elucidate the biological response of novel high strength-low elastic modulus [283].

The design and fabrication of porous structures can be a promising approach to alleviate the mismatch in stiffness especially with the advancement of additive-manufacturing(AM) techniques. Porous structures have received extensive attention because of promoting osseointegration through bone ingrowth in the porous structure [274]. Hence, it may offer a viable remedy for the problem of aseptic loosening over time. Porous implants architectures are mostly constructed from periodic arrays of representative volume elements (RVEs). The mechanical characteristics of numerous RVEs, (eg; cubic, BCC, FCC, and triply-periodic minimum surface), have drawn significant interest in the study of AM porous structures.

The objective of the study described here is to explore the mechanical properties of different lattice structures and make a comparison between them. Scaffolds with RVEs of cubic-cross (CC), body-centred cubic (BCC), faced-centered cubic (FCC), Octahedron (Octa), and Octahedron-cross (Octa-C) have investigated using finite element method. The strut diameter was employed as a parameter in the FE prediction of mechanical properties of lattice structures. This factor led to different porosity and pores size.

Results showed that BCC structure have the lowest Young's modulus, which is in agreement with the previous studies [192][284][285]. Peng et al. [282] have evaluated the fatigue life prediction of various porous structures design (SC, BCC, FCC, SC-BCC). Their findings demonstrated that the body-centered cubic (BCC) unit cell has the lowest stiffness (Young’s modulus) and yield strength at all relative densities and the highest elastic modulus and yield strength for the simple cubic (SC) unit cell. Additionally, SC unit cells have the best wear resistance of any of the architectures, while BCC unit cells have the worst. Yu et al. [286] have

examined three different porous design (primitive, gyroid, octahedron) with a porosity of 65% under compressive and tensile tests. The octahedron structure was named as BCC in their study. According to their research, Gyroid scaffolds had the highest tensile and compressive strengths (It is approximately twice higher than BCC). The gyroid and primitive structures are triply periodic minimal surfaces (TPMS). These types may exhibit strut stretching and buckling as compared to solid strut structures.

In the present study, the Octa-C scaffold was almost 2 times that of Octa structure, The Octa-C scaffold was therefore better suited for load-bearing. This is due to Octa-C lattice structure has the largest cross-sectional area at any strut diameter. This improves the structure's ability to transmit stress in the direction of loading.

Design of porous orthopaedic implants is based on knowledge of how bone ingrowth affects the mechanical characteristics of osseointegrated scaffolds. The diversity of designs offered in dentistry for dental implants for production from materials with different properties by companies poses a question for dentists to choose the optimal material for a particular clinical case. The result of the analysis gave an overview of the use of porous titanium grade 5 (Ti-6Al-4V) with different mechanical properties and showed the possibility of the development of a new orthopedic and dental implant to improve the results of treatment of patients with partial or complete edentulism who suffer from bone deficiency.

V.6 Conclusion

In this work, five different models of porous Ti6Al4V scaffolds (CC, BCC, FCC, Octa, Octa-C) with different strut diameters of 0.1, 0.2, 0.3 mm were modelled. The mechanical properties of porous titanium grade 5 scaffolds were determined by compression test using finite element method. The main conclusions are as follows:

(1) The increase in the strut diameter of the unit cell increases the volume (cross-section) of the scaffold and thus the porosity decreases.

(2) The lower the porosity the lower the stiffness at any structure.

(3) BCC lattice structure showed the lowest Young's modulus and yield strength at any strut diameter, while the Octa-C showed the highest Young's modulus and yield strength.

(4) The Octa and Octa-C scaffolds can make the structure has better stress transmission at any loading direction.

(5) The CC and FCC with strut diameter of 0.1 mm can be suitable for cancellous bone ingrowth due to their largest pore size (900 μm) and similair Young's modulus (522 MPa, 1370 MPa, respectively).

Table des matières

General Conclusion and Future Studies

In conclusion, the use of porous dental implants and Functionally Graded Material (FGM) porous implants with low stiffness to mimic the host bone and avoid stress shielding has been shown to be a promising approach. The Finite Element Method (FEM) was used to simulate the mechanical behavior of the implant and the surrounding bone. The results demonstrated that porous implants with lower stiffness were able to reduce stress shielding and promote bone ingrowth. The FEM was a powerful tool to investigate the mechanical behavior of the implants and to optimize their design. Therefore, porous implants with low stiffness can be considered a viable option for dental implant applications.

Future studies should focus on the development of composite materials to enhance the mechanical properties of the porous implants while maintaining their biocompatibility. The use of artificial intelligence (AI) to predict the results of the FEM simulations and optimize the design of the implants could also be explored. More experimental studies, both in vitro and in vivo, should be performed to further validate the findings of this study and to assess the long-term performance of the implants. Additionally, clinical trials are needed to evaluate the efficacy and safety of these new implant designs in human patients. These future studies could lead to the development of more advanced and effective dental implant solutions.

References

[1] M. Dermience, G. Lognay, F. Mathieu, P. Goyens, Effects of thirty elements on bone metabolism, J. Trace Elem. Med. Biol. 32 (2015) 86–106. https://doi.org/10.1016/j.jtemb.2015.06.005.

[2] R. Zhou, Q. Guo, Y. Xiao, Q. Guo, Y. Huang, C. Li, X. Luo, Endocrine role of bone in the regulation of energy metabolism, Bone Res. 9 (2021) 25. https://doi.org/10.1038/s41413-021-00142-4.

[3] B. Corrieri, N. Márquez-Grant, What do Bones Tell us? The Study of Human Skeletons from the Perspective of Forensic Anthropology, Sci. Prog. 98 (2015) 391–402. https://doi.org/10.3184/003685015X14470674934021.

[4] J. Kim, M.G. Bixel, Intravital Multiphoton Imaging of the Bone and Bone Marrow Environment, Cytom. Part A. 97 (2020) 496–503. https://doi.org/10.1002/cyto.a.23937.

[5] Y. Han, X. You, W. Xing, Z. Zhang, W. Zou, Paracrine and endocrine actions of bone—the functions of secretory proteins from osteoblasts, osteocytes, and osteoclasts, Bone Res. 6 (2018) 16. https://doi.org/10.1038/s41413-018-0019-6.

[6] C. Higham, B. Abrahamsen, Regulation of bone mass in endocrine diseases including diabetes, Best Pract. Res. Clin. Endocrinol. Metab. 36 (2022) 101614. https://doi.org/10.1016/j.beem.2022.101614.

[7] J. Kim, G. Lee, W.S. Chang, S. hyoung Ki, J.-C. Park, Comparison and Contrast of Bone and Dentin in Genetic Disorder, Morphology and Regeneration: A Review, J. Bone Metab. 28 (2021) 1–10. https://doi.org/10.11005/jbm.2021.28.1.1.

[8] M.A. Zoroddu, J. Aaseth, G. Crisponi, S. Medici, M. Peana, V.M. Nurchi, The essential metals for humans: a brief overview, J. Inorg. Biochem. 195 (2019) 120–129. https://doi.org/10.1016/j.jinorgbio.2019.03.013.

[9] N. Rosa, M.F.S.F. Moura, S. Olhero, R. Simoes, F.D. Magalhães, A.T. Marques, J.P.S. Ferreira, A.R. Reis, M. Carvalho, M. Parente, Bone: An Outstanding Composite Material, Appl. Sci. 12 (2022) 3381. https://doi.org/10.3390/app12073381.

[10] D.R. Halloran, B. Heubel, C. MacMurray, D. Root, M. Eskander, S.P. McTague, H. Pelkey, A. Nohe, Differentiation of Cells Isolated from Human Femoral Heads into Functional Osteoclasts, J. Dev. Biol. 10 (2022) 6. https://doi.org/10.3390/jdb10010006.

[11] A. Mallorie, B. Shine, Normal bone physiology, remodelling and its hormonal regulation, Surg. 40 (2022) 163–168. https://doi.org/10.1016/j.mpsur.2021.12.001.

[12] T. Ono, T. Nakashima, Oral bone biology, J. Oral Biosci. 64 (2022) 8–17. https://doi.org/10.1016/j.job.2022.01.008.

[13] J. Wolff, Das gestetz der transformation der knochem, Verlag von August Hirschwald. (1892).

[14] H.M. Frost, Bone ?mass? and the ?mechanostat?: A proposal, Anat. Rec. 219 (1987) 1–9. https://doi.org/10.1002/ar.1092190104.

[15] R. Korabi, K. Shemtov-Yona, A. Dorogoy, D. Rittel, The Failure Envelope Concept Applied To The Bone-Dental Implant System, Sci. Rep. 7 (2017) 2051. https://doi.org/10.1038/s41598-017-02282-2.

[16] S. Song, Y. Guo, Y. Yang, D. Fu, Advances in pathogenesis and therapeutic strategies for

osteoporosis, Pharmacol. Ther. 237 (2022) 108168. https://doi.org/10.1016/j.pharmthera.2022.108168.

[17] J.E. Compston, M.R. McClung, W.D. Leslie, Osteoporosis, Lancet. 393 (2019) 364–376. https://doi.org/10.1016/S0140-6736(18)32112-3.

[18] T. Vilaca, R. Eastell, M. Schini, Osteoporosis in men, Lancet Diabetes Endocrinol. 10 (2022) 273–283. https://doi.org/10.1016/S2213-8587(22)00012-2.

[19] A. Pavek, C. Nartker, M. Saleh, M. Kirkham, S. Khajeh Pour, A. Aghazadeh-Habashi, J.J. Barrott, Tissue Engineering Through 3D Bioprinting to Recreate and Study Bone Disease, Biomedicines. 9 (2021) 551. https://doi.org/10.3390/biomedicines9050551.

[20] V. Garcia-Giner, Z. Han, F. Giuliani, A.E. Porter, Nanoscale Imaging and Analysis of Bone Pathologies, Appl. Sci. 11 (2021) 12033. https://doi.org/10.3390/app112412033.

[21] J. Mitchell, A.H. van Heteren, A literature review of the spatial organization of lamellar bone, Comptes Rendus Palevol. 15 (2016) 23–31. https://doi.org/10.1016/j.crpv.2015.04.007.

[22] T. Hoenig, K.E. Ackerman, B.R. Beck, M.L. Bouxsein, D.B. Burr, K. Hollander, K.L. Popp, T. Rolvien, A.S. Tenforde, S.J. Warden, Bone stress injuries, Nat. Rev. Dis. Prim. 8 (2022) 26. https://doi.org/10.1038/s41572-022-00352-y.

[23] M. Ferretti, C. Palumbo, Static Osteogenesis versus Dynamic Osteogenesis: A Comparison between Two Different Types of Bone Formation, Appl. Sci. 11 (2021) 2025. https://doi.org/10.3390/app11052025.

[24] F. Bosco, V. Musolino, M. Gliozzi, S. Nucera, C. Carresi, M.C. Zito, F. Scarano, M.

Scicchitano, F. Reale, S. Ruga, J. Maiuolo, R. Macrì, L. Guarnieri, A.R. Coppoletta, R. Mollace, C. Muscoli, E. Palma, V. Mollace, The muscle to bone axis (and viceversa): An encrypted language affecting tissues and organs and yet to be codified?, Pharmacol. Res. 165 (2021) 105427. https://doi.org/10.1016/j.phrs.2021.105427.

[25] N.H. Hart, R.U. Newton, J. Tan, T. Rantalainen, P. Chivers, A. Siafarikas, S. Nimphius, Biological basis of bone strength: anatomy, physiology and measurement, J. Musculoskelet. Neuronal Interact. 20 (2020) 347.

[26] G.L. Koons, M. Diba, A.G. Mikos, Materials design for bone-tissue engineering, Nat. Rev. Mater. 5 (2020) 584–603. https://doi.org/10.1038/s41578-020-0204-2.

[27] D. Casari, J. Michler, P. Zysset, J. Schwiedrzik, Microtensile properties and failure mechanisms of cortical bone at the lamellar level, Acta Biomater. 120 (2021) 135–145. https://doi.org/10.1016/j.actbio.2020.04.030.

[28] X. Cai, L. Peralta, R. Brenner, G. Iori, D. Cassereau, K. Raum, P. Laugier, Q. Grimal, Anisotropic elastic properties of human cortical bone tissue inferred from inverse homogenization and resonant ultrasound spectroscopy, Materialia. 11 (2020) 100730. https://doi.org/10.1016/j.mtla.2020.100730.

[29] M. Asgari, J. Abi-Rafeh, G.N. Hendy, D. Pasini, Material anisotropy and elasticity of cortical and trabecular bone in the adult mouse femur via AFM indentation, J. Mech. Behav. Biomed. Mater. 93 (2019) 81–92. https://doi.org/10.1016/j.jmbbm.2019.01.024.

[30] G. Zhang, J. Luo, G. Zheng, Z. Bai, L. Cao, H. Mao, Is the 0.2%-Strain-Offset Approach Appropriate for Calculating the Yield Stress of Cortical Bone?, Ann. Biomed. Eng. 49 (2021) 1747–1760. https://doi.org/10.1007/s10439-020-02719-2.

[31] C.-Y. Lin, J.-H. Kang, Mechanical Properties of Compact Bone Defined by the Stress-Strain Curve Measured Using Uniaxial Tensile Test: A Concise Review and Practical Guide, Materials (Basel). 14 (2021) 4224. https://doi.org/10.3390/ma14154224.

[32] D.L. Albert, M.J. Katzenberger, A.M. Agnew, A.R. Kemper, A comparison of rib cortical bone compressive and tensile material properties: Trends with age, sex, and loading rate, J. Mech. Behav. Biomed. Mater. 122 (2021) 104668. https://doi.org/10.1016/j.jmbbm.2021.104668.

[33] D. Wu, P. Isaksson, S.J. Ferguson, C. Persson, Young's modulus of trabecular bone at the tissue level: A review, Acta Biomater. 78 (2018) 1–12. https://doi.org/10.1016/j.actbio.2018.08.001.

[34] L. Wang, Q. Chen, P.K.D.V. Yarlagadda, F. Zhu, Q. Li, Z. Li, Single-parameter mechanical design of a 3D-printed octet truss topological scaffold to match natural cancellous bones, Mater. Des. 209 (2021) 109986. https://doi.org/10.1016/j.matdes.2021.109986.

[35] É. Lakatos, L. Magyar, I. Bojtár, Material Properties of the Mandibular Trabecular Bone, J. Med. Eng. 2014 (2014) 1–7. https://doi.org/10.1155/2014/470539.

[36] F. Fan, X. Cai, H. Follet, F. Peyrin, P. Laugier, H. Niu, Q. Grimal, Cortical bone viscoelastic damping assessed with resonant ultrasound spectroscopy reflects porosity and mineral content, J. Mech. Behav. Biomed. Mater. 117 (2021) 104388. https://doi.org/10.1016/j.jmbbm.2021.104388.

[37] A. Shahin-Shamsabadi, A. Hashemi, M. Tahriri, F. Bastami, M. Salehi, F. Mashhadi Abbas, Mechanical, material, and biological study of a PCL/bioactive glass bone scaffold:

Importance of viscoelasticity, Mater. Sci. Eng. C. 90 (2018) 280–288. https://doi.org/10.1016/j.msec.2018.04.080.

[38] X. Chen, R. Hughes, N. Mullin, R.J. Hawkins, I. Holen, N.J. Brown, J.K. Hobbs, Mechanical Heterogeneity in the Bone Microenvironment as Characterized by Atomic Force Microscopy, Biophys. J. 119 (2020) 502–513. https://doi.org/10.1016/j.bpj.2020.06.026.

[39] R.N. Yadav, P. Sihota, D. Neradi, J.C. Bose, V. Dhiman, S. Karn, S. Sharma, S. Aggarwal, V.G. Goni, S.K. Bhadada, N. Kumar, Effects of type 2 diabetes on the viscoelastic behavior of human trabecular bone, Med. Eng. Phys. 104 (2022) 103810. https://doi.org/10.1016/j.medengphy.2022.103810.

[40] Y. Yue, H. Yang, Y. Li, H. Zhong, Q. Tang, J. Wang, R. Wang, H. He, W. Chen, D. Chen, Combining ultrasonic and computed tomography scanning to characterize mechanical properties of cancellous bone in necrotic human femoral heads, Med. Eng. Phys. 66 (2019) 12–17. https://doi.org/10.1016/j.medengphy.2019.02.002.

[41] B. Bai, X. Bai, C. Wang, Mapping research trends of temporomandibular disorders from 2010 to 2019: A bibliometric analysis, J. Oral Rehabil. 48 (2021) 517–530. https://doi.org/10.1111/joor.13143.

[42] C. Hague, W. Beasley, L. Dixon, S. Gaito, K. Garcez, A. Green, L.W. Lee, M. Maranzano, A. McPartlin, H. Mistry, D. Mullan, A.J. Sykes, D. Thomson, M. Van Herk, C.M. West, N. Slevin, Use of a novel atlas for muscles of mastication to reduce inter observer variability in head and neck radiotherapy contouring, Radiother. Oncol. 130 (2019) 56–61. https://doi.org/10.1016/j.radonc.2018.10.030.

[43] D. Lee, B. Chua, Gummy bear-based gnathodynamometer for masticatory diagnostics, Sensors Actuators A Phys. 290 (2019) 80–89. https://doi.org/10.1016/j.sna.2019.03.013.

[44] H.J. Kim, S. Ji, J.Y. Han, H. Bin Cho, Y.-G. Park, D. Choi, H. Cho, J.-U. Park, W. Bin Im, Detection of cracked teeth using a mechanoluminescence phosphor with a stretchable photodetector array, NPG Asia Mater. 14 (2022) 26. https://doi.org/10.1038/s41427-022-00374-8.

[45] P. Jindal, M. Juneja, F.L. Siena, D. Bajaj, P. Breedon, Mechanical and geometric properties of thermoformed and 3D printed clear dental aligners, Am. J. Orthod. Dentofac. Orthop. 156 (2019) 694–701. https://doi.org/10.1016/j.ajodo.2019.05.012.

[46] D. Sybil, K. Gopalkrishnan, Assessment of Masticatory Function Using Bite Force Measurements in Patients Treated for Mandibular Fractures, Craniomaxillofac. Trauma Reconstr. 6 (2013) 247–250. https://doi.org/10.1055/s-0033-1356755.

[47] R. Buser, V. Ziltener, S. Samietz, M. Fontolliet, T. Nef, M. Schimmel, Validation of a purpose-built chewing gum and smartphone application to evaluate chewing efficiency, J. Oral Rehabil. 45 (2018) 845–853. https://doi.org/10.1111/joor.12696.

[48] E.A. Mokhtar, V. Rattan, S. Rai, S.S. Jolly, V. Lal, Analysis of maximum bite force and chewing efficiency in unilateral temporomandibular joint ankylosis cases treated with buccal fat pad interpositional arthroplasty, Br. J. Oral Maxillofac. Surg. 60 (2022) 313–319. https://doi.org/10.1016/j.bjoms.2021.07.007.

[49] V. Pitchika, R.A. Jordan, O. Norderyd, B. Rolander, A. Welk, H. Völzke, B. Holtfreter, T. Kocher, Factors influencing tooth loss in European populations, J. Clin. Periodontol. 49 (2022) 642–653. https://doi.org/10.1111/jcpe.13642.

[50] G.T. Vu, B.B. Little, P.C. Lai, G.-L. Cheng, Tooth loss and uncontrolled diabetes among US adults, J. Am. Dent. Assoc. 153 (2022) 542–551. https://doi.org/10.1016/j.adaj.2021.11.008.

[51] E. Emami, R.F. de Souza, M. Kabawat, J.S. Feine, The Impact of Edentulism on Oral and General Health, Int. J. Dent. 2013 (2013) 1–7. https://doi.org/10.1155/2013/498305.

[52] O. Şakar, Classification of Partially Edentulous Arches, in: Removable Partial Dentures, Springer International Publishing, Cham, 2016: pp. 17–21. https://doi.org/10.1007/978-3-319-20556-4_3.

[53] M.Q. Mubaraki, M.M. Al Moaleem, A.H. Alzahrani, M. Shariff, S.M. Alqahtani, A. Porwal, F.A. Al-Sanabani, S. Bhandi, J.P.M. Tribst, A. Heboyan, S. Patil, Assessment of Conventionally and Digitally Fabricated Complete Dentures: A Comprehensive Review, Materials (Basel). 15 (2022) 3868. https://doi.org/10.3390/ma15113868.

[54] P.-I. Brånemark, U. Breine, R. Adell, B.O. Hansson, J. Lindström, Å. Ohlsson, Intra-Osseous Anchorage of Dental Prostheses: I. Experimental Studies, Scand. J. Plast. Reconstr. Surg. 3 (1969) 81–100. https://doi.org/10.3109/02844316909036699.

[55] F.A. Shah, P. Thomsen, A. Palmquist, Osseointegration and current interpretations of the bone-implant interface, Acta Biomater. 84 (2019) 1–15. https://doi.org/10.1016/j.actbio.2018.11.018.

[56] A. Vollmer, B. Saravi, G. Lang, N. Adolphs, D. Hazard, V. Giers, P. Stoll, Factors Influencing Primary and Secondary Implant Stability—A Retrospective Cohort Study with 582 Implants in 272 Patients, Appl. Sci. 10 (2020) 8084. https://doi.org/10.3390/app10228084.

[57] S. Schnutenhaus, W. Götz, J. Dreyhaupt, H. Rudolph, R.G. Luthardt, C. Edelmann, Associations among Primary Stability, Histomorphometric Findings, and Bone Density: A Prospective Randomized Study after Alveolar Ridge Preservation with a Collagen Cone, Dent. J. 8 (2020) 112. https://doi.org/10.3390/dj8040112.

[58] A. Ibrahim, M. Heitzer, A. Bock, F. Peters, S.C. Möhlhenrich, F. Hölzle, A. Modabber, K. Kniha, Relationship between Implant Geometry and Primary Stability in Different Bony Defects and Variant Bone Densities: An In Vitro Study, Materials (Basel). 13 (2020) 4349. https://doi.org/10.3390/ma13194349.

[59] N. Meredith, D. Alleyne, P. Cawley, Quantitative determination of the stability of the implant-tissue interface using resonance frequency analysis, Clin. Oral Implants Res. 7 (1996) 261–267. https://doi.org/10.1034/j.1600-0501.1996.070308.x.

[60] A. Sachdeva, P. Dhawan, S. Sindwani, Assessment of Implant Stability: Methods and Recent Advances, Br. J. Med. Med. Res. 12 (2016) 1–10. https://doi.org/10.9734/BJMMR/2016/21877.

[61] L. Pagliani, L. Sennerby, A. Petersson, D. Verrocchi, S. Volpe, P. Andersson, The relationship between resonance frequency analysis (RFA) and lateral displacement of dental implants: an in vitro study, J. Oral Rehabil. 40 (2013) 221–227. https://doi.org/10.1111/joor.12024.

[62] U. Lekholm, Patient selection and preparation, Tissue Integr. Prothes. (1985) 199–209.

[63] M.R. Norton, C. Gamble, Bone classification: an objective scale of bone density using the computerized tomography scan, Clin. Oral Implants Res. 12 (2001) 79–84.

[64] R.A. de Medeiros, E.P. Pellizzer, A.J. Vechiato Filho, D.M. dos Santos, E.V.F. da Silva,

M.C. Goiato, Evaluation of marginal bone loss of dental implants with internal or external connections and its association with other variables: A systematic review, J. Prosthet. Dent. 116 (2016) 501-506.e5. https://doi.org/10.1016/j.prosdent.2016.03.027.

[65] C.A.A. Lemos, V.E. de Souza Batista, D.A. de F. Almeida, J.F. Santiago Júnior, F.R. Verri, E.P. Pellizzer, Evaluation of cement-retained versus screw-retained implant-supported restorations for marginal bone loss, J. Prosthet. Dent. 115 (2016) 419–427. https://doi.org/10.1016/j.prosdent.2015.08.026.

[66] W. Niu, P. Wang, S. Zhu, Z. Liu, P. Ji, Marginal bone loss around dental implants with and without microthreads in the neck: A systematic review and meta-analysis, J. Prosthet. Dent. 117 (2017) 34–40. https://doi.org/10.1016/j.prosdent.2016.07.003.

[67] K. Yasuda, S. Okada, Y. Okazaki, K. Hiasa, K. Tsuga, Y. Abe, Bone turnover markers to assess jawbone quality prior to dental implant treatment: a case-control study, Int. J. Implant Dent. 6 (2020) 67. https://doi.org/10.1186/s40729-020-00264-0.

[68] T. Albrektsson, G. Zarb, P. Worthington, A.R. Eriksson, The long-term efficacy of currently used dental implants: a review and proposed criteria of success, Int j Oral Maxillofac Implant. 1 (1986) 11–25.

[69] D.E. Smith, G.A. Zarb, Criteria for success of osseointegrated endosseous implants, J. Prosthet. Dent. 62 (1989) 567–572. https://doi.org/10.1016/0022-3913(89)90081-4.

[70] K. Karthik, Sivakumar, Sivaraj, V. Thangaswamy, Evaluation of implant success: A review of past and present concepts, J. Pharm. Bioallied Sci. 5 (2013) 117. https://doi.org/10.4103/0975-7406.113310.

[71] S. Park, J. Park, I. Kang, H. Lee, G. Noh, Effects of assessing the bone remodeling process

in biomechanical finite element stability evaluations of dental implants, Comput. Methods Programs Biomed. 221 (2022) 106852. https://doi.org/10.1016/j.cmpb.2022.106852.

[72] B. Jafari, H.R. Katoozian, M. Tahani, N. Ashjaee, A comparative study of bone remodeling around hydroxyapatite-coated and novel radial functionally graded dental implants using finite element simulation, Med. Eng. Phys. 102 (2022) 103775. https://doi.org/10.1016/j.medengphy.2022.103775.

[73] A.C. Dayrell, C.T. Pimenta de Araújo, R.L. Rocha, C.P. Isolan, P.Y. Noritomi, M.F. Mesquita, Biomechanics of internal connection in mandibular implant-supported prosthesis under effect of loadings and number of implants: A 3D finite element analysis, Comput. Biol. Med. 148 (2022) 105755. https://doi.org/10.1016/j.compbiomed.2022.105755.

[74] H.-C. Chang, C.-H. Chang, H.-Y. Li, C.-H. Wang, Biomechanical analysis of the press-fit effect in a conical Morse taper implant system by using an in vitro experimental test and finite element analysis, J. Prosthet. Dent. 127 (2022) 601–608. https://doi.org/10.1016/j.prosdent.2020.10.022.

[75] B. Xie, J. Chen, T. Zhao, J. Shen, I. Dörsam, Y. He, Three-dimensional finite element analysis of anterior fixed partial denture supported by implants with different materials, Ann. Anat. - Anat. Anzeiger. 243 (2022) 151943. https://doi.org/10.1016/j.aanat.2022.151943.

[76] L. Zupancic Cepic, M. Frank, A.G. Reisinger, B. Sagl, D.H. Pahr, W. Zechner, A. Schedle, Experimental validation of a micro-CT finite element model of a human cadaveric mandible rehabilitated with short-implant-supported partial dentures, J. Mech. Behav.

Biomed. Mater. 126 (2022) 105033. https://doi.org/10.1016/j.jmbbm.2021.105033.

[77] L.-S. Huang, Y.-C. Huang, C. Yuan, S.-J. Ding, M. Yan, Biomechanical evaluation of bridge span with three implant abutment designs and two connectors for tooth-implant supported prosthesis: A finite element analysis, J. Dent. Sci. 18 (2023) 248–263. https://doi.org/10.1016/j.jds.2022.05.026.

[78] S. Chen, R. Li, Z. Wu, J. Wang, G. Xie, H. Xie, X. Pei, An implant-supported overdenture for a mandibular defect after tumor resection guided by 3-dimensional finite element analysis: A clinical report, J. Prosthet. Dent. (2022). https://doi.org/10.1016/j.prosdent.2022.04.031.

[79] F. Sun, L.-T. Lv, D.-D. Xiang, D.-C. Ba, Z. Lin, G.-Q. Song, Effect of central screw taper angles on the loosening performance and fatigue characteristics of dental implants, J. Mech. Behav. Biomed. Mater. 129 (2022) 105136. https://doi.org/10.1016/j.jmbbm.2022.105136.

[80] P.G. Patil, L.L. Seow, R. Uddanwadikar, A. Pau, P.D. Ukey, Different implant diameters and their effect on stress distribution pattern in 2-implant mandibular overdentures: A 3D finite element analysis study, J. Prosthet. Dent. (2022). https://doi.org/10.1016/j.prosdent.2022.04.018.

[81] W. Yu, X. Li, X. Ma, X. Xu, Biomechanical analysis of inclined and cantilever design with different implant framework materials in mandibular complete-arch implant restorations, J. Prosthet. Dent. 127 (2022) 783.e1-783.e10. https://doi.org/10.1016/j.prosdent.2022.02.018.

[82] M. Armentia, M. Abasolo, I. Coria, N. Sainitier, Effect of the geometry of butt-joint

implant-supported restorations on the fatigue life of prosthetic screws, J. Prosthet. Dent. 127 (2022) 477.e1-477.e9. https://doi.org/10.1016/j.prosdent.2021.12.010.

[83] A.M.A. Mohamed, M.G. Askar, M.E.-M.B. El Homossany, Stresses induced by one piece and two piece dental implants in All-on-4® implant supported prosthesis under simulated lateral occlusal loading: non linear finite element analysis study, BMC Oral Health. 22 (2022) 196. https://doi.org/10.1186/s12903-022-02228-9.

[84] A. Mohammadi Anari, E. Selahi, Progressive damage analysis of functionally graded dental implants due to pre-tightening loads using extended finite element method, J. Brazilian Soc. Mech. Sci. Eng. 44 (2022) 283. https://doi.org/10.1007/s40430-022-03581-0.

[85] L. Zupancic Cepic, M. Frank, A. Reisinger, D. Pahr, W. Zechner, A. Schedle, Biomechanical finite element analysis of short-implant-supported, 3-unit, fixed CAD/CAM prostheses in the posterior mandible, Int. J. Implant Dent. 8 (2022) 8. https://doi.org/10.1186/s40729-022-00404-8.

[86] C. Liu, Y. Xing, Y. Li, Y. Lin, J. Xu, D. Wu, Bone quality effect on short implants in the edentulous mandible: a finite element study, BMC Oral Health. 22 (2022) 139. https://doi.org/10.1186/s12903-022-02164-8.

[87] K.-C. Cheng, P.-H. Liu, H.-S. Chen, T.-H. Lan, Stress Distribution of Four-Unit Implant-Supported Fixed Partial Prosthesis with Different Numbers and Positions of Fixtures in Maxilla Anterior Region-3D FEA, J. Med. Biol. Eng. 42 (2022) 526–533. https://doi.org/10.1007/s40846-022-00729-0.

[88] L. Bassi-Junior, R. Oliveira de Souza Silva, V.H. Dias dos Santos, A. da Rocha Lourenço,

P.V. Trevizoli, H. Gaêta-Araujo, P.M. Queiroz, V.D. Gottardo, Mechanical analysis of prosthetic bars and dental implants in 3 and 4 implant-supported overdenture protocols using finite element analysis, J. Oral Biol. Craniofacial Res. 11 (2021) 438–441. https://doi.org/10.1016/j.jobcr.2021.05.007.

[89] P. Ausiello, J.P.M. Tribst, M. Ventre, E. Salvati, A.E. di Lauro, M. Martorelli, A. Lanzotti, D.C. Watts, The role of cortical zone level and prosthetic platform angle in dental implant mechanical response: A 3D finite element analysis, Dent. Mater. 37 (2021) 1688–1697. https://doi.org/10.1016/j.dental.2021.08.022.

[90] H. Lee, M. Jo, G. Noh, Biomechanical effects of dental implant diameter, connection type, and bone density on microgap formation and fatigue failure: A finite element analysis, Comput. Methods Programs Biomed. 200 (2021) 105863. https://doi.org/10.1016/j.cmpb.2020.105863.

[91] L.S. Silva, F.R. Verri, C.A.A. Lemos, C.M. Martins, E.P. Pellizzer, V.E. de Souza Batista, Biomechanical effect of an occlusal device for patients with an implant-supported fixed dental prosthesis under parafunctional loading: A 3D finite element analysis, J. Prosthet. Dent. 126 (2021) 223.e1-223.e8. https://doi.org/10.1016/j.prosdent.2021.04.024.

[92] D. Fabris, M.C. Fredel, J.C.M. Souza, F.S. Silva, B. Henriques, Biomechanical behavior of functionally graded S53P4 bioglass-zirconia dental implants: Experimental and finite element analyses, J. Mech. Behav. Biomed. Mater. 120 (2021) 104565. https://doi.org/10.1016/j.jmbbm.2021.104565.

[93] A. Jafariandehkordi, Z. Jafariandehkordi, A finite element optimization of the design variables of a dental implant screw based on the Mechanostat Theory, Comput. Methods

Programs Biomed. Updat. 1 (2021) 100033. https://doi.org/10.1016/j.cmpbup.2021.100033.

[94] J. Chen, L. Wang, L. Yang, X. Zhang, B. Huang, J. Li, The prosthetic screw loosening of two-implant supported screw-retained fixed dental prostheses in the posterior region: A retrospective evaluation and finite element analysis, J. Biomech. 122 (2021) 110423. https://doi.org/10.1016/j.jbiomech.2021.110423.

[95] C. Liu, J. Lin, L. Tang, Z. Liu, Z. Jiang, K. Lian, Design of metal-polymer structure for dental implants with stiffness adaptable to alveolar bone, Compos. Commun. 24 (2021) 100660. https://doi.org/10.1016/j.coco.2021.100660.

[96] O. Cantó-Navés, X. Marimon, M. Ferrer, J. Cabratosa-Termes, Comparison between experimental digital image processing and numerical methods for stress analysis in dental implants with different restorative materials, J. Mech. Behav. Biomed. Mater. 113 (2021) 104092. https://doi.org/10.1016/j.jmbbm.2020.104092.

[97] H. Lee, M. Jo, I. Sailer, G. Noh, Effects of implant diameter, implant-abutment connection type, and bone density on the biomechanical stability of implant components and bone: A finite element analysis study, J. Prosthet. Dent. 128 (2022) 716–728. https://doi.org/10.1016/j.prosdent.2020.08.042.

[98] M. Gibreel, A. Sameh, S. Hegazy, T.O. Närhi, P.K. Vallittu, L. Perea-Lowery, Effect of specific retention biomaterials for ball attachment on the biomechanical response of single implant-supported overdenture: A finite element analysis, J. Mech. Behav. Biomed. Mater. 122 (2021) 104653. https://doi.org/10.1016/j.jmbbm.2021.104653.

[99] E. Kul, İ.H. Korkmaz, Effect of different design of abutment and implant on stress

distribution in 2 implants and peripheral bone: A finite element analysis study, J. Prosthet. Dent. 126 (2021) 664.e1-664.e9. https://doi.org/10.1016/j.prosdent.2020.09.058.

[100] B.S. Honório Tonin, Y. He, N. Ye, H.P. Chew, A. Fok, Effects of tightening torque on screw stress and formation of implant-abutment microgaps: A finite element analysis, J. Prosthet. Dent. 127 (2022) 882–889. https://doi.org/10.1016/j.prosdent.2020.11.026.

[101] C.A.A. Lemos, F.R. Verri, P.Y. Noritomi, D.T. Kemmoku, V.E. de Souza Batista, R.S. Cruz, J.M. de Luna Gomes, E.P. Pellizzer, Effect of bone quality and bone loss level around internal and external connection implants: A finite element analysis study, J. Prosthet. Dent. 125 (2021) 137.e1-137.e10. https://doi.org/10.1016/j.prosdent.2020.06.029.

[102] P.G. Patil, L.L. Seow, R. Uddanwadikar, P.D. Ukey, Biomechanical behavior of mandibular overdenture retained by two standard implants or 2 mini implants: A 3-dimensional finite element analysis, J. Prosthet. Dent. 125 (2021) 138.e1-138.e8. https://doi.org/10.1016/j.prosdent.2020.09.015.

[103] A. Darwich, A. Alammar, O. Heshmeh, S. Szabolcs, H. Nazha, Fatigue Loading Effect in Custom-Made All-on-4 Implants System: A 3D Finite Elements Analysis, IRBM. 43 (2022) 372–379. https://doi.org/10.1016/j.irbm.2021.06.008.

[104] S. Giner, J.F. Bartolomé, P. Gomez-Cogolludo, C. Castellote, G. Pradíes, Fatigue fracture resistance of titanium and chairside CAD-CAM zirconia implant abutments supporting zirconia crowns: An in vitro comparative and finite element analysis study, J. Prosthet. Dent. 125 (2021) 503.e1-503.e9. https://doi.org/10.1016/j.prosdent.2020.09.025.

[105] G.A. Borges, A.G.C. Presotto, R.A. Caldas, M.X. Pisani, M.F. Mesquita, Is one dental

mini-implant biomechanically appropriate for the retention of a mandibular overdenture? A comparison with Morse taper and external hexagon platforms, J. Prosthet. Dent. 125 (2021) 491–499. https://doi.org/10.1016/j.prosdent.2020.01.038.

[106] H.-Y. Lee, S.-W. Yang, Y.-J. Kang, K.C. Oh, J.-H. Kim, Influence of shoulder coverage difference of abutment on stress distribution and screw stability in tissue-level internal connection implants: A finite element analysis and in vitro study, J. Prosthet. Dent. 125 (2021) 682.e1-682.e10. https://doi.org/10.1016/j.prosdent.2020.08.022.

[107] E. Sato, R. Shigemitsu, T. Mito, N. Yoda, J. Rasmussen, K. Sasaki, The effects of bone remodeling on biomechanical behavior in a patient with an implant-supported overdenture, Comput. Biol. Med. 129 (2021) 104173. https://doi.org/10.1016/j.compbiomed.2020.104173.

[108] A. Mourya, R. Nahar, S.K. Mishra, R. Chowdhary, Stress distribution around different abutments on titanium and CFR-PEEK implant with different prosthetic crowns under parafunctional loading: A 3D FEA study, J. Oral Biol. Craniofacial Res. 11 (2021) 313–320. https://doi.org/10.1016/j.jobcr.2021.03.005.

[109] P. Oyar, R. Durkan, G. Deste, The effect of the design of a mandibular implant-supported zirconia prosthesis on stress distribution, J. Prosthet. Dent. 125 (2021) 502.e1-502.e11. https://doi.org/10.1016/j.prosdent.2020.05.027.

[110] P. Ercal, A.E. Taysi, D.C. Ayvalioglu, M.M. Eren, S. Sismanoglu, Impact of peri-implant bone resorption, prosthetic materials, and crown to implant ratio on the stress distribution of short implants: a finite element analysis, Med. Biol. Eng. Comput. 59 (2021) 813–824. https://doi.org/10.1007/s11517-021-02342-w.

[111] J.J. da Rocha Ferreira, L.F.M. Machado, J.M. Oliveira, J.C.T. Ramos, Effect of crown-to-implant ratio and crown height space on marginal bone stress: a finite element analysis, Int. J. Implant Dent. 7 (2021) 81. https://doi.org/10.1186/s40729-021-00368-1.

[112] Ö.Ö. Zincir, A. Parlar, Comparison of stresses in monoblock tilted implants and conventional angled multiunit abutment-implant connection systems in the all-on-four procedure, BMC Oral Health. 21 (2021) 646. https://doi.org/10.1186/s12903-021-02023-y.

[113] A. Manafi Khajeh Pasha, R. Mahmoudi Sheykhsarmast, S. Manafi Khajeh Pasha, E. Khashabi, Influence of Treatment Plans on Stress and Deformation Distribution in Mandibular Implant-Supported Overdenture and Mandibular Bone under Traumatic Load: A 3D FEA, J. Med. Biol. Eng. 41 (2021) 543–557. https://doi.org/10.1007/s40846-021-00639-7.

[114] M. Pirmoradian, H.A. Naeeni, M. Firouzbakht, D. Toghraie, M.K. Khabaz, R. Darabi, Finite element analysis and experimental evaluation on stress distribution and sensitivity of dental implants to assess optimum length and thread pitch, Comput. Methods Programs Biomed. 187 (2020) 105258. https://doi.org/10.1016/j.cmpb.2019.105258.

[115] A. Chakraborty, P. Datta, S. Majumder, S.C. Mondal, A. Roychowdhury, Finite element and experimental analysis to select patient's bone condition specific porous dental implant, fabricated using additive manufacturing, Comput. Biol. Med. 124 (2020) 103839. https://doi.org/10.1016/j.compbiomed.2020.103839.

[116] R. Alaqeely, N. Babay, M. AlQutub, Dental implant primary stability in different regions of the Jawbone: CBCT-based 3D finite element analysis, Saudi Dent. J. 32 (2020) 101–107. https://doi.org/10.1016/j.sdentj.2019.06.001.

[117] J.F. Valera-Jiménez, G. Burgueño-Barris, S. Gómez-González, J. López-López, E. Valmaseda-Castellón, E. Fernández-Aguado, Finite element analysis of narrow dental implants, Dent. Mater. 36 (2020) 927–935. https://doi.org/10.1016/j.dental.2020.04.013.

[118] O. Kayabasi, Design methodology for dental implant using approximate solution techniques, J. Stomatol. Oral Maxillofac. Surg. 121 (2020) 684–695. https://doi.org/10.1016/j.jormas.2020.01.003.

[119] A.Y.-J. Wu, J.-T. Hsu, L.-J. Fuh, H.-L. Huang, Biomechanical effect of implant design on four implants supporting mandibular full-arch fixed dentures: In vitro test and finite element analysis, J. Formos. Med. Assoc. 119 (2020) 1514–1523. https://doi.org/10.1016/j.jfma.2019.12.001.

[120] Z.-H. Jin, M.-D. Peng, Q. Li, The effect of implant neck microthread design on stress distribution of peri-implant bone with different level: A finite element analysis, J. Dent. Sci. 15 (2020) 466–471. https://doi.org/10.1016/j.jds.2019.12.003.

[121] F. Bayata, C. Yildiz, The effects of design parameters on mechanical failure of Ti-6Al-4V implants using finite element analysis, Eng. Fail. Anal. 110 (2020) 104445. https://doi.org/10.1016/j.engfailanal.2020.104445.

[122] E.J. Moreira de Melo, C.E. Francischone, Three-dimensional finite element analysis of two angled narrow-diameter implant designs for an all-on-4 prosthesis, J. Prosthet. Dent. 124 (2020) 477–484. https://doi.org/10.1016/j.prosdent.2019.09.015.

[123] T.A. Dantas, J.P. Carneiro Neto, J.L. Alves, P.C.S. Vaz, F.S. Silva, In silico evaluation of the stress fields on the cortical bone surrounding dental implants: Comparing root-analogue and screwed implants, J. Mech. Behav. Biomed. Mater. 104 (2020) 103667.

https://doi.org/10.1016/j.jmbbm.2020.103667.

[124] E. de Souza Rendohl, W.C. Brandt, Stress distribution with extra-short implants in an angled frictional system: A finite element analysis study, J. Prosthet. Dent. 124 (2020) 728.e1-728.e9. https://doi.org/10.1016/j.prosdent.2020.04.022.

[125] A. Bachiri, N. Djebbar, B. Boutabout, B. Serier, Effect of different impactor designs on biomechanical behavior in the interface bone-implant: A comparative biomechanics study, Comput. Methods Programs Biomed. 197 (2020) 105723. https://doi.org/10.1016/j.cmpb.2020.105723.

[126] A. Ayali, M. Altagar, O. Ozan, S. Kurtulmus-Yilmaz, Biomechanical comparison of the All-on-4, M-4, and V-4 techniques in an atrophic maxilla: A 3D finite element analysis, Comput. Biol. Med. 123 (2020) 103880. https://doi.org/10.1016/j.compbiomed.2020.103880.

[127] J. Zhong, M. Guazzato, J. Chen, Z. Zhang, G. Sun, X. Huo, X. Liu, R. Ahmad, Q. Li, Effect of different implant configurations on biomechanical behavior of full-arch implant-supported mandibular monolithic zirconia fixed prostheses, J. Mech. Behav. Biomed. Mater. 102 (2020) 103490. https://doi.org/10.1016/j.jmbbm.2019.103490.

[128] M.R. Niroomand, M. Arabbeiki, Implant stability in different implantation stages: Analysis of various interface conditions, Informatics Med. Unlocked. 19 (2020) 100317. https://doi.org/10.1016/j.imu.2020.100317.

[129] M. Stocchero, Y. Jinno, M. Toia, R. Jimbo, C. Lee, S. Yamaguchi, S. Imazato, J.P. Becktor, In silico multi-scale analysis of remodeling peri-implant cortical bone: a comparison of two types of bone structures following an undersized and non-undersized

technique, J. Mech. Behav. Biomed. Mater. 103 (2020) 103598. https://doi.org/10.1016/j.jmbbm.2019.103598.

[130] J. Morita, M. Wada, T. Mameno, Y. Maeda, K. Ikebe, Ideal placement of an implant considering the positional relationship to an opposing tooth in the first molar region: a three-dimensional finite element analysis, Int. J. Implant Dent. 6 (2020) 31. https://doi.org/10.1186/s40729-020-00223-9.

[131] H. Araki, T. Nakano, S. Ono, H. Yatani, Three-dimensional finite element analysis of extra short implants focusing on implant designs and materials, Int. J. Implant Dent. 6 (2020) 5. https://doi.org/10.1186/s40729-019-0202-6.

[132] M. Shash, H. Nazha, W. Abbas, Influence of Different Abutment Designs on the Biomechanical Behavior of One-Piece Zirconia Dental Implants and Their Surrounding Bone: A 3D-FEA, IRBM. 40 (2019) 313–319. https://doi.org/10.1016/j.irbm.2019.07.001.

[133] A. Brune, M. Stiesch, M. Eisenburger, A. Greuling, The effect of different occlusal contact situations on peri-implant bone stress – A contact finite element analysis of indirect axial loading, Mater. Sci. Eng. C. 99 (2019) 367–373. https://doi.org/10.1016/j.msec.2019.01.104.

[134] S. Chatterjee, S. Sarkar, S.R. Kalidindi, B. Basu, Periprosthetic biomechanical response towards dental implants, with functional gradation, for single/multiple dental loss, J. Mech. Behav. Biomed. Mater. 94 (2019) 249–258. https://doi.org/10.1016/j.jmbbm.2019.03.001.

[135] W. Jung, W. Lee, H.-B. Kwon, Effects of abutment screw preload in two implant connection systems: A 3D finite element study, J. Prosthet. Dent. 122 (2019) 474.e1-474.e8. https://doi.org/10.1016/j.prosdent.2019.04.025.

[136] F. Azcarate-Velázquez, R. Castillo-Oyagüe, L.-G. Oliveros-López, D. Torres-Lagares, Á.-J. Martínez-González, A. Pérez-Velasco, C.D. Lynch, J.-L. Gutiérrez-Pérez, M.-Á. Serrera-Figallo, Influence of bone quality on the mechanical interaction between implant and bone: A finite element analysis, J. Dent. 88 (2019) 103161. https://doi.org/10.1016/j.jdent.2019.06.008.

[137] V. Demenko, I. Linetskiy, L. Linetska, O. Yefremov, Load-carrying capacity of short implants in edentulous posterior maxilla: A finite element study, Med. Eng. Phys. 71 (2019) 30–37. https://doi.org/10.1016/j.medengphy.2019.02.003.

[138] H.-C. Chang, H.-Y. Li, Y.-N. Chen, C.-H. Chang, C.-H. Wang, Mechanical analysis of a dental implant system under 3 contact conditions and with 2 mechanical factors, J. Prosthet. Dent. 122 (2019) 376–382. https://doi.org/10.1016/j.prosdent.2018.10.008.

[139] A. Aslam, S.H. Hassan, H.M. Aslam, D.A. Khan, Effect of platform switching on peri-implant bone: A 3D finite element analysis, J. Prosthet. Dent. 121 (2019) 935–940. https://doi.org/10.1016/j.prosdent.2018.08.011.

[140] G. Berger, L.F. de O. Pereira, E.M. de Souza, R.N. Rached, A 3D finite element analysis of glass fiber reinforcement designs on the stress of an implant-supported overdenture, J. Prosthet. Dent. 121 (2019) 865.e1-865.e7. https://doi.org/10.1016/j.prosdent.2019.02.010.

[141] R. Kasani, B.K. Rama Sai Attili, V.K. Dommeti, A. Merdji, J.K. Biswas, S. Roy, Stress distribution of overdenture using odd number implants – A Finite Element Study, J. Mech. Behav. Biomed. Mater. 98 (2019) 369–382. https://doi.org/10.1016/j.jmbbm.2019.06.030.

[142] H. Lee, S. Park, G. Noh, Biomechanical analysis of 4 types of short dental implants in a resorbed mandible, J. Prosthet. Dent. 121 (2019) 659–670.

https://doi.org/10.1016/j.prosdent.2018.07.013.

[143] H.A. Bulaqi, A. Barzegar, M. Paknejad, H. Safari, Assessment of preload, remaining torque, and removal torque in abutment screws under different frictional conditions: A finite element analysis, J. Prosthet. Dent. 121 (2019) 548.e1-548.e7. https://doi.org/10.1016/j.prosdent.2018.10.035.

[144] G.P. Petris, J.P. De Carli, L.R. Paranhos, P.L. Santos, P. Benetti, M. Walber, E.S. Linden, M.S.S. Linden, Morse taper performance: A finite element analysis study, Clinics. 74 (2019) e852. https://doi.org/10.6061/clinics/2019/e852.

[145] G. de la Rosa Castolo, S. V. Guevara Perez, P.-J. Arnoux, L. Badih, F. Bonnet, M. Behr, Implant-supported overdentures with different clinical configurations: Mechanical resistance using a numerical approach, J. Prosthet. Dent. 121 (2019) 546.e1-546.e10. https://doi.org/10.1016/j.prosdent.2018.09.023.

[146] C.C. Mello, J.F. Santiago Junior, C.A.A. Lemos, G.A. Galhano, E. Evangelisti, R. Scotti, F.R. Verri, E.P. Pellizzer, Evaluation of the accuracy and stress distribution of 3-unit implant supported prostheses obtained by different manufacturing methods, Mater. Sci. Eng. C. 102 (2019) 66–74. https://doi.org/10.1016/j.msec.2019.03.059.

[147] Y.-C. Cheng, C.-P. Jiang, D.-H. Lin, Finite element based optimization design for a one-piece zirconia ceramic dental implant under dynamic loading and fatigue life validation, Struct. Multidiscip. Optim. 59 (2019) 835–849. https://doi.org/10.1007/s00158-018-2104-2.

[148] V. Sharanraj, C.M. Ramesha, V. Kumar, M. Sadashiva, Finite Element Analysis of Zirconia Ceramic Biomaterials Used in Medical Dental Implants, Interceram - Int. Ceram.

Rev. 68 (2019) 24–31. https://doi.org/10.1007/s42411-019-0004-0.

[149] E. Dávila, M. Ortiz-Hernández, R.A. Perez, M. Herrero-Climent, M. Cerrolaza, F.J. Gil, Crestal module design optimization of dental implants: finite element analysis and in vivo studies, J. Mater. Sci. Mater. Med. 30 (2019) 90. https://doi.org/10.1007/s10856-019-6291-1.

[150] Z. Li, S. Gao, H. Chen, R. Ma, T. Wu, H. Yu, Micromotion of implant-abutment interfaces (IAI) after loading: correlation of finite element analysis with in vitro performances, Med. Biol. Eng. Comput. 57 (2019) 1133–1144. https://doi.org/10.1007/s11517-018-1937-6.

[151] P. Dhatrak, V. Girme, U. Shirsat, S. Sumanth, V. Deshmukh, Significance of Orthotropic Material Models to Predict Stress Around Bone-Implant Interface Using Numerical Simulation, Bionanoscience. 9 (2019) 652–659. https://doi.org/10.1007/s12668-019-00649-5.

[152] J. Li, J.A. Jansen, X.F. Walboomers, J.J. van den Beucken, Mechanical aspects of dental implants and osseointegration: A narrative review, J. Mech. Behav. Biomed. Mater. 103 (2020) 103574. https://doi.org/10.1016/j.jmbbm.2019.103574.

[153] E. Vidal, D. Torres, J. Guillem-Marti, G. Scionti, J.M. Manero, M.-P. Ginebra, D. Rodríguez, E. Rupérez, Titanium Scaffolds by Direct Ink Writing: Fabrication and Functionalization to Guide Osteoblast Behavior, Metals (Basel). 10 (2020) 1156. https://doi.org/10.3390/met10091156.

[154] G.E. Romanos, R.A. Delgado-Ruiz, D. Sacks, J.L. Calvo-Guirado, Influence of the implant diameter and bone quality on the primary stability of porous tantalum trabecular metal dental implants: an in vitro biomechanical study, Clin. Oral Implants Res. 29 (2018)

649–655. https://doi.org/10.1111/clr.12792.

[155] G. Yamako, D. Janssen, S. Hanada, T. Anijs, K. Ochiai, K. Totoribe, E. Chosa, N. Verdonschot, Improving stress shielding following total hip arthroplasty by using a femoral stem made of β type Ti-33.6Nb-4Sn with a Young's modulus gradation, J. Biomech. 63 (2017) 135–143. https://doi.org/10.1016/j.jbiomech.2017.08.017.

[156] S. Lascano, C. Arévalo, I. Montealegre-Melendez, S. Muñoz, J. Rodriguez-Ortiz, P. Trueba, Y. Torres, Porous Titanium for Biomedical Applications: Evaluation of the Conventional Powder Metallurgy Frontier and Space-Holder Technique, Appl. Sci. 9 (2019) 982. https://doi.org/10.3390/app9050982.

[157] A. Rodriguez-Contreras, M. Punset, J.A. Calero, F.J. Gil, E. Ruperez, J.M. Manero, Powder metallurgy with space holder for porous titanium implants: A review, J. Mater. Sci. Technol. 76 (2021) 129–149. https://doi.org/10.1016/j.jmst.2020.11.005.

[158] E. Liverani, G. Rogati, S. Pagani, S. Brogini, A. Fortunato, P. Caravaggi, Mechanical interaction between additive-manufactured metal lattice structures and bone in compression: implications for stress shielding of orthopaedic implants, J. Mech. Behav. Biomed. Mater. 121 (2021) 104608. https://doi.org/10.1016/j.jmbbm.2021.104608.

[159] C. Domínguez-Trujillo, F. Ternero, J.A. Rodríguez-Ortiz, J.J. Pavón, I. Montealegre-Meléndez, C. Arévalo, F. García-Moreno, Y. Torres, Improvement of the balance between a reduced stress shielding and bone ingrowth by bioactive coatings onto porous titanium substrates, Surf. Coatings Technol. 338 (2018) 32–37. https://doi.org/10.1016/j.surfcoat.2018.01.019.

[160] A. Manoj, A.K. Kasar, P.L. Menezes, Tribocorrosion of Porous Titanium Used in

Biomedical Applications, J. Bio- Tribo-Corrosion. 5 (2019) 3. https://doi.org/10.1007/s40735-018-0194-4.

[161] Z. Chen, X. Yan, S. Yin, L. Liu, X. Liu, G. Zhao, W. Ma, W. Qi, Z. Ren, H. Liao, M. Liu, D. Cai, H. Fang, Influence of the pore size and porosity of selective laser melted Ti6Al4V ELI porous scaffold on cell proliferation, osteogenesis and bone ingrowth, Mater. Sci. Eng. C. 106 (2020) 110289. https://doi.org/10.1016/j.msec.2019.110289.

[162] J. LI, P. HABIBOVIC, M. VANDENDOEL, C. WILSON, J. DEWIJN, C. VANBLITTERSWIJK, K. DEGROOT, Bone ingrowth in porous titanium implants produced by 3D fiber deposition, Biomaterials. 28 (2007) 2810–2820. https://doi.org/10.1016/j.biomaterials.2007.02.020.

[163] T. Liu, Y. Chen, A. Apicella, Z. Mu, T. Yu, Y. Huang, C. Wang, Effect of Porous Microstructures on the Biomechanical Characteristics of a Root Analogue Implant: An Animal Study and a Finite Element Analysis, ACS Biomater. Sci. Eng. 6 (2020) 6356–6367. https://doi.org/10.1021/acsbiomaterials.0c01096.

[164] K. Bari, A. Arjunan, Extra low interstitial titanium based fully porous morphological bone scaffolds manufactured using selective laser melting, J. Mech. Behav. Biomed. Mater. 95 (2019) 1–12. https://doi.org/10.1016/j.jmbbm.2019.03.025.

[165] S. Kholgh Eshkalak, E. Rezvani Ghomi, Y. Dai, D. Choudhury, S. Ramakrishna, The role of three-dimensional printing in healthcare and medicine, Mater. Des. 194 (2020) 108940. https://doi.org/10.1016/j.matdes.2020.108940.

[166] R. Kumar, M. Kumar, J.S. Chohan, The role of additive manufacturing for biomedical applications: A critical review, J. Manuf. Process. 64 (2021) 828–850.

https://doi.org/10.1016/j.jmapro.2021.02.022.

[167] M. Salmi, Additive Manufacturing Processes in Medical Applications, Materials (Basel). 14 (2021) 191. https://doi.org/10.3390/ma14010191.

[168] M. Revilla-León, M. Sadeghpour, M. Özcan, A Review of the Applications of Additive Manufacturing Technologies Used to Fabricate Metals in Implant Dentistry, J. Prosthodont. 29 (2020) 579–593. https://doi.org/10.1111/jopr.13212.

[169] Y. Wei, Y. Hu, M. Li, D. Li, Fabrication of Sr-functionalized micro/nano-hierarchical structure ceramic coatings on 3D printing titanium, Surf. Eng. 37 (2021) 373–380. https://doi.org/10.1080/02670844.2020.1748349.

[170] S. Ghods, R. Schur, E. Schultz, R. Pahuja, A. Montelione, C. Wisdom, D. Arola, M. Ramulu, Powder reuse and its contribution to porosity in additive manufacturing of Ti6Al4V, Materialia. 15 (2021) 100992. https://doi.org/10.1016/j.mtla.2020.100992.

[171] M. Vignesh, G. Ranjith Kumar, M. Sathishkumar, M. Manikandan, G. Rajyalakshmi, R. Ramanujam, N. Arivazhagan, Development of Biomedical Implants through Additive Manufacturing: A Review, J. Mater. Eng. Perform. 30 (2021) 4735–4744. https://doi.org/10.1007/s11665-021-05578-7.

[172] C. Tan, J. Zou, S. Li, P. Jamshidi, A. Abena, A. Forsey, R.J. Moat, K. Essa, M. Wang, K. Zhou, M.M. Attallah, Additive manufacturing of bio-inspired multi-scale hierarchically strengthened lattice structures, Int. J. Mach. Tools Manuf. 167 (2021) 103764. https://doi.org/10.1016/j.ijmachtools.2021.103764.

[173] Y. Zhang, Z. Wang, Y. Zhang, S. Gomes, A. Bernard, Bio-inspired generative design for support structure generation and optimization in Additive Manufacturing (AM), CIRP

Ann. 69 (2020) 117–120. https://doi.org/10.1016/j.cirp.2020.04.091.

[174] M. Doblaré, J.M. García, M.J. Gómez, Modelling bone tissue fracture and healing: a review, Eng. Fract. Mech. 71 (2004) 1809–1840. https://doi.org/10.1016/j.engfracmech.2003.08.003.

[175] E. Anitua, N. Larrazabal Saez de Ibarra, I. Morales Martín, L. Saracho Rotaeche, Influence of Dental Implant Diameter and Bone Quality on the Biomechanics of Single-Crown Restoration. A Finite Element Analysis, Dent. J. 9 (2021) 103. https://doi.org/10.3390/dj9090103.

[176] G. Osterhoff, E.F. Morgan, S.J. Shefelbine, L. Karim, L.M. McNamara, P. Augat, Bone mechanical properties and changes with osteoporosis, Injury. 47 (2016) S11–S20. https://doi.org/10.1016/S0020-1383(16)47003-8.

[177] R. Florencio-Silva, G.R. da S. Sasso, E. Sasso-Cerri, M.J. Simões, P.S. Cerri, Biology of Bone Tissue: Structure, Function, and Factors That Influence Bone Cells, Biomed Res. Int. 2015 (2015) 1–17. https://doi.org/10.1155/2015/421746.

[178] S.C. Cowin, Wolff's Law of Trabecular Architecture at Remodeling Equilibrium, J. Biomech. Eng. 108 (1986) 83–88. https://doi.org/10.1115/1.3138584.

[179] H.M. Frost, Skeletal structural adaptations to mechanical usage (SATMU): 1. Redefining Wolff's Law: The bone modeling problem, Anat. Rec. 226 (1990) 403–413. https://doi.org/10.1002/ar.1092260402.

[180] H.M. Frost, A 2003 update of bone physiology and Wolff's Law for clinicians, Angle Orthod. 74 (2004) 3–15.

[181] G.S. Beaupré, T.E. Orr, D.R. Carter, An approach for time-dependent bone modeling and remodeling-theoretical development, J. Orthop. Res. 8 (1990) 651–661. https://doi.org/10.1002/jor.1100080506.

[182] S.C. Cowin, D.H. Hegedus, Bone remodeling I: theory of adaptive elasticity, J. Elast. 6 (1976) 313–326. https://doi.org/10.1007/BF00041724.

[183] R. Huiskes, H. Weinans, H.J. Grootenboer, M. Dalstra, B. Fudala, T.J. Slooff, Adaptive bone-remodeling theory applied to prosthetic-design analysis, J. Biomech. 20 (1987) 1135–1150. https://doi.org/10.1016/0021-9290(87)90030-3.

[184] A. Madeo, D. George, T. Lekszycki, M. Nierenberger, Y. Rémond, A second gradient continuum model accounting for some effects of micro-structure on reconstructed bone remodelling, Comptes Rendus Mécanique. 340 (2012) 575–589. https://doi.org/10.1016/j.crme.2012.05.003.

[185] A. Merdji, B. Bachir Bouiadjra, B. Ould Chikh, R. Mootanah, L. Aminallah, B. Serier, I.M. Muslih, Stress distribution in dental prosthesis under an occlusal combined dynamic loading, Mater. Des. 36 (2012) 705–713. https://doi.org/10.1016/j.matdes.2011.12.006.

[186] H.M.S. Duarte, J.R. Andrade, L.M.J.S. Dinis, R.M.N. Jorge, J. Belinha, Numerical analysis of dental implants using a new advanced discretization technique, Mech. Adv. Mater. Struct. 23 (2016) 467–479. https://doi.org/10.1080/15376494.2014.987410.

[187] D. Jia, F. Li, C. Zhang, K. Liu, Y. Zhang, Design and simulation analysis of Lattice bone plate based on finite element method, Mech. Adv. Mater. Struct. 28 (2021) 1311–1321. https://doi.org/10.1080/15376494.2019.1665759.

[188] D.-S. Son, H. Mehboob, S.-H. Chang, Simulation of the bone healing process of fractured

long bones applied with a composite bone plate with consideration of the blood vessel growth, Compos. Part B Eng. 58 (2014) 443–450. https://doi.org/10.1016/j.compositesb.2013.10.058.

[189] H. Mehboob, F. Tarlochan, A. Mehboob, S.-H. Chang, S. Ramesh, W.S.W. Harun, K. Kadirgama, A novel design, analysis and 3D printing of Ti-6Al-4V alloy bio-inspired porous femoral stem, J. Mater. Sci. Mater. Med. 31 (2020) 78. https://doi.org/10.1007/s10856-020-06420-7.

[190] H. Mehboob, F. Ahmad, F. Tarlochan, A. Mehboob, S.H. Chang, A comprehensive analysis of bio-inspired design of femoral stem on primary and secondary stabilities using mechanoregulatory algorithm, Biomech. Model. Mechanobiol. 19 (2020) 2213–2226. https://doi.org/10.1007/s10237-020-01334-3.

[191] A.Z.E.-A. Arab, A. Merdji, A. Benaissa, S. Roy, B.-A. Bachir Bouiadjra, K. Layadi, A. Ouddane, O.M. Mukdadi, Finite-Element analysis of a lateral femoro-tibial impact on the total knee arthroplasty, Comput. Methods Programs Biomed. 192 (2020) 105446. https://doi.org/10.1016/j.cmpb.2020.105446.

[192] H. Mehboob, F. Tarlochan, A. Mehboob, S.-H. Chang, Finite element modelling and characterization of 3D cellular microstructures for the design of a cementless biomimetic porous hip stem, Mater. Des. 149 (2018) 101–112. https://doi.org/10.1016/j.matdes.2018.04.002.

[193] A. Benaissa, A. Merdji, M.Z. Bendjaballah, P. Ngan, O.M. Mukdadi, Stress influence on orthodontic system components under simulated treatment loadings, Comput. Methods Programs Biomed. 195 (2020) 105569. https://doi.org/10.1016/j.cmpb.2020.105569.

[194] A. Mehboob, S.H.A. Rizvi, S.-H. Chang, H. Mehboob, Comparative study of healing fractured tibia assembled with various composite bone plates, Compos. Sci. Technol. 197 (2020) 108248. https://doi.org/10.1016/j.compscitech.2020.108248.

[195] F. Tarlochan, H. Mehboob, A. Mehboob, S.-H. Chang, Influence of functionally graded pores on bone ingrowth in cementless hip prosthesis: a finite element study using mechano-regulatory algorithm, Biomech. Model. Mechanobiol. 17 (2018) 701–716. https://doi.org/10.1007/s10237-017-0987-2.

[196] A. Mehboob, H. Mehboob, S.-H. Chang, Evaluation of unidirectional BGF/PLA and Mg/PLA biodegradable composites bone plates-scaffolds assembly for critical segmental fractures healing, Compos. Part A Appl. Sci. Manuf. 135 (2020) 105929. https://doi.org/10.1016/j.compositesa.2020.105929.

[197] H. Mehboob, J. Kim, A. Mehboob, S.-H. Chang, How post-operative rehabilitation exercises influence the healing process of radial bone shaft fractures fixed by a composite bone plate, Compos. Struct. 159 (2017) 307–315. https://doi.org/10.1016/j.compstruct.2016.09.081.

[198] S.E. Alkhatib, F. Tarlochan, H. Mehboob, R. Singh, K. Kadirgama, W.S.B.W. Harun, Finite element study of functionally graded porous femoral stems incorporating body-centered cubic structure, Artif. Organs. 43 (2019). https://doi.org/10.1111/aor.13444.

[199] A. Mehboob, H. Mehboob, S.-H. Chang, F. Tarlochan, Effect of composite intramedullary nails (IM) on healing of long bone fractures by means of reamed and unreamed methods, Compos. Struct. 167 (2017) 76–87. https://doi.org/10.1016/j.compstruct.2017.01.076.

[200] Y.-M. Huang, I.-C. Chou, C.-P. Jiang, Y.-S. Wu, S.-Y. Lee, Finite Element Analysis of

Dental Implant Neck Effects on Primary Stability and Osseointegration in a Type IV Bone Mandible, Biomed. Mater. Eng. 24 (2014) 1407–1415. https://doi.org/10.3233/BME-130945.

[201] M.-D. Jeng, Y.-S. Lin, C.-L. Lin, Biomechanical Evaluation of the Effects of Implant Neck Wall Thickness and Abutment Screw Size: A 3D Nonlinear Finite Element Analysis, Appl. Sci. 10 (2020) 3471. https://doi.org/10.3390/app10103471.

[202] P. Marcián, J. Wolff, L. Horáčková, J. Kaiser, T. Zikmund, L. Borák, Micro finite element analysis of dental implants under different loading conditions, Comput. Biol. Med. 96 (2018) 157–165. https://doi.org/10.1016/j.compbiomed.2018.03.012.

[203] H. Mehboob, A. Mehboob, F. Abbassi, F. Ahmad, A.S. Khan, S. Miran, Bioinspired porous dental implants using the concept of 3D printing to investigate the effect of implant type and porosity on patient's bone condition, Mech. Adv. Mater. Struct. (2021) 1–15. https://doi.org/10.1080/15376494.2021.1971347.

[204] R.M. Jones, Deformation theory of plasticity, Bull Ridge Corporation, 2009.

[205] C. Öhman, M. Baleani, C. Pani, F. Taddei, M. Alberghini, M. Viceconti, M. Manfrini, Compressive behaviour of child and adult cortical bone, Bone. 49 (2011) 769–776. https://doi.org/10.1016/j.bone.2011.06.035.

[206] B. Liu, W. Xu, X. Lu, M. Tamaddon, M. Chen, J. Dong, Y. Liu, L. Guo, J. Zhang, X. Qu, X. He, C. Liu, The Optimization of Ti Gradient Porous Structure Involves the Finite Element Simulation Analysis, Front. Mater. 8 (2021). https://doi.org/10.3389/fmats.2021.642135.

[207] L.C. Gerhardt, A.R. Boccaccini, Bioactive glass and glass-ceramic scaffolds for bone

tissue engineering, Materials (Basel). 3 (2010) 3867–3910. https://doi.org/10.3390/ma3073867.

[208] E.F. Morgan, T.M. Keaveny, Dependence of yield strain of human trabecular bone on anatomic site, J. Biomech. 34 (2001) 569–577. https://doi.org/10.1016/S0021-9290(01)00011-2.

[209] F.J. Quevedo González, J.D. Lipman, D. Lo, I. De Martino, P.K. Sculco, T.P. Sculco, F. Catani, T.M. Wright, Mechanical performance of cementless total knee replacements: It is not all about the maximum loads, J. Orthop. Res. 37 (2019) 350–357. https://doi.org/10.1002/jor.24194.

[210] A. Mahnama, M. Tafazzoli-Shadpour, F. Geramipanah, M. Mehdi Dehghan, Verification of the mechanostat theory in mandible remodeling after tooth extraction: Animal study and numerical modeling, J. Mech. Behav. Biomed. Mater. 20 (2013) 354–362. https://doi.org/10.1016/j.jmbbm.2013.02.013.

[211] J.P.M. Kan, R.B. Judge, J.E.A. Palamara, In vitro bone strain analysis of implant following occlusal overload, Clin. Oral Implants Res. 25 (2014) e73–e82. https://doi.org/10.1111/clr.12059.

[212] K. Pałka, R. Pokrowiecki, Porous Titanium Implants: A Review, Adv. Eng. Mater. 20 (2018) 1700648. https://doi.org/10.1002/adem.201700648.

[213] Z. Wally, W. van Grunsven, F. Claeyssens, R. Goodall, G. Reilly, Porous Titanium for Dental Implant Applications, Metals (Basel). 5 (2015) 1902–1920. https://doi.org/10.3390/met5041902.

[214] A. El-Gazzar, W. Högler, Mechanisms of Bone Fragility: From Osteogenesis Imperfecta to

Secondary Osteoporosis, Int. J. Mol. Sci. 22 (2021) 625. https://doi.org/10.3390/ijms22020625.

[215] R. Pokrowiecki, A. Mielczarek, T. Zaręba, S. Tyski, Oral microbiome and peri-implant diseases: where are we now?, Ther. Clin. Risk Manag. Volume 13 (2017) 1529–1542. https://doi.org/10.2147/TCRM.S139795.

[216] T.J. Sego, Y.-T. Hsu, T.-M.G. Chu, A. Tovar, On the Significance and Predicted Functional Effects of the Crown-to-Implant Ratio: A Finite Element Study of Long-Term Implant Stability Using High-Resolution, Nonlinear Numerical Analysis, in: Vol. 3 Biomed. Biotechnol. Eng., American Society of Mechanical Engineers, 2016. https://doi.org/10.1115/IMECE2016-67654.

[217] O.M. Ugarte, I.O. Gialain, N.M. de Carvalho, G.L. Fukuoka, R.Y. Ballester, P.M. Cattaneo, M.G. Roscoe, J.B.C. Meira, Can maxilla and mandible bone quality explain differences in orthodontic mini-implant failures?, Biomater. Investig. Dent. 8 (2021) 1–10. https://doi.org/10.1080/26415275.2020.1863155.

[218] A. Civantos, M. Giner, P. Trueba, S. Lascano, M.-J. Montoya-García, C. Arévalo, M.Á. Vázquez, J.P. Allain, Y. Torres, In Vitro Bone Cell Behavior on Porous Titanium Samples: Influence of Porosity by Loose Sintering and Space Holder Techniques, Metals (Basel). 10 (2020) 696. https://doi.org/10.3390/met10050696.

[219] A.M. Crovace, L. Lacitignola, D.M. Forleo, F. Staffieri, E. Francioso, A. Di Meo, J. Becerra, A. Crovace, L. Santos-Ruiz, 3D Biomimetic Porous Titanium (Ti6Al4V ELI) Scaffolds for Large Bone Critical Defect Reconstruction: An Experimental Study in Sheep, Animals. 10 (2020) 1389. https://doi.org/10.3390/ani10081389.

[220] F.A. Shah, M. Trobos, P. Thomsen, A. Palmquist, Commercially pure titanium (cp-Ti) versus titanium alloy (Ti6Al4V) materials as bone anchored implants — Is one truly better than the other?, Mater. Sci. Eng. C. 62 (2016) 960–966. https://doi.org/10.1016/j.msec.2016.01.032.

[221] M. Dallago, V. Fontanari, E. Torresani, M. Leoni, C. Pederzolli, C. Potrich, M. Benedetti, Fatigue and biological properties of Ti-6Al-4V ELI cellular structures with variously arranged cubic cells made by selective laser melting, J. Mech. Behav. Biomed. Mater. 78 (2018) 381–394. https://doi.org/10.1016/j.jmbbm.2017.11.044.

[222] L. Shi, L. Shi, L. Wang, Y. Duan, W. Lei, Z. Wang, J. Li, X. Fan, X. Li, S. Li, Z. Guo, The Improved Biological Performance of a Novel Low Elastic Modulus Implant, PLoS One. 8 (2013) e55015. https://doi.org/10.1371/journal.pone.0055015.

[223] J.M. Shum, B.C. Gadomski, S.J. Tredinnick, W. Fok, J. Fernandez, B. Nelson, R.H. Palmer, K.C. McGilvray, G.J. Hooper, C. Puttlitz, J. Easley, T.B.F. Woodfield, Enhanced bone formation in locally-optimised, low-stiffness additive manufactured titanium implants: An in silico and in vivo tibial advancement study, Acta Biomater. (2022). https://doi.org/https://doi.org/10.1016/j.actbio.2022.04.006.

[224] M. Emmert, A. Gülses, E. Behrens, F. Karayürek, Y. Acil, J. Wiltfang, J.H. Spille, An experimental study on the effects of the cortical thickness and bone density on initial mechanical anchorage of different Straumann® implant designs, Int. J. Implant Dent. 7 (2021) 83. https://doi.org/10.1186/s40729-021-00367-2.

[225] L. Salou, A. Hoornaert, G. Louarn, P. Layrolle, Enhanced osseointegration of titanium implants with nanostructured surfaces: An experimental study in rabbits, Acta Biomater.

11 (2015) 494–502. https://doi.org/10.1016/j.actbio.2014.10.017.

[226] F.S. Alzahrani, I.A. Abbas, Analytical estimations of temperature in a living tissue generated by laser irradiation using experimental data, J. Therm. Biol. 85 (2019) 102421. https://doi.org/10.1016/j.jtherbio.2019.102421.

[227] F.S. Alzahrani, I.A. Abbas, Analytical solutions of thermal damage in living tissues due to laser irradiation, Waves in Random and Complex Media. 31 (2021) 1443–1456. https://doi.org/10.1080/17455030.2019.1676934.

[228] H. Deppe, M. Ahrens, A. V. Behr, C. Marr, A. Sculean, P. Mela, L.M. Ritschl, Thermal effect of a 445 nm diode laser on five dental implant systems: an in vitro study, Sci. Rep. 11 (2021) 20174. https://doi.org/10.1038/s41598-021-99709-8.

[229] A. Ghanmi, I.A. Abbas, An analytical study on the fractional transient heating within the skin tissue during the thermal therapy, J. Therm. Biol. 82 (2019) 229–233. https://doi.org/10.1016/j.jtherbio.2019.04.003.

[230] A. Hobiny, I. Abbas, Thermal response of cylindrical tissue induced by laser irradiation with experimental study, Int. J. Numer. Methods Heat Fluid Flow. 30 (2019) 4013–4023. https://doi.org/10.1108/HFF-10-2019-0777.

[231] A. Hobiny, I. Abbas, Analytical solutions of fractional bioheat model in a spherical tissue, Mech. Based Des. Struct. Mach. 49 (2021) 430–439. https://doi.org/10.1080/15397734.2019.1702055.

[232] A. Hobiny, F. Alzahrani, I. Abbas, Analytical Estimation of Temperature in Living Tissues Using the TPL Bioheat Model with Experimental Verification, Mathematics. 8 (2020) 1188. https://doi.org/10.3390/math8071188.

[233] A. Hobiny, F. Alzahrani, I. Abbas, M. Marin, The Effect of Fractional Time Derivative of Bioheat Model in Skin Tissue Induced to Laser Irradiation, Symmetry (Basel). 12 (2020) 602. https://doi.org/10.3390/sym12040602.

[234] A.D. Hobiny, I.A. Abbas, Theoretical analysis of thermal damages in skin tissue induced by intense moving heat source, Int. J. Heat Mass Transf. 124 (2018) 1011–1014. https://doi.org/10.1016/j.ijheatmasstransfer.2018.04.018.

[235] Y. Yao, Z. Mo, G. Wu, J. Guo, J. Li, L. Wang, Y. Fan, A personalized 3D-printed plate for tibiotalocalcaneal arthrodesis: Design, fabrication, biomechanical evaluation and postoperative assessment, Comput. Biol. Med. 133 (2021) 104368. https://doi.org/10.1016/j.compbiomed.2021.104368.

[236] J. Li, H. Yuan, A. Chandrakar, L. Moroni, P. Habibovic, 3D porous Ti6Al4V-beta-tricalcium phosphate scaffolds directly fabricated by additive manufacturing, Acta Biomater. 126 (2021) 496–510. https://doi.org/10.1016/j.actbio.2021.03.021.

[237] B.M. Ferguson, A. Entezari, J. Fang, Q. Li, Optimal placement of fixation system for scaffold-based mandibular reconstruction, J. Mech. Behav. Biomed. Mater. 126 (2022) 104855. https://doi.org/10.1016/j.jmbbm.2021.104855.

[238] F. Günther, M. Wagner, S. Pilz, A. Gebert, M. Zimmermann, Design procedure for triply periodic minimal surface based biomimetic scaffolds, J. Mech. Behav. Biomed. Mater. 126 (2022) 104871. https://doi.org/10.1016/j.jmbbm.2021.104871.

[239] V.S. Cheong, B.C. Roberts, V. Kadirkamanathan, E. Dall'Ara, Bone remodelling in the mouse tibia is spatio-temporally modulated by oestrogen deficiency and external mechanical loading: A combined in vivo/in silico study, Acta Biomater. 116 (2020) 302–

317. https://doi.org/10.1016/j.actbio.2020.09.011.

[240] M.M.A. Peyroteo, J. Belinha, R.M. Natal Jorge, A mathematical biomechanical model for bone remodeling integrated with a radial point interpolating meshless method, Comput. Biol. Med. 129 (2021) 104170. https://doi.org/10.1016/j.compbiomed.2020.104170.

[241] G. Rouhi, M. Tahani, B. Haghighi, W. Herzog, Prediction of Stress Shielding Around Orthopedic Screws: Time-Dependent Bone Remodeling Analysis Using Finite Element Approach, J. Med. Biol. Eng. 35 (2015) 545–554. https://doi.org/10.1007/s40846-015-0066-z.

[242] A. Ouldyerou, A. Merdji, L. Aminallah, V. Msomi, P.L. Chong, S. Roy, BIOMECHANICAL EVALUATION OF MARGINAL BONE LOSS IN THE SURROUNDING BONE UNDER DIFFERENT LOADING: 3D FINITE ELEMENT ANALYSIS STUDY, Int. J. Multiscale Comput. Eng. 20 (2022) 43–56. https://doi.org/10.1615/IntJMultCompEng.2022043707.

[243] A.O. Ghaziani, R. Soheilifard, S. Kowsar, The effect of functionally graded materials on bone remodeling around osseointegrated trans-femoral prostheses, J. Mech. Behav. Biomed. Mater. 118 (2021) 104426. https://doi.org/10.1016/j.jmbbm.2021.104426.

[244] A. Ouldyerou, L. Aminallah, A. Merdji, A. Mehboob, H. Mehboob, Finite element analyses of porous dental implant designs based on 3D printing concept to evaluate biomechanical behaviors of healthy and osteoporotic bones, Mech. Adv. Mater. Struct. (2022) 1–13. https://doi.org/10.1080/15376494.2022.2053908.

[245] R.D. Carpenter, B.S. Klosterhoff, F.B. Torstrick, K.T. Foley, J.K. Burkus, C.S.D. Lee, K. Gall, R.E. Guldberg, D.L. Safranski, Effect of porous orthopaedic implant material and

structure on load sharing with simulated bone ingrowth: A finite element analysis comparing titanium and PEEK, J. Mech. Behav. Biomed. Mater. 80 (2018) 68–76. https://doi.org/10.1016/j.jmbbm.2018.01.017.

[246] D.R. Carter, W.C. Hayes, The compressive behavior of bone as a two-phase porous structure., J. Bone Joint Surg. Am. 59 (1977) 954–62.

[247] K. Su, L. Yuan, J. Yang, J. Du, Numerical Simulation of Mandible Bone Remodeling under Tooth Loading: A Parametric Study, Sci. Rep. 9 (2019) 14887. https://doi.org/10.1038/s41598-019-51429-w.

[248] T.R. Morneburg, P.A. Pröschel, Measurement of masticatory forces and implant loads: a methodologic clinical study., Int. J. Prosthodont. 15 (2002).

[249] M. Piccinini, J. Cugnoni, J. Botsis, P. Ammann, A. Wiskott, Numerical prediction of peri-implant bone adaptation: Comparison of mechanical stimuli and sensitivity to modeling parameters, Med. Eng. Phys. 38 (2016) 1348–1359. https://doi.org/10.1016/j.medengphy.2016.08.008.

[250] B. Chrcanovic, T. Albrektsson, A. Wennerberg, Bone Quality and Quantity and Dental Implant Failure: A Systematic Review and Meta-analysis, Int. J. Prosthodont. 30 (2017) 219–237. https://doi.org/10.11607/ijp.5142.

[251] S.B. Mada, S. Reddi, N. Kumar, R. Kumar, S. Kapila, R. Kapila, R. Trivedi, A. Karvande, N. Ahmad, Antioxidative peptide from milk exhibits antiosteopenic effects through inhibition of oxidative damage and bone-resorbing cytokines in ovariectomized rats, Nutrition. 43–44 (2017) 21–31. https://doi.org/10.1016/j.nut.2017.06.010.

[252] D. Kawahara, A. Saito, S. Ozawa, Y. Nagata, Image synthesis with deep convolutional

generative adversarial networks for material decomposition in dual-energy CT from a kilovoltage CT, Comput. Biol. Med. 128 (2021) 104111. https://doi.org/10.1016/j.compbiomed.2020.104111.

[253] K. Zheng, N. Yoda, J. Chen, Z. Liao, J. Zhong, C. Wu, B. Wan, S. Koyama, K. Sasaki, C. Peck, M. Swain, Q. Li, Bone remodeling following mandibular reconstruction using fibula free flap, J. Biomech. 133 (2022) 110968. https://doi.org/10.1016/j.jbiomech.2022.110968.

[254] J.E. Gubaua, G.W.O. Dicati, J. da Silva, J.L. do Vale, J.T. Pereira, Techniques for mitigating the checkerboard formation: application in bone remodeling simulations, Med. Eng. Phys. 99 (2022) 103739. https://doi.org/10.1016/j.medengphy.2021.103739.

[255] F. Cozzolino, D. Apicella, G. Wang, A. Apicella, R. Sorrentino, Implant-to-bone force transmission: a pilot study for in vivo strain gauge measurement technique, J. Mech. Behav. Biomed. Mater. 90 (2019) 173–181. https://doi.org/10.1016/j.jmbbm.2018.10.014.

[256] E. Yılmaz, F. Kabataş, A. Gökçe, F. Fındık, Production and Characterization of a Bone-Like Porous Ti/Ti-Hydroxyapatite Functionally Graded Material, J. Mater. Eng. Perform. 29 (2020) 6455–6467. https://doi.org/10.1007/s11665-020-05165-2.

[257] L. Li, J. Shi, K. Zhang, L. Yang, F. Yu, L. Zhu, H. Liang, X. Wang, Q. Jiang, Early osteointegration evaluation of porous Ti6Al4V scaffolds designed based on triply periodic minimal surface models, J. Orthop. Transl. 19 (2019) 94–105. https://doi.org/10.1016/j.jot.2019.03.003.

[258] K.S. Rappe, M. Ortiz-Hernandez, M. Punset, M. Molmeneu, A. Barba, C. Mas-Moruno, J. Guillem-Marti, C. Caparrós, E. Rupérez, J. Calero, M.-C. Manzanares, J. Gil, J. Franch, On-Growth and In-Growth Osseointegration Enhancement in PM Porous Ti-Scaffolds by

Two Different Bioactivation Strategies: Alkali Thermochemical Treatment and RGD Peptide Coating, Int. J. Mol. Sci. 23 (2022) 1750. https://doi.org/10.3390/ijms23031750.

[259] C. Han, Y. Li, Q. Wang, S. Wen, Q. Wei, C. Yan, L. Hao, J. Liu, Y. Shi, Continuous functionally graded porous titanium scaffolds manufactured by selective laser melting for bone implants, J. Mech. Behav. Biomed. Mater. 80 (2018) 119–127. https://doi.org/10.1016/j.jmbbm.2018.01.013.

[260] A. Dutta, K. Mukherjee, S. Dhara, S. Gupta, Design of porous titanium scaffold for complete mandibular reconstruction: The influence of pore architecture parameters, Comput. Biol. Med. 108 (2019) 31–41. https://doi.org/10.1016/j.compbiomed.2019.03.004.

[261] F. Yang, C. Chen, Q. Zhou, Y. Gong, R. Li, C. Li, F. Klämpfl, S. Freund, X. Wu, Y. Sun, X. Li, M. Schmidt, D. Ma, Y. Yu, Laser beam melting 3D printing of Ti6Al4V based porous structured dental implants: fabrication, biocompatibility analysis and photoelastic study, Sci. Rep. 7 (2017) 45360. https://doi.org/10.1038/srep45360.

[262] D. Mahmoud, M. Elbestawi, Lattice Structures and Functionally Graded Materials Applications in Additive Manufacturing of Orthopedic Implants: A Review, J. Manuf. Mater. Process. 1 (2017) 13. https://doi.org/10.3390/jmmp1020013.

[263] Y. Zhang, N. Sun, M. Zhu, Q. Qiu, P. Zhao, C. Zheng, Q. Bai, Q. Zeng, T. Lu, The contribution of pore size and porosity of 3D printed porous titanium scaffolds to osteogenesis, Biomater. Adv. 133 (2022) 112651. https://doi.org/10.1016/j.msec.2022.112651.

[264] A.I. Torres Pérez, M. Fernández Fairén, Á.A. Torres Pérez, J. Gil Mur, Use of Porous

Titanium Trabecular as a Bone Defect Regenerator: In Vivo Study, Metals (Basel). 12 (2022) 327. https://doi.org/10.3390/met12020327.

[265] G. Zhang, P. Zhao, L. Lin, L. Qin, Z. Huan, S. Leeflang, A.A. Zadpoor, J. Zhou, L. Wu, Surface-treated 3D printed Ti-6Al-4V scaffolds with enhanced bone regeneration performance: an in vivo study, Ann. Transl. Med. 9 (2021) 39–39. https://doi.org/10.21037/atm-20-3829.

[266] Y. Wang, X. Chen, C. Zhang, W. Feng, P. Zhang, Y. Chen, J. Huang, Y. Luo, J. Chen, Studies on the performance of selective laser melting porous dental implant by finite element model simulation, fatigue testing and in vivo experiments, Proc. Inst. Mech. Eng. Part H J. Eng. Med. 233 (2019) 170–180. https://doi.org/10.1177/0954411918816114.

[267] J.S. Pelz, N. Ku, M.A. Meyers, L.R. Vargas-Gonzalez, Additive manufacturing of structural ceramics: a historical perspective, J. Mater. Res. Technol. 15 (2021) 670–695. https://doi.org/10.1016/j.jmrt.2021.07.155.

[268] E. Strumza, P. Landau, G. Kimmel, Y.I. Ganor, O. Yeheskel, S. Hayun, Thermophysical properties of Ti-6Al-4V fabricated by powder bed fusion methods, Addit. Manuf. 58 (2022) 103045. https://doi.org/10.1016/j.addma.2022.103045.

[269] L. C. B. Carolo, R.E. Cooper O., A review on the influence of process variables on the surface roughness of Ti-6Al-4V by electron beam powder bed fusion, Addit. Manuf. 59 (2022) 103103. https://doi.org/10.1016/j.addma.2022.103103.

[270] Q. Luo, L. Yin, T.W. Simpson, A.M. Beese, Effect of processing parameters on pore structures, grain features, and mechanical properties in Ti-6Al-4V by laser powder bed fusion, Addit. Manuf. 56 (2022) 102915. https://doi.org/10.1016/j.addma.2022.102915.

[271] C. Hou, Y. Liu, W. Xu, X. Lu, L. Guo, Y. Liu, S. Tian, B. Liu, J. Zhang, C. Wen, Additive manufacturing of functionally graded porous titanium scaffolds for dental applications, Biomater. Adv. 139 (2022) 213018. https://doi.org/10.1016/j.bioadv.2022.213018.

[272] N. Taniguchi, S. Fujibayashi, M. Takemoto, K. Sasaki, B. Otsuki, T. Nakamura, T. Matsushita, T. Kokubo, S. Matsuda, Effect of pore size on bone ingrowth into porous titanium implants fabricated by additive manufacturing: An in vivo experiment, Mater. Sci. Eng. C. 59 (2016) 690–701. https://doi.org/10.1016/j.msec.2015.10.069.

[273] J.M. Shum, B.C. Gadomski, S.J. Tredinnick, W. Fok, J. Fernandez, B. Nelson, R.H. Palmer, K.C. McGilvray, G.J. Hooper, C. Puttlitz, J. Easley, T.B.F. Woodfield, Enhanced bone formation in locally-optimised, low-stiffness additive manufactured titanium implants: An in silico and in vivo tibial advancement study, Acta Biomater. 156 (2023) 202–213. https://doi.org/10.1016/j.actbio.2022.04.006.

[274] C. Sun, E. Dong, J. Chen, J. Zheng, J. Kang, Z. Jin, C. Liu, L. Wang, D. Li, The Promotion of Mechanical Properties by Bone Ingrowth in Additive-Manufactured Titanium Scaffolds, J. Funct. Biomater. 13 (2022) 127. https://doi.org/10.3390/jfb13030127.

[275] T. Fujii, R. Murakami, N. Kobayashi, K. Tohgo, Y. Shimamura, Uniform porous and functionally graded porous titanium fabricated via space holder technique with spark plasma sintering for biomedical applications, Adv. Powder Technol. 33 (2022) 103598. https://doi.org/10.1016/j.apt.2022.103598.

[276] A.H. Foroughi, M.J. Razavi, Multi-objective Shape Optimization of Bone Scaffolds: Enhancement of Mechanical Properties and Permeability, Acta Biomater. 146 (2022) 317–

340. https://doi.org/10.1016/j.actbio.2022.04.051.

[277] K.-M. Park, G.-O. Kim, J.-G. Kim, Y. Roh, Mechanical properties of additive manufactured variable-density Kelvin lattice structures: a novel design method for Kelvin unit cells, J. Struct. Integr. Maint. 7 (2022) 34–45. https://doi.org/10.1080/24705314.2021.1971893.

[278] E.A.A. Alkebsi, T. Outtas, A. Almutawakel, H. Ameddah, T. Kanit, Design of mechanically compatible lattice structures cancellous bone fabricated by fused filament fabrication of Z-ABS material, Mech. Adv. Mater. Struct. (2022) 1–14. https://doi.org/10.1080/15376494.2022.2053904.

[279] J. Zhao, H. Liu, Y. Zhou, Y. Chen, J. Gong, Effect of relative density on the compressive properties of Ti6Al4V diamond lattice structures with shells, Mech. Adv. Mater. Struct. 29 (2022) 3301–3315. https://doi.org/10.1080/15376494.2021.1893418.

[280] J. Zhang, J. Zhao, Q. Rong, W. Yu, X. Li, R.D.K. Misra, Machine learning guided prediction of mechanical properties of TPMS structures based on finite element simulation for biomedical titanium, Mater. Technol. (2021) 1–8. https://doi.org/10.1080/10667857.2021.1999558.

[281] V.S. Sufiiarov, A. V. Orlov, E. V. Borisov, V. V. Sokolova, M.O. Chukovenkova, A. V. Soklakov, D.S. Mikhaluk, A.A. Popovich, Design and mechanical properties simulation of graded lattice structures for additive manufacturing endoprostheses, Mech. Adv. Mater. Struct. 28 (2021) 1656–1662. https://doi.org/10.1080/15376494.2019.1700432.

[282] C. Peng, P. Tran, H. Nguyen-Xuan, A.J.M. Ferreira, Mechanical performance and fatigue life prediction of lattice structures: Parametric computational approach, Compos. Struct.

235 (2020) 111821. https://doi.org/10.1016/j.compstruct.2019.111821.

[283] K.C. Nune, R.D.K. Misra, S.J. Li, Y.L. Hao, R. Yang, Osteoblast cellular activity on low elastic modulus Ti–24Nb–4Zr–8Sn alloy, Dent. Mater. 33 (2017) 152–165. https://doi.org/10.1016/j.dental.2016.11.005.

[284] K. Refai, M. Montemurro, C. Brugger, N. Saintier, Determination of the effective elastic properties of titanium lattice structures, Mech. Adv. Mater. Struct. 27 (2020) 1966–1982. https://doi.org/10.1080/15376494.2018.1536816.

[285] T. Tancogne-Dejean, D. Mohr, Stiffness and specific energy absorption of additively-manufactured metallic BCC metamaterials composed of tapered beams, Int. J. Mech. Sci. 141 (2018) 101–116. https://doi.org/10.1016/j.ijmecsci.2018.03.027.

[286] G. Yu, Z. Li, S. Li, Q. Zhang, Y. Hua, H. Liu, X. Zhao, D.T. Dhaidhai, W. Li, X. Wang, The select of internal architecture for porous Ti alloy scaffold: A compromise between mechanical properties and permeability, Mater. Des. 192 (2020) 108754. https://doi.org/10.1016/j.matdes.2020.108754.

Published Works

Publication	International Quartile	Dgrsdt category	Impact factor
Ouldyerou, A., Merdji, A., Aminallah, L., Msomi, V., Chong, P. L., & Roy, S. (2022). BIOMECHANICAL EVALUATION OF MARGINAL BONE LOSS IN THE SURROUNDING BONE UNDER DIFFERENT LOADING: 3D FINITE ELEMENT ANALYSIS STUDY. International Journal for Multiscale Computational Engineering, 20(4). https://doi.org/10.1615/IntJMultCompEng.2022043707	**Q3**	**A**	**1.59**
- **Ouldyerou**, A., Aminallah, L., Merdji, A., Mehboob, A., & Mehboob, H. (2023). Finite element analyses of porous dental implant designs based on 3D printing concept to evaluate biomechanical behaviors of healthy and osteoporotic bones. Mechanics of Advanced Materials and Structures, 30(11), 2328-2340. https://doi.org/10.1080/15376494.2022.2053908	**Q2**	**A**	**3.33**
- **Ouldyerou**, A., Merdji, A., Aminallah, L., Roy, S., Mehboob, H., & Özcan, M. (2022). Biomechanical performance of Ti-PEEK dental implants in bone: An in-	**Q2**	**A**	**4.04**

	silico analysis. Journal of the Mechanical Behavior of Biomedical Materials, 134, 105422. https://doi.org/10.1016/j.jmbbm.2022.105422			
-	**Ouldyerou**, A., Mehboob, H., Merdji, A., Aminallah, L., Mehboob, A., & Mukdadi, O. M. (2022). Biomechanical analysis of printable functionally graded material (FGM) dental implants for different bone densities. Computers in Biology and Medicine, 150, 106111. https://doi.org/10.1016/j.compbiomed.2022.106111	**Q1**	**A**	**6.69**
-	**Ouldyerou**, A., Merdji, A., Aminallah, L., Mehboob, H., Mehboob, A., Roy, S., ... & Tarlochan, F. (2023). Functionally graded ceramics (FGC) dental abutment with implant-supported cantilever crown: finite element analysis. Composites Communications, 38, 101514. https://doi.org/10.1016/j.coco.2023.101514	**Q1**	**A**	**7.56**